Spring 2007

Dynamic modeling and simulations of solid oxide fuel cells for grid-tied applications

Nagasmitha Akkinapragada

Department:

DYNAMIC MODELING AND SIMULATIONS OF SOLID OXIDE FUEL CELLS FOR GRID-TIED APPLICATIONS

by

NAGASMITHA AKKINAPRAGADA

A THESIS

Presented to the Faculty of the Graduate School of the

UNIVERSITY OF MISSOURI-ROLLA

In Partial Fulfillment of the Requirements for the Degree

MASTER OF SCIENCE IN ELECTRICAL ENGINEERING

2007

Approved by

_____	_____
Dr. Badrul H. Chowdhury, Advisor	Dr. Kelvin T. Erickson

_____

Dr. Norman R. Cox

ABSTRACT

As energy consumption rises, one must find suitable alternative means of generation to supplement conventional existing generation facilities. In this regard, distributed generation (DG) will continue to play a critical role in the energy supply-demand realm. The common technologies available as DG are micro-turbines, solar photovoltaic systems, fuel cells stack and wind energy systems.

In this thesis, a dynamic model of solid oxide fuel cell (SOFC) is presented. Fuel cells operate at low voltages and hence need to be boosted and inverted in order to be connected to the utility grid. The interconnection of the SOFC with a DC-DC converter and a DC-AC inverter for interfacing with the grid is presented in this thesis. These models are built in PSCAD 4.1.1

The power characteristics of the DC-AC inverter are compared with the characteristics of the DC-DC converter and the fuel cell. Fuel cells have a slow response time which prevents it from grid-tied applications. Simulations validate the improvement in the response when the power conditioning unit is connected.

ACKNOWLEDGMENTS

I would like to extend my sincere gratitude and appreciation to my advisor, Dr. Badrul H. Chowdhury, for his guidance, assistance, support and suggestions throughout my graduate studies as well as my research work. With his co-operation, I was able to complete my thesis.

I would like to thank Dr. Kelvin T. Erickson and Dr. Norman R. Cox for serving on my advisory committee, taking the time to review my thesis.

I would like to thank the U.S. National Science Foundation for funding this research project under the grant ECS-0523897.

I would also like to thank all my friends and family members for their constant emotional and moral assistance throughout my work

TABLE OF CONTENTS

LIST OF ILLUSTRATIONS

LIST OF TABLES

1. INTRODUCTION

1.1. DISTRIBUTED GENERATION

The centralized and regulated electric utilities have always been the major source of electric power production and supply. However, the increase in demand for electric power has led to the development of distributed generation (DG) which can complement the central power by providing additional capacity to the users. These are small generating units which can be located at the consumer end or anywhere within the distribution system. DG can be beneficial to the consumers as well as the utility. Consumers are interested in DG due to the various benefits associated with it: cost saving during peak demand charges, higher power quality and increased energy efficiency. The utilities can also benefit as it generally eliminates the cost needed for laying new transmission/distribution lines.

Distributed generation employs alternate resources such as micro-turbines, solar photovoltaic systems, fuel cells and wind energy systems. This thesis lays emphasis on the fuel cell technology and its integration with the utility grid.

1.2. LITERATURE REVIEW

The fuel cell is a fast growing technology and much research has been going on in this decade. Fuel cells are gaining much attention because of their light weight, compact size, low maintenance, and low acoustic and chemical emissions. They can serve as a potential source for electric power generation for stand-alone as well as for grid-tied applications.

Reference [1] provides a basic approach for fuel cell modeling suitable for distributed generation. A model for the proton exchange membrane fuel cell (PEMFC) has been developed by various researchers in [2]-[4] taking its thermodynamic effect into consideration. References [5]-[9] provide the solid oxide fuel cell (SOFC) model taking the temperature effect into account. Hall and Colclaser [5] did not consider the dynamics of the chemical species. Achenbach [6] developed a mathematical model of a planar SOFC which concentrated on the effects of temperature changes on the output voltage response. The same author investigated the transient behavior of a stand-alone SOFC

caused by a load change in [7]. A non-linear dynamic model of the SOFC that can be used for dynamic and transient stability studies was developed in [8]. A physically based model for tubular SOFC was developed in [9]. Simplified models of the SOFC have been presented in [10]-[15] considering constant cell temperature. Direct reforming molten carbonate fuel cell (MCFC) stack was developed in [16]-[17].

Fuel cells operate at low DC voltages and hence need to be boosted with the help of a DC-DC converter. Various topologies such as the H-bridge series resonant, buck and boost converters have been presented in [18]. The advantage of the H-bridge resonant converter is its inherited short-circuit protection and no saturation problem of the transformer. These converters provide dc isolation for the inverter. Buck and boost converters can be used if isolation is not required and the voltage conversion ratio is not high. These converters are known as non-isolated DC-DC converters. A current fed push-pull converter has been presented in [19]. This topology decreases the conduction losses in the switches due to the low fuel cell voltage. An interleaved front-end boost converter has been discussed in [20]. This topology considerably reduces the current ripple flowing into the fuel cell. A dual loop control strategy (current and voltage loop) has been used for the interleaved converter. A Z-source converter has been introduced in [21]. This is a new concept in which a shoot-through vector directly steps up the DC source voltage without using a boost DC-DC converter. The boost voltage rate depends on the total duration of the shoot-through zero vectors over one switching period [21]. In this thesis, a non-isolated buck-boost DC-DC converter with a closed loop PWM (pulse width modulation) control strategy as described in Reference [22] has been employed.

DC-AC inverter converts the DC power of the fuel cell system into AC power for stand alone as well as grid connected applications. The voltage source inverter (VSI) plays a vital role in interfacing the fuel cell-DC-DC system with the utility grid. Various control strategies have been proposed for the VSI in references [21], [23]-[32]. References [24]-[25] and [32] deal with the flux vector control for choosing the inverter voltage vectors and an ideal inverter has been used in [27]. A real and reactive power control using *dq* transformation has been employed in reference [23] and [28]. Reference [15] discusses modeling of one-cycle controlled inverter. Most of the controllers are based on PWM control whereas in reference [29] hysteresis control has been used.

PEM fuel cells for transportation, backup power and light mobility have already been commercialized and are available in the market. Ballard Power systems designs, develops and manufactures zero-emission PEM fuel cells and associated power electronic devices to meet the needs of a diverse and demanding customer base [33]. Siemens-Westinghouse Power Corp. has developed its first prototype of 125kW system for cogeneration applications and is in the process of commercialization [34]. GE global research has successfully developed a 6kW prototype of a SOFC system with the support of U.S. Department of Energy for testing purposes [35].

Fuel cell prototypes have been developed and tested for stand-alone and transportation applications. Grid-tied application is a major concern and a challenge for most researchers and developers. Accumentrics Corporation (USA) has installed a 5kW SOFC system near Cleveland, Ohio [36]. This unit is being operated in a grid-parallel mode and is in the process of commercialization. UTC Power (USA) has developed Pure Cell 200 Power Solution which is a grid connected unit, operating in parallel with electric utilities [36]. It can either be operated in grid connection or grid independent mode and produces 200kW of electric power. Plug Power (USA) is currently developing GenSys systems for off-grid prime power applications where backup power is critical [36]. Plug Power has worked in conjunction with Valliant (Germany) on the virtual fuel cell power plant [37]. This plant being centrally controlled and grid connected, contributes to meet peak energy demand in the public utility grid. These systems have been tested in German, Dutch and Australian households since 2002. Idatech (USA) has developed ElectraGen which is designed to run either in grid parallel mode or sole power in case of grid failure [38]. Japan Energy (Japan), in conjunction with Toshiba Fuel Cell Power Systems, has installed a number of LPG-fuelled 700W fuel cells into homes that it serves [38]. Wartsila Corporation (USA) is developing WF50, a 50kW distributed generation power unit for commercialization [36]. Ztek (USA) plans to develop a half megawatt and full megawatt version for the distributed electricity market, based on the 200kW SOFC/gas turbine system which is still under construction [39]. Mitsubishi Materials (Japan) working with Kansai Electric (Japan) and Kyushu University have developed 10kW units for on-site power generation and is in the process of commercialization [39]. Considerable research is being carried out to study the capabilities of the fuel cell system

during the grid-connected mode. Reference [40] presents case studies for the control of grid connected fuel cells for transient stability enhancement.

1.3. OBJECTIVE OF THE THESIS

High-temperature fuel cells such as the solid oxide fuel cells (SOFC) have the potential for centralized power generation as well as combined heat and power. Compared to the other fuel cells, SOFCs are capable of handling more convenient forms of hydrocarbon fuels; they are highly efficient; and tolerant to impurities and its high temperature enables internal reforming. This thesis employs the SOFC model presented in [14].

The DC-DC converter boosts the low voltage of the fuel cell as well as regulates the voltage. In reference [23] and [28] a non-isolated boost converter with a conventional PI controller has been used for the converter control. In this thesis, a non-isolated buck-boost converter with a PWM closed loop control has been employed for the converter control based on the control procedure presented in [22] because it uses small signal analysis and is simple to implement.

The DC-AC inverter plays a key role in making the fuel cell DC power available for stand-alone as well as for the grid connection. This thesis focuses on the interfacing of the fuel cell system with the utility grid. The inverter switching control determines the amount of real and reactive power injection into the grid. The proposed strategy involves real and reactive power control similar to the strategies presented earlier. In this thesis, the method employed for determination of the duty cycle terms required for the sine triangle modulation is different compared to the other strategies.

In this thesis, the AC power of the inverter is compared with the characteristics of the converter and the fuel cell. Fuel cells have slow response time which prevents it from grid-tie applications. Simulation results validate the improvement in the response when the power conditioning unit (DC-DC converter and DC-AC inverter) is connected.

1.4. SOFTWARE USED

Modeling of dynamic systems can be done in MATLAB/Simulink [41] as well as in PSCAD [42]. Both PSCAD and Simulink have a graphical user interface with the same

level of capabilities. In this thesis, PSCAD 4.1.1 has been used to model the fuel cell, DC-DC converter and the DC-AC inverter.

The reason for using PSCAD over Simulink is the computation time which is faster in the case of PSCAD. In terms of implementation of the models and accuracy in the results, both pieces of software are similar in nature. PSCAD was developed primarily for power system analysis.

Another feature of PSCAD that makes it an ideal choice for modeling is its data import and export facilities. Data can be exchanged between the main system and the subsystems without having any connection between them.

1.5. OUTLINE OF THE THESIS

Since this thesis is basically concerned with the fuel cell, the converter and the inverter, there is a separate section for each subsystem. Section 2 deals with the overview of the fuel cells, discusses the fuel cell system and the operating principle. The solid oxide fuel cell (SOFC) is discussed in detail in this subsection. This subsection consists of the fuel cell equations and the model parameters.

Section 3 deals with the power conditioning unit. The DC-DC converter and the DC-AC inverter are described in separate subsections. The converter subsection deals with the converter topologies, discusses the buck-boost converter and the PWM closed loop control strategy. The inverter subsection deals with the three-phase PWM VSI, controller design and the duty cycle modulation calculations.

Section 4 consists of the dynamic model of the integrated system, i.e., the SOFC, the converter and the inverter connected to a utility grid. It also deals with the simulation results obtained for the system.

Section 5 contains the conclusions drawn from the simulation results and discusses the scope for further studies on fuel cell integration with the utility grid.

2. FUEL CELLS

2.1. OVERVIEW

Fuel cell technology is a relatively new energy-saving technology that has the potential to compete with the conventional existing generation facilities. Among the various DG technologies available, fuel cells are being considered as a potential source of electricity because they have no geographic limitations and can be placed anywhere on a distribution system. Fuel cells have numerous benefits which make them superior compared to the other technologies. Benefits include high efficiency, high power quality and service reliability, few or no moving parts which leads to low noise, fuel flexibility, modularity and low maintenance.

Fuel cells find application in space shuttles due to their light weight and compact size. They serve as a power source in remote locations where utility transmission lines cannot be reached. Since they have no location limitations, they find application in transportation purposes as in cars, trucks and buses. Lower temperature fuel cells like the PEMFC and PAFC (phosphoric acid fuel cell) are well suited for transportation applications. The higher temperature fuel cells like the SOFC and MCFC produce high grade waste heat which can be used to heat water or air or to provide cooling [6]. Fuel cells can also be used in industrial equipment, off-road utility vehicles, airport ground service equipment and golf carts. Fuel cells for cellular phones, laptop computers, video cameras and portable electronics are on their way to the market. Many hospitals, credit card centers, police stations, and banks are now using fuel cells to provide backup power to their facilities. Some wastewater treatment plants and landfills are using fuel cells to convert the methane gas they produce into electricity. The possibilities are seemingly endless [35].

Though the fuel cell stack is a good source of electric power, it has a major drawback which presents difficulties in connecting to the utility grid or for use in stand-alone applications. Fuel cells have a slow electrochemical and thermodynamic response. The slow response is associated with the time for the fuel cell stack to modify the chemical reaction parameters after a change in the flow of reactants [14]. Hence it can be a good source in the steady state but cannot respond quickly to electrical load transients.

Fuel cells have to be connected to power conditioning devices, which enhance their performance, in order to the connected to the power grid.

Despite the benefits, fuel cells are unable to penetrate the market owing to their high capital cost. Fuel cells need to become more competitive in terms of their capital and the installed cost in order to compete with conventional power facilities. The installed cost in the stationary power market is around $4000 per kilowatt; $1500 per kilowatt would make fuel cells competitive. In the automobile sector, the competitive cost is in the order of $60-$100 per kilowatt. Considerable efforts are being made in specific areas to reduce the capital cost. These specific areas include, material reduction, exploration of low-cost materials, minimizing temperature constraints, increasing power density, streamlining the manufacturing processes, improving fuel flexibility and endurance and reliability [43].

2.2. THE FUEL CELL SYSTEM

A fuel cell is an electrochemical device that converts the chemical energy of the fuel (hydrogen) into electrical energy. It is centered on a chemical reaction between the fuel and the oxidant (generally oxygen) to produce electricity where water and heat are byproducts. This conversion of the fuel into energy takes place without combustion. Generally, efficiency of the fuel cells ranges from 40-60% and can be improved to 80-90% in cogeneration applications. The waste heat produced by the lower temperature cells is undesirable since it cannot be used for any application and thus limits the efficiency of the system. The higher temperature fuel cells have higher efficiency since the heat produced can be used for heating purposes.

2.2.1. Operating Principle. The structure and the functioning of a fuel cell is similar to that of a battery except that the fuel can be continuously fed into the cell. The cell consists of two electrodes, anode (negative electrode) and cathode (positive electrode) separated by an electrolyte. Fuel is fed into the anode where electrochemical oxidation takes place and the oxidant is fed into the cathode where electrochemical reduction takes place to produce electric current and water is the primary product of the cell reaction. Figure 2.1 shows the flows of reactants in a simplified fuel cell.

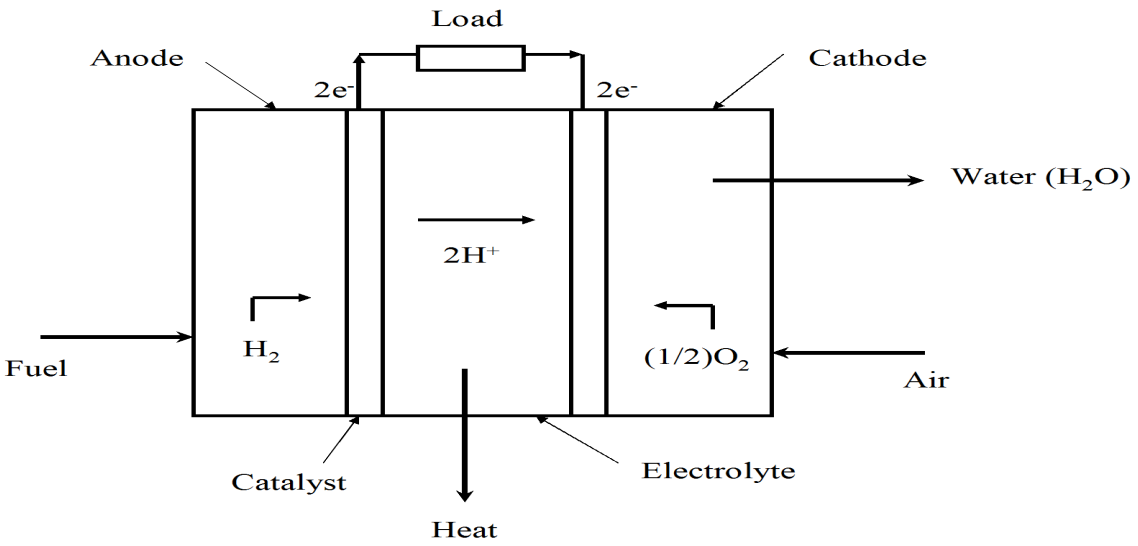

Figure 2.1 Schematic of an individual fuel cell [44]

The hydrogen which enters the anode side is broken into hydrogen ions and electrons with the help of the catalyst. In case of lower temperature cells like the PEMFC and the PAFC, the hydrogen ions move through the electrolyte and the electrons flow through the external circuit. The oxygen which enters through the cathode side combines with these hydrogen ions and electrons to form water as shown in the above figure. As this water is removed, more ions are passed through the electrolyte to continue the reaction which results in further power production. In the SOFC, it is not the hydrogen ions which move through the electrolyte, but the oxygen radicals. In case of MCFC, carbon dioxide combines with the oxygen and electrons to form carbonate ions, which are transmitted through the electrolyte [45]. Fuel cells are classified based on the type of electrolyte used. A solid polymer membrane electrolyte is fitted between two platinum-catalyzed porous electrodes for PEM fuel cells [46]. MCFCs have a liquid lithium-potassium or lithium-sodium based electrolyte while SOFCs employ a solid yittra-stablized zirconia ceramic electrolyte. The catalyst used for SOFC and MCFC are perovsikites and nickel, respectively, the cost of which is comparatively lower than that

used for PEMFC. The typical anode and cathode reactions for a hydrogen fuel cell are given by Equations (1) and (2), respectively.

$$H_2 \rightarrow 2H^+ + 2e^- \tag{1}$$

$$\frac{1}{2}O_2 + 2H^+ + 2e^- \rightarrow H_2O \tag{2}$$

An individual fuel cell produces less than a volt of electric potential. A large number of cells are stacked on top of each other and connected in series (with bipolar connects) to produce higher voltages. Figure 2.2 shows cell stacks which consists of repeating units, each comprising an anode, cathode, electrolyte and a bipolar separator plate. The number of cells depends on the desired power output.

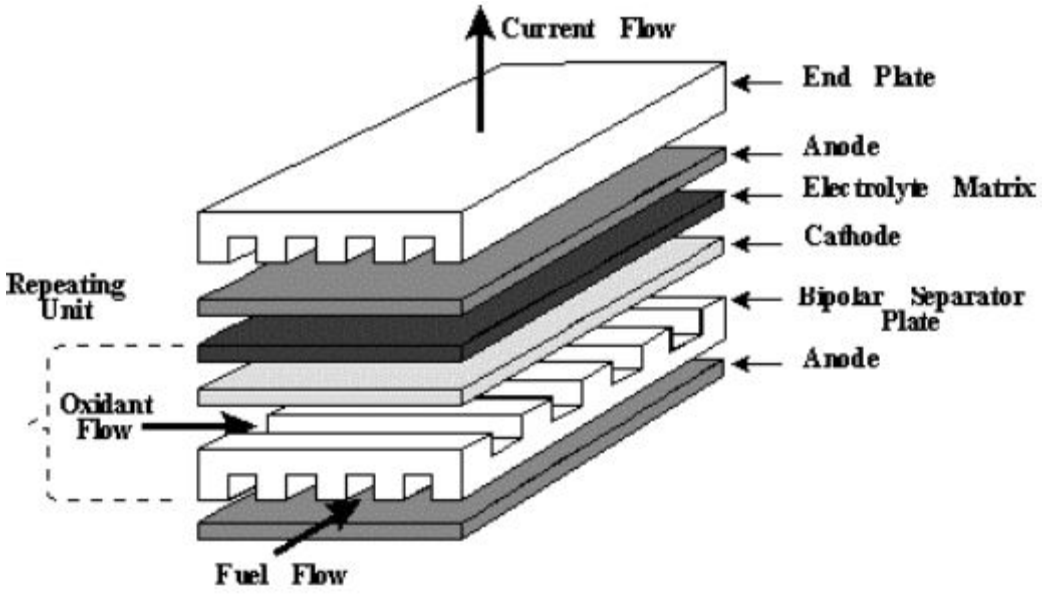

Figure 2.2 Components of a fuel cell stack [46]

2.2.2. Fuel Cell Voltage and Nernst Equation. The chemical energy of the fuel cell is defined by enthalpy of formation and Gibbs free energy. Gibbs free energy is the energy available to do external work which involves moving electrons around an external circuit. Enthalpy of formation is the sum of Gibbs free energy and the energy connected with entropy. In fuel cells, change in Gibbs free energy of formation (ΔG_f) is considered, as this change is responsible for the energy released. This change is the difference between the free energy of the products and the reactants, as shown in Equation (3) [47].

$$\Delta G_f = G_f \text{ products} - G_f \text{ reactants} \tag{3}$$

These quantities can be expressed in their 'per mole' form to make the comparisons easier. They are indicated by ¯ over the lower case letter ($\overline{g_f}$) which is given by Equation (4) [47].

$$\Delta \overline{g_f} = \overline{g_f} \text{ products} - \overline{g_f} \text{ reactants} \tag{4}$$

For the hydrogen fuel cell, two electrons pass through the external circuit for each water molecule produced and each molecule of hydrogen used, as given in Equation (1). In a lossless system, electrical work done is equal to the change in Gibbs free energy. Further, electrical work done to move a charge of *2F* (to move two electrons) for a voltage of *E* is given by Equation (5) [47].

$$\text{Electrical work done} = -2FE \text{ joules} \tag{5}$$

Therefore *E* can be written as shown in Equation (6). This voltage is the open circuit voltage of the fuel cell [47].

$$E = -\frac{\Delta \overline{g_f}}{2F} \tag{6}$$

Consider a general reaction given as $jJ + kK \rightarrow mM$ where j moles of J and k moles of K react with each other to produce m moles of M. These reactants and products have an activity (a) associated with them. This activity is the ratio of the partial pressure of the gas and the standard pressure. Hence Gibbs free energy can be written as shown in the Equation (7) [47]. $\Delta\overline{g_f}^o$ is the change in the Gibbs free energy of formation at standard pressure.

$$\Delta\overline{g_f} = \Delta\overline{g_f}^o - RT\ln\left(\frac{a_J{}^j . a_K{}^k}{a_M{}^m}\right) \tag{7}$$

Equation (7) can be applied to a typical hydrogen fuel cell reaction, where the reactants are hydrogen and oxygen and the product is water. Since activity is the pressure of the gas to its standard pressure, activity can be replaced by pressure in Equation (7). Further, the standard pressure is considered to be unity. Hence, Equations (6) and (7) can be combined together to obtain an equation for voltage as shown in Equation (8), also known as the Nernst equation [47].

$$E = -\frac{\Delta\overline{g_f}^o}{2F} + \frac{RT}{2F}\ln\left(\frac{p_{H2} \cdot p_{O2}{}^{\frac{1}{2}}}{p_{H2O}}\right) \tag{8}$$

2.2.3. Types of Fuel Cells. Fuel cells are classified according to the type of electrolyte used. There are various fuel cell types at different stages of development. The various types of fuel cells in the increasing order of their operating temperature are:

- Proton exchange membrane fuel cell (PEMFC-175^o F)
- Phosphoric acid fuel cell (PAFC-400^o F)
- Molten carbonate fuel cell (MCFC-1250^o F)
- Solid oxide fuel cell (SOFC-1800^o F)

Each of these fuel cell types differ in the electrolyte and fuel used, operating temperature and pressure, construction materials, power density and efficiency. Table 2.1 gives a basic summary of the characteristics and requirements of the fuel cell types mentioned above.

The most important component of a fuel cell is the fuel processor and the reformer since hydrogen is not readily available. Fossil fuels such as gasoline, natural gas and coal gases need to be processed and reformed to obtain enriched hydrogen. Natural gas is the most easily available fuel source. Bio-fuels can also be used as a source to obtain hydrogen. Biological methods such as photosynthesis and fermentation can be used to produce hydrogen. Though there are different methods to produce hydrogen, a proper and feasible method which can be commercialized is not yet available.

Storage of hydrogen is an important aspect of the fuel cell systems because the fuel has to be readily available for continuous supply of electric power. Sometimes, electrical energy is used to divide water into hydrogen and oxygen with the help of electrolysers during times of high supply and low demand. Fuel cells have to be compact and portable for mobile applications; hence storage of hydrogen is essential for such applications. Hydrogen needs to be handled with great care because it is a highly volatile and flammable gas. It has a high leak rate due to which the gas tends to escape through small orifices, faster than the other gases. Hence storage of hydrogen plays a key role in the fuel cell systems. Hydrogen can be stored as a compressed gas in pressurized cylinders and is the most common method of storage. This method is simple, indefinite storage time and there are no purity limits on the gas. It is used in places where demand for hydrogen is variable and not high. The next method of storage is as a cryogenic liquid at a temperature of 22K. This method is used for storing large quantities of hydrogen. Storing hydrogen at low temperatures is not a preferred method due to the safety problems associated with it. Frostbite is a major concern for this method of storage. Hydrogen can also be stored as a metal hydride. This method basically consists of a reversible reaction between a metal and hydrogen. Hydrogen is supplied to the metal alloy at slightly above atmospheric pressure to form the metal hydride. The reaction is mildly exothermic and normal air cooling would be sufficient for the reaction. Once the metal has reacted with hydrogen, it is stored in a vessel and sealed. Since the reaction is

reversible, hydrogen can be obtained from the hydride whenever required. Though this method is safe it can be used only for storing small quantities of hydrogen. The specific energy is poor where large quantities have to be used and further, high purity hydrogen should be used in order to prevent metal contamination. None of these methods have a satisfactory performance. Other methods are being developed which rely on the use of chemical 'hydrogen carriers' [47]. Chemicals such as methanol, ammonia, ethanol, hydrazine and hydrides such as sodium, calcium, aluminium and potassium hydrides can be used as potential hydrogen storage materials. These methods are preferred because the manufacturing process is simple, costs are lower for carrying out the reactions and they are safe to handle.

A fuel processor converts the primary fuel source (hydrocarbons) into the fuel gas (hydrogen) required by the fuel cell stack. The processor uses a catalytic reaction to break the fuel into hydrogen and separate it from the carbon based gases. Each of the fuel cell types has specific fuel requirements. Natural gas and petroleum liquids contain sulphur compounds and have to be desulphurized before they can be used as a fuel. The anode catalysts are intolerant of sulphur and it must be removed before it degrades catalyst performance. There is a risk of carbon formation in fuel cell systems which can be reduced by carrying out pre-reforming of the fuel gas before it is fed to the reformer reactor. Carbon monoxide can be used as a fuel for SOFC and MCFC because it can be internally converted to hydrogen whereas the PEMFC should be completely free from it. Carbon monoxide has high affinity for anode catalyst (especially platinum) and it prevents the flow of fuel in the PEMFC. Ammonia is a poison for all the fuel cell types due to its adverse effects on the cell life except for SOFC, where it can be internally reformed.

Lower-temperature fuel cells require an external reformer to obtain the hydrogen rich fuel, thus increasing the cost and thereby reducing the efficiency. Higher temperature fuel cells do not require an external reformer; its high temperature allows direct conversion of natural gas to hydrogen. High temperature requires stringent materials which increases the cost of the fuel cells. Hence, researchers are working to combine the benefits of the PEMFC and the PAFC to obtain intermediate temperature cells, often referred to as high temperature PEM.

Table 2.1 Summary of characteristics of fuel cell types [1] [35] [46]

Criteria	PEMFC	PAFC	MCFC	SOFC
Operating Temperature	< 210^{o} F	~ 400^{o} F	~ 1250^{o} F	~ 1800^{o} F
Operating Pressure	1-5 atm	1-8 atm	1-3 atm	1-13 atm
Size Range	3-250 kW	100-200 kW	250Kw-10 MW	1kW-10 MW
Efficiency	35-40%	35-40%	50-55%	45-50%
Fuel	H_2	H_2	H_2, CO, CH_4	H_2,CO,CH_4, NH_3
Poison	CO,NH_3,Cl_2,S_2	CO,NH_3,Cl_2,S_2	Cl_2, S_2	S_2
Charge Carrier	H^+	H^+	CO_3^{2-}	O^{2-}
Construction Material	Graphite carbon	Graphite carbon	Ni and stainless steel	Ceramics and Metals
Cooling Medium	Water	Boiling water	Excess air	Excess air

2.3. SOLID OXIDE FUEL CELL (SOFC)

The SOFC is a high-temperature operating fuel cell which has high potential in stationary applications. The efficiency of SOFC is in the range of 45-50% and when integrated with a gas turbine, it reaches a high efficiency of 70-75%. It is a solid-state device that uses an oxide ion-conducting non-porous ceramic material as an electrolyte. Since the electrolyte is a solid, the cells do not have to be constructed in the plate-like configuration typical of other fuel cell types. Corrosion is less compared to MCFC and no water management problems as in PEMFCs due to the solid electrolyte. High-temperature operation removes the need for a precious-metal catalyst, thereby reducing the cost. It also allows SOFCs to reform fuels internally, which enables the use of a variety of fuels and reduces the cost associated with adding a reformer to the system.

Two different geometries which are being developed are tubular and planar. Tubular designs are more costly and advanced compared to the planar designs and is closer to commercialization.

The electrolyte used is a ceramic oxide (yttria stabilized zirconia). The anode used is nickel-zirconia cermet and the cathode is a strontium doped lanthanum manganite. The use of ceramic materials increases the cost of SOFCs. High operating temperature requires stringent materials to be used which further drives up the cost. Research is being carried out to reduce the operating temperature and use less stringent materials. Reduction of temperature improves the starting time, cheaper materials can be used, durability and robustness can be increased. Intermediate-temperature SOFCs cannot be used for all applications. Higher temperature is required for fuel cell micro-turbine hybrid systems. However, for smaller systems intermediate temperature SOFCs would be ideal.

Since SOFCs have fuel-flexibility, the input to the anode can be hydrogen, carbon monoxide or methane. Hydrogen or carbon monoxide may enter the anode. At the cathode, electrochemical reduction takes place to obtain oxide ions. These ions pass through the electrolyte layer to the anode where hydrogen is oxidized to obtain water. In case of carbon monoxide, it is oxidized to carbon dioxide. The cathode, anode and cell reactions are shown in Equations (8), (9) and (10) [5].

$$O_2 + 4e^- \rightarrow 2O^{2-} \tag{8}$$

$$\left.\begin{aligned} H_2 + O^{2-} &\rightarrow H_2O + 2e^- \\ CO + O^{2-} &\rightarrow CO_2 + 2e^- \end{aligned}\right\} \text{ Anode reactions} \tag{9}$$

$$H_2 + O_2 + CO \rightarrow H_2O + CO_2 \tag{10}$$

Hydrogen is the fuel that has been used in this analysis. Operating voltage (V_{fc}) of the fuel cell at a current I is obtained by applying the Nernst's equation and taking the losses into account is shown in Equation (11) [47].

$$V_{fc} = E - V_{act} - V_{conc} - rI \tag{11}$$

E is given by the Equation12.

$$E = N(E^o + \frac{RT}{2F}\ln\left(\frac{pH_2.pO_2^{\frac{1}{2}}}{pH_2O}\right) \tag{12}$$

E – Reversible open circuit voltage (V)

E^o – Standard reversible cell potential (V)

p_i – Partial pressure of species i (Pa)

V_{act} – Drop due to activation loss (V)

V_{conc} – Drop due to concentration loss (V)

r – Internal resistance of stack (Ω)

I – Stack current (A)

N – Number of cells in stack

R – Universal gas constant (J/ mol K)

T – Stack temperature (K)

F – Faraday's constant (C/mol)

Typical values for the above parameters are shown in Table A.1 of the Appendix. Activation loss is due to the slow rate of the electrochemical reaction between the fuel and the oxidant. A part of the voltage generated is lost in initiating the electrochemical reaction. Concentration loss results from the change in concentration of the reactants at the surface of the electrodes as the fuel is used. When the reactants are being consumed at the respective electrode, there will be a slight reduction in the concentrations. This change in concentrations leads to a drop in the partial pressures which results in a reduction in the voltage [47]. In this analysis, a reduced model of the fuel cell has been taken into account, neglecting the activation and concentration losses as well as the double charging effect. The loss due to internal resistance of the stack is basically due to the resistance to the flow of ions in the electrolyte as well as the material of the electrode.

In general, it is mainly caused by the electrolyte. Figure 2.3 shows the typical volt-amp characteristics of SOFC. Fuel cells have drooping voltage characteristics: an increase in the load current causes a decrease in the stack voltage. The number of cells is taken to be 384 and the standard cell potential is 1.18V (from reference [14]). Hence the open circuit voltage (OCV) is 453V which decreases as the load current increases as seen in Figure 2.3. The drop is fairly linear in the middle region, known as region of ohmic polarization This is the operating region for the fuel cell. The voltage varies rapidly at lower and higher currents.

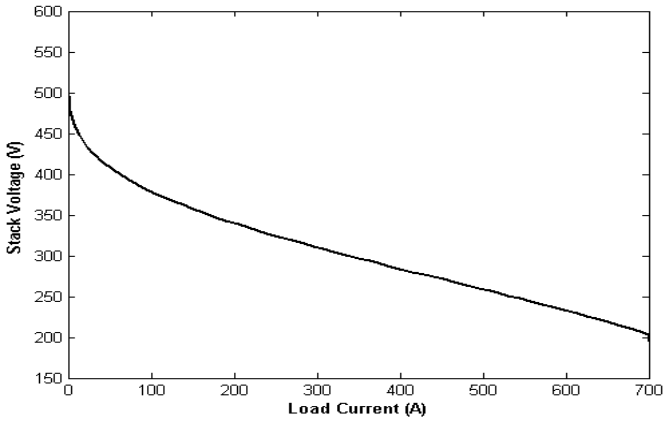

Figure 2.3 Volt-amp characteristics of SOFC

Partial pressure of hydrogen, oxygen and water are given in Equations (13), (14) and (15). The slow dynamics of the fuel cell current is represented by Equation (16) [15].

$$pH_2 = \left(\frac{\frac{1}{KH_2}}{1+\tau_{H2}s} \right)(qH_2 - 2K_r I) \tag{13}$$

$$pO_2 = \left(\frac{\frac{1}{KO_2}}{1 + \tau_{O2} s} \right) (qO_2 - K_r I) \tag{14}$$

$$pH_2O = \left(\frac{\frac{1}{KH_2O}}{1 + \tau_{H2O} s} \right) (2K_r I) \tag{15}$$

$$I = \left(\frac{I_{ref}}{1 + \tau_e s} \right) \tag{16}$$

I_{ref} is the reference current which is given by Equation (17). Fuel and oxygen flow are given by Equations (18) and (19) [15].

$$I_{ref} = \left(\frac{P_{ref}}{V_{fc}} \right) \tag{17}$$

$$qH_2 = \frac{2K_r}{U_{opt}} \left(\frac{1}{1 + \tau_f s} \right) \tag{18}$$

$$qO_2 = \frac{qH_2}{r_{HO}} \tag{19}$$

Fuel utilization is the ratio between the fuel flow that reacts and the input fuel flow given by Equation (20) [14]. Fuel utilization in the range of 80-90% is generally used. The fuel flow that reacts is given by Equation (21) [14].

$$U_f = \frac{qH_2{}^r}{qH_2} \tag{20}$$

$$qH_2{}^r = 2K_r I \tag{21}$$

The fuel cell current is restricted by the minimum and maximum fuel utilization and the fuel flow, given by Equation (22) [14].

$$\frac{0.8qH_2}{2K_r} \le I \le \frac{0.9qH_2}{2K_r} \tag{22}$$

qH_2 – Fuel flow (mol/s)

qO_2 – Oxygen flow (mol/s)

KH_2 – Valve molar constant for hydrogen (kmol/s atm)

KO_2 – Valve molar constant for oxygen (kmol/s atm)

KH_2O – Valve molar constant for water (kmol/s atm)

τ_{H2} – Response time for hydrogen (s)

τ_{O2} – Response time for oxygen (s)

τ_{H2O} – Response time for water (s)

τ_e – Electrical response time (s)

τ_f – Fuel response time (s)

U_{opt} – Optimum fuel utilization

r_{HO} – Ratio of hydrogen to oxygen

K_r – Constant (kmol/s A)

P_{ref} – Reference power (kW)

Typical values for all relevant parameters are given in Table A.1 of the Appendix. The block diagram representation of the SOFC dynamic model is shown in the Figure 2.4.

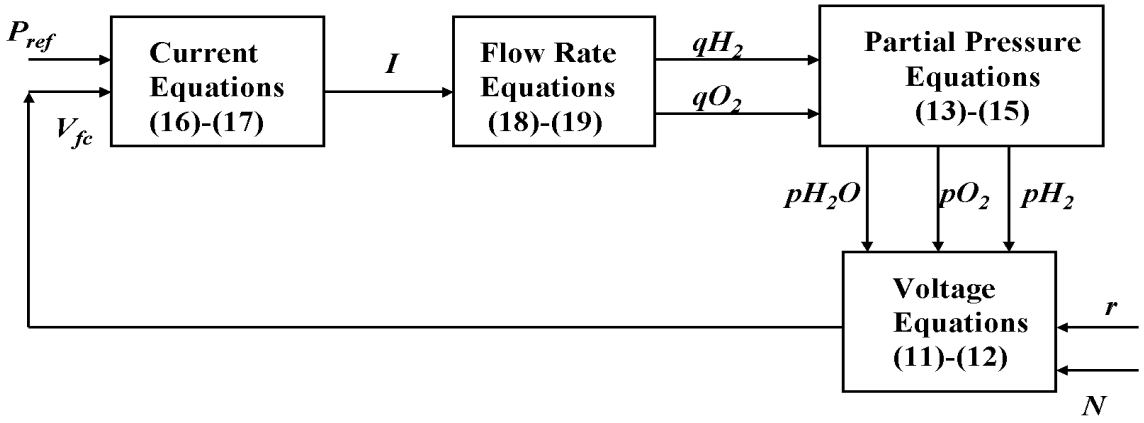

Figure 2.4 Block diagram for dynamic model of SOFC

3. POWER CONDITIONING UNIT

3.1. DC-DC CONVERTER

The DC input from the fuel cells is unregulated. The switch-mode DC-DC converter converts the unregulated DC input into regulated and controlled DC output at a desired voltage level [22]. The output voltage level can be lower, higher or even negative lower or higher compared to the input voltage. The drawback associated with these converters is the noise that they generate at higher frequencies which must be filtered out. These devices can be non-isolated or isolated. Isolated DC-DC converters maintain electrical isolation between the input and the output with the help of an electrical isolation transformer. Various non-isolated and isolated converter topologies presented in [18] are:

- Non-isolated DC-DC converters: Buck, Boost and Buck-Boost converters
- Isolated DC-DC converters: H-bridge, series resonant H-bridge and push-pull converters

Due to its slow response, a fuel cell stack cannot be directly connected to the load. Further, the voltage generated by the stack is low. This voltage must be boosted to a higher level in order to invert this dc voltage into ac voltage for grid interconnection. Hence a boost or buck-boost converter is required to be connected between the fuel cell and the inverter. Figure 3.1 shows the circuit diagram of the non-isolated buck-boost converter. The parameters used for the buck-boost DC-DC converter are given in Table A.2 of the Appendix.

A buck-boost converter is preferred over the boost converter topology due to a higher range of input voltage control and smoother output voltage. These converters can have lower or higher output voltage based on the duty cycle. If the duty cycle is less than 0.5, it operates like a buck converter otherwise it operates like a boost converter. A buck-boost converter can be obtained by the cascade connection of the buck and the boost converter.

Design of the buck-boost converter involves determination of the inductance L and the capacitance C. R is the equivalent load resistance and L_f is the filter inductance in

series with the load resistance to smoothen the output current and provides energy during the slow operation of the fuel cell. L and C can be obtained by Equations (1) and (2), respectively [22].

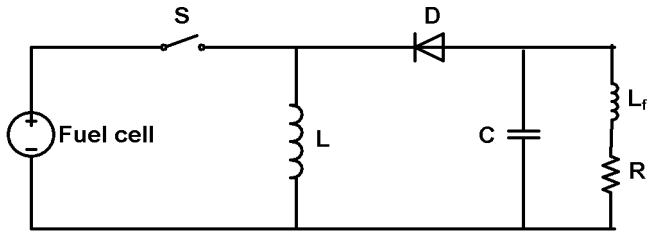

Figure 3.1 Non-isolated DC-DC buck-boost converter [22]

$$L > \frac{(1-D)^2 R}{2f} \tag{1}$$

$$C > \frac{D}{Rf\left(\frac{\Delta V}{V_o}\right)} \tag{2}$$

Where D is the duty cycle, f is the switching frequency and $\left(\frac{\Delta V}{V_o}\right)$ is the voltage ripple. Figure 3.2 shows the block diagram model of the buck-boost converter connected to the fuel cell system with the feedback control system. The input to the converter is the fuel cell voltage (V_{fc}). The output voltage of the converter (V_o) is compared with the reference output voltage (V_{oref}). The error signal is compensated to obtain the control voltage (V_c). This control voltage is used to adjust the duty cycle (d) of the switch in the

converter. The output voltage has to be regulated to be within a specified tolerance band in response to changes in the output load and the input voltage.

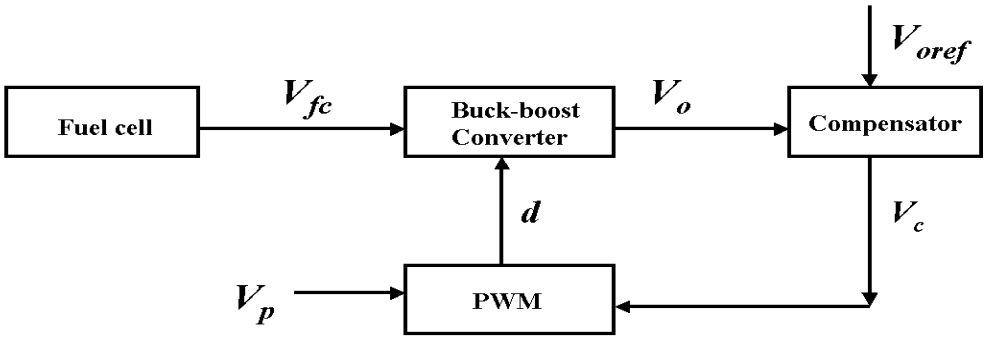

Figure 3.2 Fuel cell-converter system

Small signal transfer functions can be obtained by using small perturbations in output voltage and the duty cycle around their steady-state dc operating values V_o and D. Figure 3.3 shows the linearized feedback control system for any DC converter.

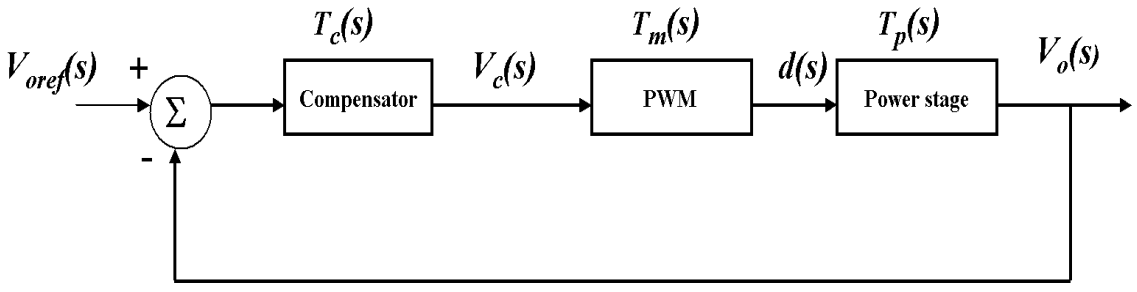

Figure 3.3 Linearized feedback control system for the converter [22]

The power stage, compensator and PWM transfer functions are given by Equation (3), (4) and (5), respectively.

$$T_p(s) = \left(\frac{V_{in}(R(1-D)^2 - DLs)}{(1-D)^2} \right) \left(\frac{1}{LCRs^2 + Ls + R(1-D)^2} \right) \tag{3}$$

$$T_c(s) = \frac{1}{R_1 C_2} \frac{(s+\omega_z)}{s(s+\omega_p)} \tag{4}$$

$$T_m(s) = \left(\frac{1}{V_p} \right) \tag{5}$$

Where V_{in} and D are the steady-state dc values of the input voltage (here it is fuel cell voltage) and the duty cycle, V_p is the amplitude of the carrier signal, R_1 and C_2 are parameters in the compensator and ω_z is the zero and ω_p is the pole in the transfer function. These equations are used to design a suitable compensator for the buck-boost converter. The detailed design procedure is given in reference [22]. The zero and pole are given by Equations (6) and (7), respectively.

$$\omega_z = \frac{1}{R_2 C_1} \tag{6}$$

$$\omega_p = \frac{1}{R_2 C_2} \tag{7}$$

Figure 3.4 shows the analog representation of the error amplifier (compensator), where R_1, R_2, C_1 and C_2 are the parameters of the compensator. Inputs to the amplifier are the output voltage (V_o) and the reference voltage (V_{oref}) and the output is the control voltage (V_c).

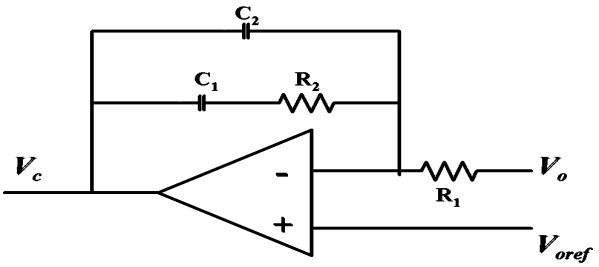

Figure 3.4 Error amplifier [22]

3.2. DC-AC INVERTER

A three phase six-switch PWM VSI is used to convert the power available at the DC bus to AC power. The SOFC-DC converter system is connected to the utility grid through a DC-AC inverter. The transistor switching signals for the inverter are obtained from the real and the reactive power control system. Figure 3.5 shows the three-phase DC-AC voltage source inverter connected to the infinite source (utility grid) through a transformer and a coupling reactance.

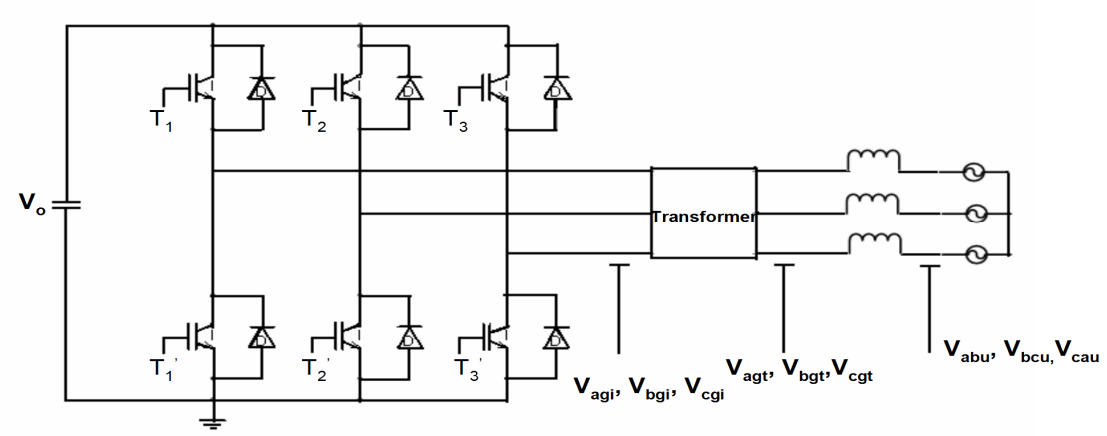

Figure 3.5 Three phase six-switch inverter connected to the grid through a transformer

V_o: DC voltage from the DC-DC converter

T_1-T_3: Transistor (switching) signals

V_{agi}, V_{bgi}, V_{cgi}: Line to ground voltages on the inverter side

V_{agt}, V_{bgt}, V_{cgt}: Line to ground voltages on the transformer side

V_{abu}, V_{bcu}, V_{cau}: Line to line voltages on the utility side

The control scheme proposed in this thesis is the decoupled PQ control. This controller controls the phase angle and amplitude of the voltage across the transformer. The difference in the phase angle between the voltage across the transformer and the utility side voltage determines the direction of the real and reactive power flow. Since the phase angle on the utility side is zero, phase angle of the voltage across the transformer determines the direction of the power flow. This control is basically a real power control since the reactive power is assumed to be zero. Figure 3.6 shows the block diagram of the overall inverter control system.

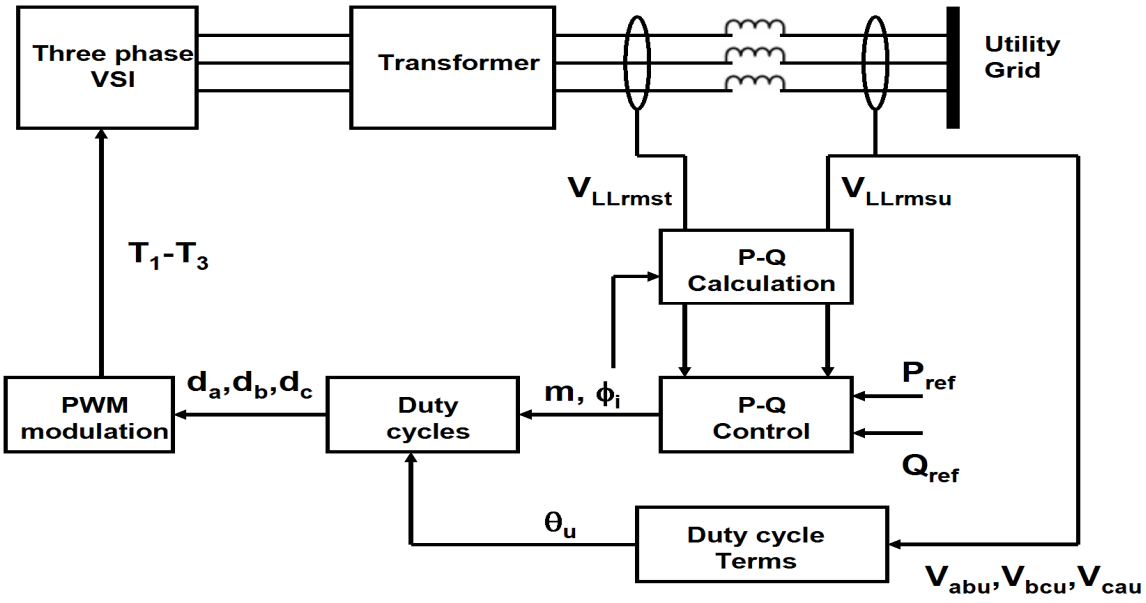

Figure 3.6 Block diagram of the overall control system of the inverter

The figure consists of various sub blocks to be dealt with, apart from the P-Q controller. The line-line voltage across the transformer and the utility side are measured from the system to calculate the real and reactive power flow. The P-Q controller compares the actual values with the reference real and reactive powers to obtain the phase angle of the transformer voltage and the modulation index, respectively. These control variables are used to determine the duty cycle control signals which when compared with the triangular wave, produce the switching signals for the inverter.

3.2.1. P-Q Control. This subsection consists of the real and reactive power calculation and the decoupled P and Q controller. The line-line voltage on the utility side (V_{LLrmsu}) and the transformer (V_{LLrmst}) are measured from the system. The real and reactive power flows are given by Equations (8) and (9), respectively.

$$P = \frac{V_{LLrmst} V_{LLrmsu} \sin(\phi_i)}{\omega L_t} \tag{8}$$

$$Q = V_{LLrmst} \left(\frac{V_{LLrmst} - V_{LLrmsu} \cos(\phi_i)}{\omega L_t} \right) \tag{9}$$

Where ϕ_i is the phase angle of the voltage on the inverter side and L_t is the leakage inductance of the transformer. For calculation purposes, the transformer is considered to be ideal; hence the angle lag due to Y-Δ connection is neglected.

The P-Q controller basically consists of PI controllers to control the phase angle and the modulation index. The main requirement for the inverter switching signals is the phase angle and amplitude of the inverter voltage. Figure 3.7 shows the real and reactive power control system. The real power flow is given by Equation (8). The voltages and the reactance terms are more or less constant. The real power is directly proportional to the phase angle if the angle is small. Hence the real power flow can be used to control the phase angle of the inverter. Reactive power flow controls the amplitude of the transformer voltage. The error between the reference and the measured real power is fed into a PI controller to control the phase angle of the inverter as shown in the figure below. The inverter voltage is used to determine the amplitude of the modulation signals. The

voltage, in turn, depends on the reactive power. The error between the reference and the measured reactive power is fed into the PI controller. The output of the controller is summed with the term $V_{LLrmst}\cos(\phi_i)$ based on Equation (9) to obtain the voltage on the transformer side. The control of the transformer voltage is proportional to the control of the inverter voltage.

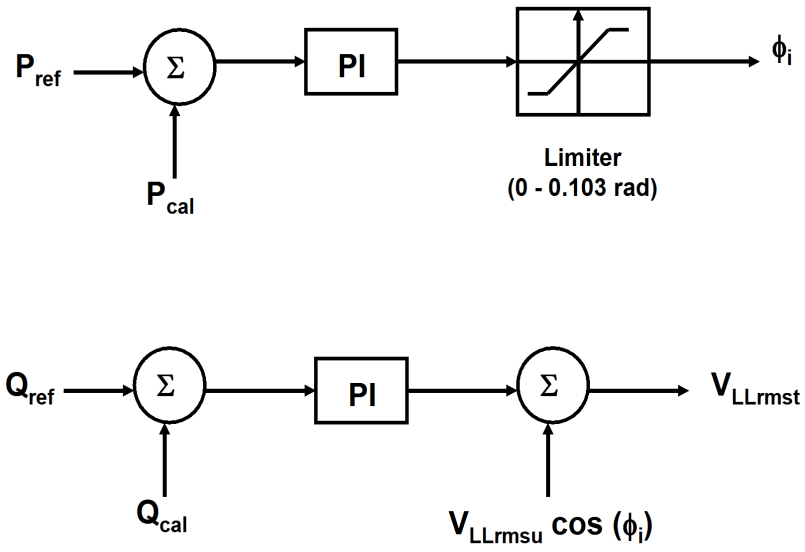

Figure 3.7 Real and reactive power control system

The modulation index is given by Equation (10). K_t is the turns ratio in this Equation.

$$m = V_{LLrmst}\sqrt{\frac{2}{3}}\frac{2}{V_o}\frac{1}{K_t} \tag{10}$$

3.2.2. Duty Cycle Signals. The duty cycle control signals depend on the phase angle and the modulation index of the inverter voltage and the phase angle on the utility side. The control signals are given by Equation (11) [48]. These control signals are compared with the triangular wave (of switching frequency 1000 Hz) to determine the switching signals for the inverter.

$$d_a = \frac{1}{2}\left(1 + m\cos(\theta_u + \phi_i) - \frac{m}{6}\cos(3\theta_u + 3\phi_i)\right)$$

$$d_b = \frac{1}{2}\left(1 + m\cos(\theta_u + \phi_i - 2\frac{\pi}{3}) - \frac{m}{6}\cos(3\theta_u + 3\phi_i)\right) \tag{11}$$

$$d_c = \frac{1}{2}\left(1 + m\cos(\theta_u + \phi_i + 2\frac{\pi}{3}) - \frac{m}{6}\cos(3\theta_u + 3\phi_i)\right)$$

The phase angle (ϕ_i) and modulation index (m) are obtained from the P-Q control explained in the subsection 3.2.1. The trigonometric terms expressed in terms of θ_u can be determined using the line-line voltages on the utility side. These voltages are measured from the system and can be expressed in equation form as given by Equation (12).

$$V_{abu} = \sqrt{3}V_u \cos\left(\theta_u + \frac{\pi}{6}\right)$$

$$V_{bcu} = -\sqrt{3}V_u \cos(\theta_u - \frac{\pi}{2}) \tag{12}$$

$$V_{cau} = -\sqrt{3}V_u \cos\left(\theta_u - \frac{\pi}{6}\right)$$

Where V_u is the peak value of the line-neutral voltage and θ_u is the utility side phase angle. This peak value can be determined using the line-line voltages, given by Equation (13). The line-line voltages are measured from the system and V_u is calculated

using Equation (13). Equation (14) is used to determine the other terms required in calculating the duty cycle signals.

$$V_u = \frac{2}{3}\sqrt{V_{abu}{}^2 + V_{bcu}{}^2 + V_{abu}V_{bcu}} \tag{13}$$

Equation (12) can be re-written as:

$$\cos\left(\theta_u + \frac{\pi}{6}\right) = \frac{V_{abu}}{\sqrt{3}V_u}$$

$$\cos(\theta_u - \frac{\pi}{2}) = \frac{-V_{bcu}}{\sqrt{3}V_u} \tag{14}$$

$$\cos\left(\theta_u - \frac{\pi}{6}\right) = \frac{-V_{cau}}{\sqrt{3}V_u}$$

4. IMPLEMENTATION AND SIMULATION RESULTS

4.1. SYSTEM MODELING

The fuel cell stack is connected to the DC-DC converter to boost the DC voltage to connect it to the utility grid via the DC-AC inverter. The fuel cell, DC-DC converter and DC-AC inverter are modeled in PSCAD 4.1.1 [42]. Figure 4.1 shows the block diagram representation of the fuel cell system connected to the utility grid through the transformer and the coupling reactance. The electrical data is given in Appendix A.3.

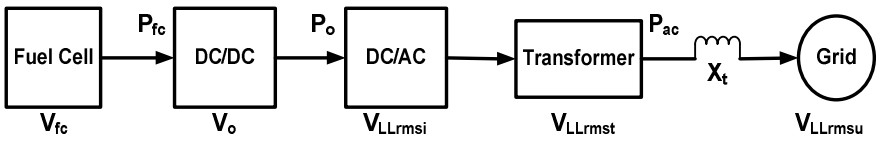

Figure 4.1 Fuel cell system [31]

Where,

V_{fc}: Fuel cell stack voltage (V)

V_o: Output voltage of DC-DC converter (V)

V_{LLrmsi}: Output voltage of the three phase inverter (V)

V_{LLrmst}: Voltage across the transformer (kV)

X_t: Leakage reactance of the transformer (Ω)

V_{LLrmsu}: Utility grid voltage (kV)

P_{fc}: Fuel cell stack power (kW)

P_o: Output power of the DC-DC converter (kW)

P_{ac}: Real power injection into the grid (kW)

The following assumptions have been made in this system:

- The three phase transformer has been considered to be ideal. The voltage across the transformer is modeled as turns ratio (K_t) times the voltage on the inverter side and the leakage reactance in series with it [31].
- Reactive power is assumed to be zero (Q).
- Switching losses of the inverter are neglected.

The following constraints have been made for simulating the fuel cell power system:

- The Line-line rms voltage across the inverter constraint is given by Inequality (1). The relationship between the inverter and the transformer voltage is expressed by Equation (2).

$$V_{LLrmsi} \le \frac{V_o}{\sqrt{2}} \qquad \text{i.e.,} \quad V_{LLrmsi} \le 424.26\,\text{V} \tag{1}$$

$$V_{LLrmst} = K_t V_{LLrmsi} \tag{2}$$

Line-line rms voltage across the transformer constraint is given by Inequality (3).

$$V_{LLrmst} \le 30.5(424.26) \qquad \text{i.e.,} \quad V_{LLrmst} \le 12.94\,\text{kV} \tag{3}$$

- The maximum fuel cell stack power is limited to 400 kW and it loses stability for any reference power beyond this limit. Higher reference power can be commanded by either increasing the number of cells, increasing the standard potential or by decreasing the internal resistance of the fuel cell. The simulations corresponding to the breakdown of the fuel cell can be seen in the results section (Figure 4.15). The maximum stack power is given by Inequality (4).

$$P_{fc\max} \le 400\ \text{kW} \tag{4}$$

- When the reactive power is considered to be zero, the power flow equation (Equation 9 in section 3.2.1.) is reduced to Equation (5).

$$V_{LLrmst} = V_{LLrmsu}\cos(\phi_i) \tag{5}$$

- The phase angle is limited to 30^o (0.523 radians) in order to provide linear power control [32]. The maximum limit on the real power injection (400kW) limits the phase angle to 5.9^o (0.103 radians). The limitation on the phase angle is given by Inequality (6) and the transformer voltage constraint due to zero reactive power injection is given by Inequality (7).

$$0 < \phi_i \leq 0.103\,\text{rad} \tag{6}$$

$$12.43 \leq V_{LLrmst} < 12.5\,\text{kV} \tag{7}$$

- The third harmonic injection increases the range of modulation index. Without the injection, the range is between 0 and 1. With the injection, the range is given by Inequality (8). The zero reactive power and the transformer voltage constraint gives rise to the modulation index constraint given by Inequality (9).

$$0 < m < 1.15 \tag{8}$$

$$1.109 \leq m < 1.115 \tag{9}$$

4.1.1. SOFC Model. The dynamic model of the SOFC is based on Figure 2.4. The ac real power injection into the utility grid is considered to be the reference power for the fuel cell. The stack voltage and the reference power are used to determine the reference current which in turn is used to determine the fuel cell stack current. The fuel flow is proportional to the stack current. The partial pressure of hydrogen, oxygen and water are determined using the flow rates of hydrogen and oxygen. The stack voltage is

based on the Nernst Equation which depends on the stack current and the partial pressures of the gases. Figure 4.2 shows the mathematical dynamic model of SOFC.

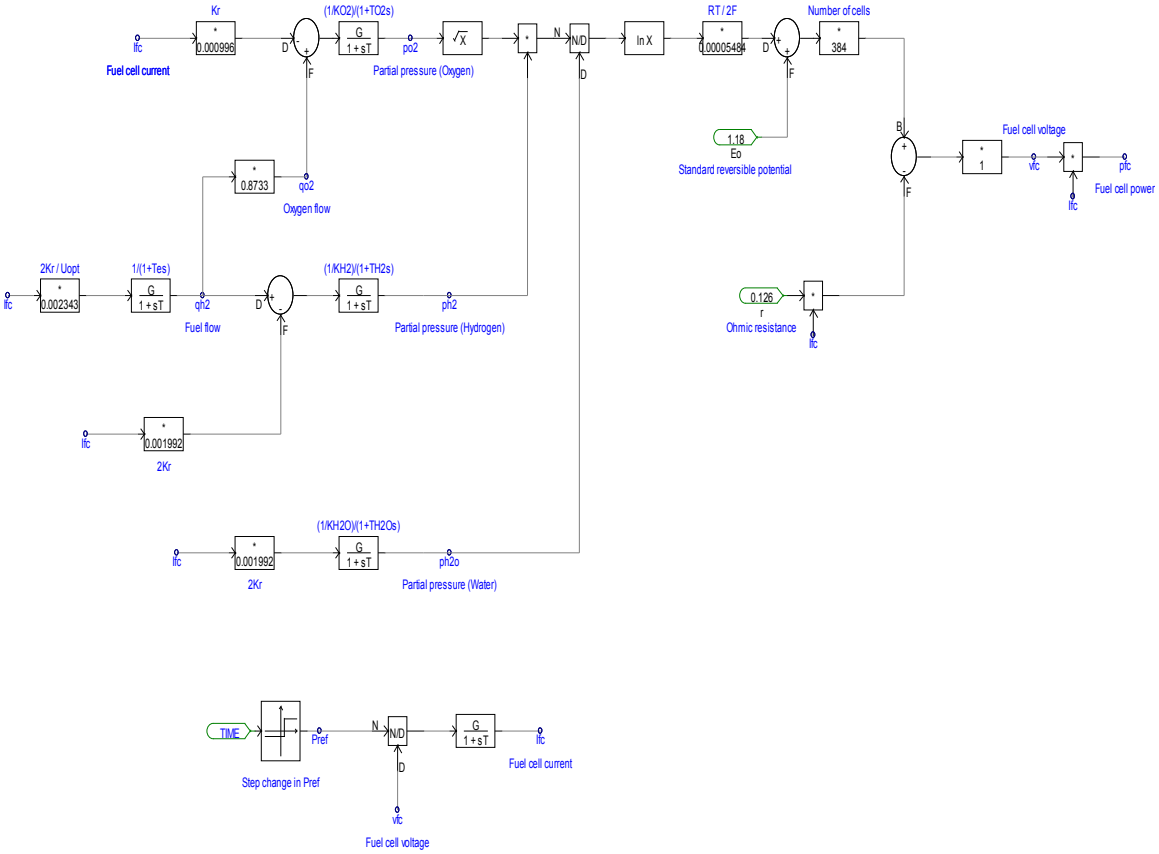

Figure 4.2 Dynamic model of SOFC in PSCAD

4.1.2. DC-DC Converter Model. The input to the converter is the fuel cell stack voltage. A step change in the equivalent load resistance is considered. The higher the value of capacitance, the smoother the output voltage. A filter inductor connected in series with the load resistance causes the output current to be smooth. Figure 4.3 shows

the dynamic model of the DC-DC buck-boost converter. Figure 4.4 shows the feedback control system of the duty cycle.

The switching signal to the GTO is given by the closed loop feedback control system. The error signal is fed into the compensator to obtain the control voltage. This voltage is compared with the PWM (triangular wave) signal to obtain the required gating signal.

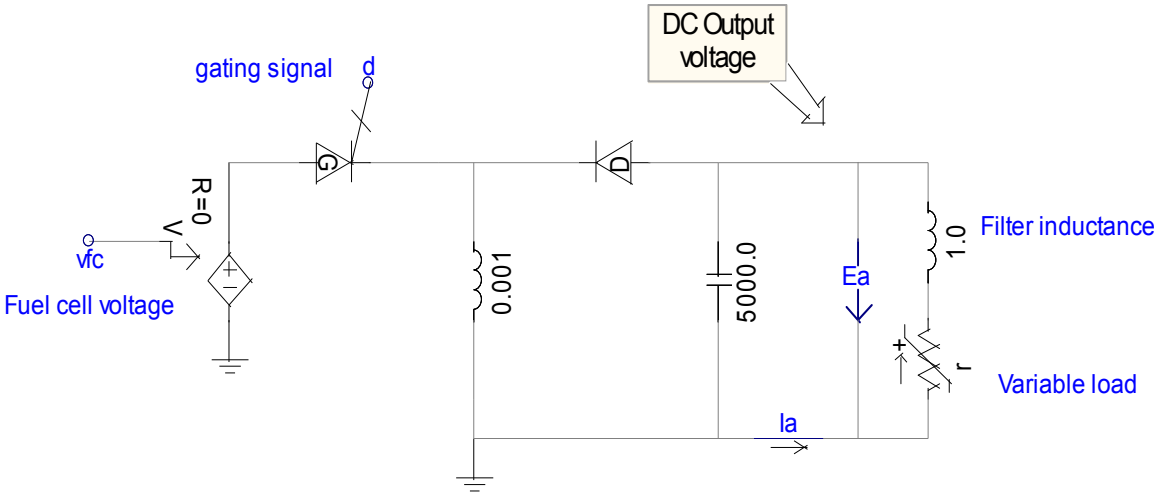

Figure 4.3 DC-DC buck-boost converter model in PSCAD

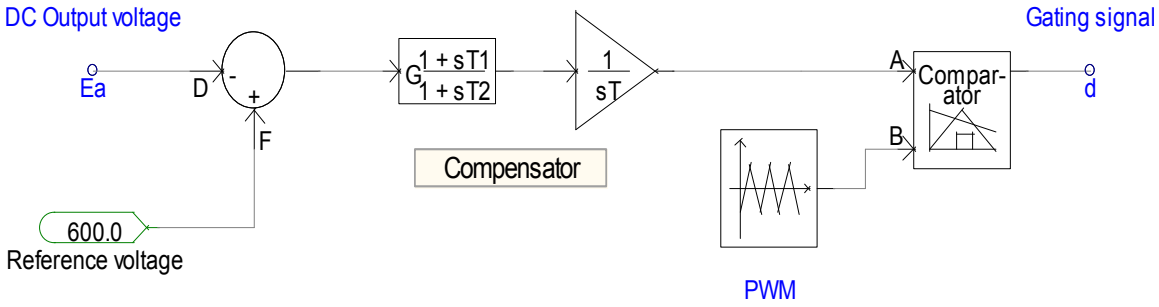

Figure 4.4 Feedback control system model in PSCAD

4.1.3. DC-AC Inverter Model. The input to the three phase inverter is the output voltage of the DC-DC converter. The output voltage of the inverter is a PWM voltage with harmonics which are filtered with an LC filter. The low voltage of the inverter is stepped up with the three phase transformer before being connected to the utility grid. Figure 4.5 shows the fuel cell system connection to the utility grid through the inverter.

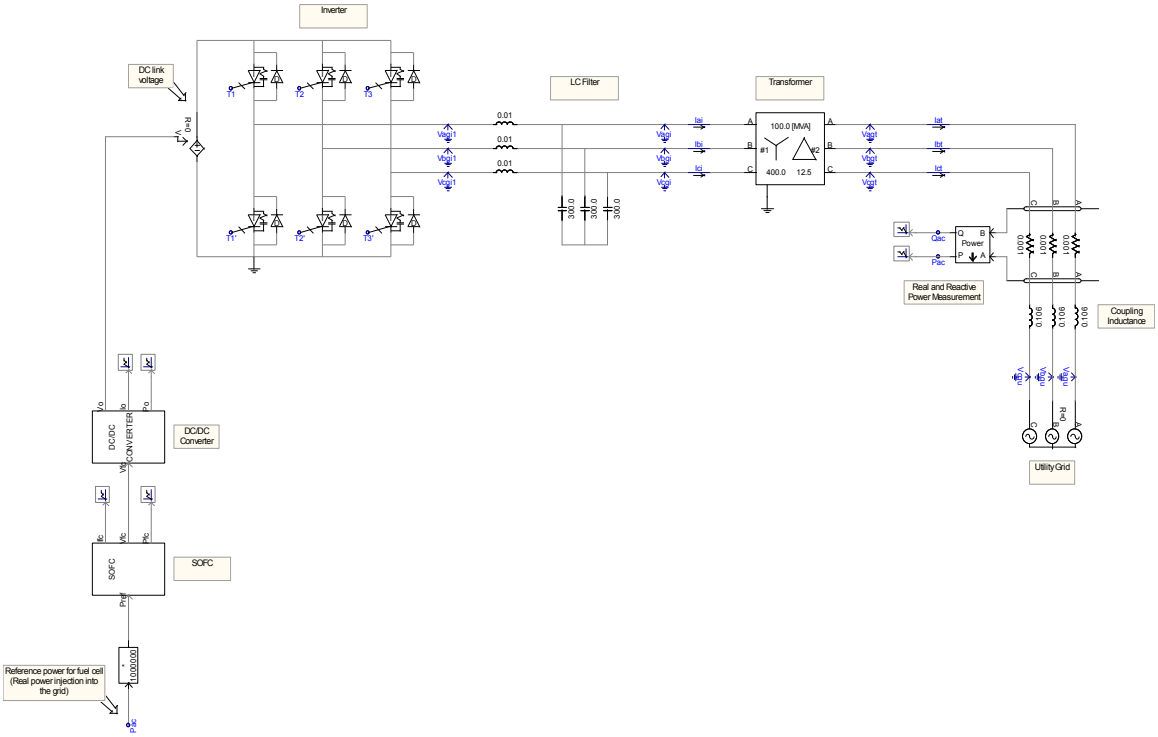

Figure 4.5 Three phase inverter-utility grid connection model in PSCAD

The main components required for the inverter control is the phase angle of the inverter and the modulation index. This work employs the decoupled real and reactive power control. The P and Q controller controls the phase angle and the amplitude of the

inverter voltage, respectively. Figures 4.6 and 4.7 show the real and reactive power control system.

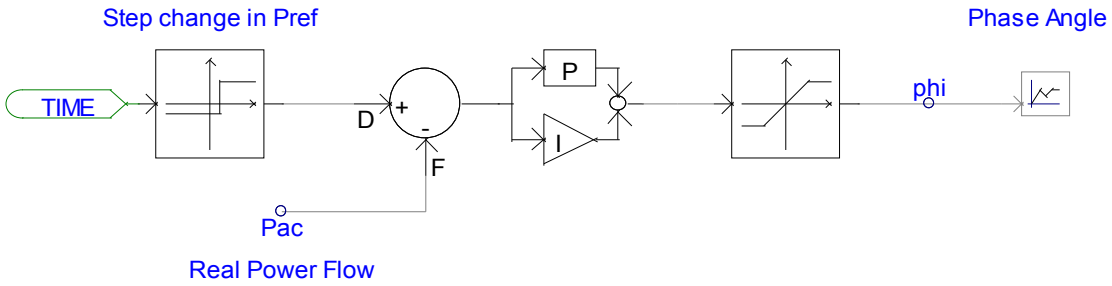

Figure 4.6 Real power control system model in PSCAD

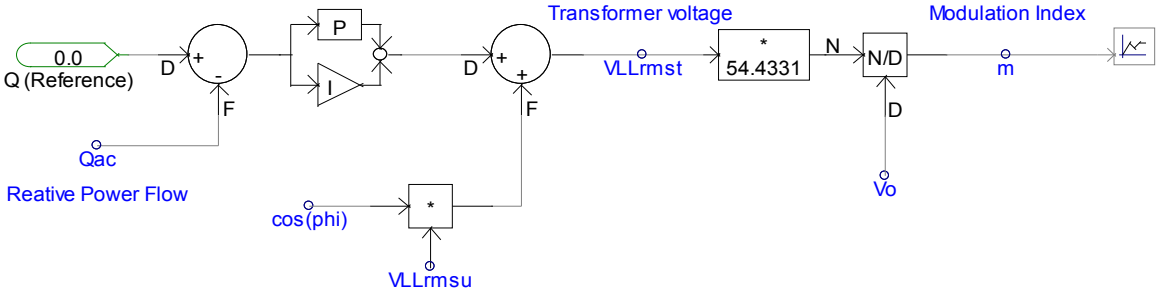

Figure 4.7 Reactive power control system model in PSCAD

The line-line rms voltages (V_{abu}, V_{bcu}, and V_{cau}) on the utility side are measured by running the simulation model shown in Figure 4.5. These voltages are used to determine the peak value of the line-neutral voltage (V_u) as shown Equation (13) (Section 3.2). The mathematical PSCAD model of this equation is shown in Figure 4.8.

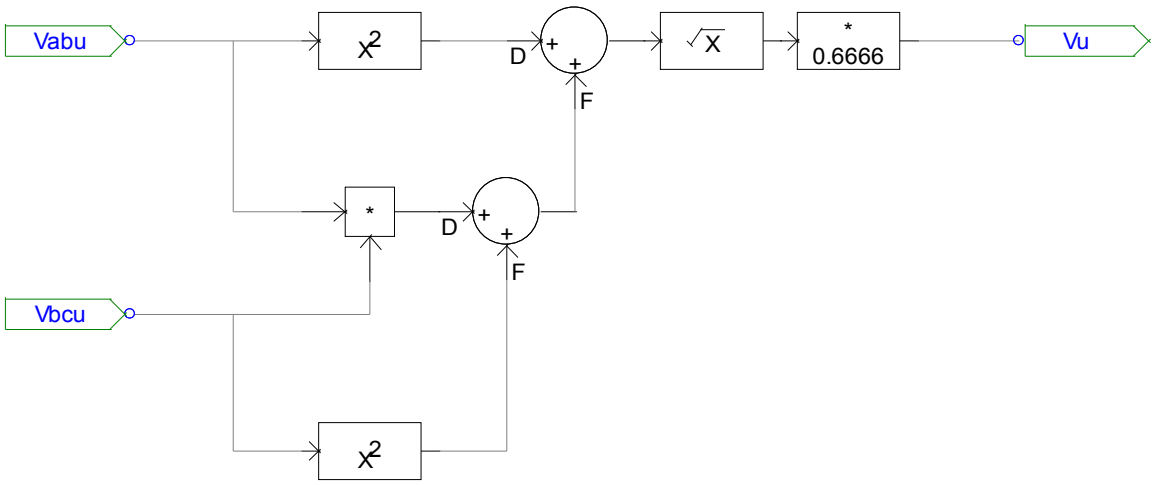

Figure 4.8 Determination of the peak voltage model in PSCAD

In Section 3.2, Equation (12) was re-written as Equation (14). Equation (12) corresponds to the line-line voltages on the utility side expressed in terms of the peak value of the voltage and the utility phase angle. The line-line voltages measured from the simulation model and the peak value obtained from Figure 4.8 are used to express the contents of Equation (14). Figure 4.9 shows the mathematical model of Equation (14). The terms obtained from Figure 4.9 and the control parameters (phase angle and modulation index) obtained from Figures 4.6 and 4.7, respectively, are used to determine the duty cycle control signals. These signals are given by Equation (11) in Section 3.2. Figures 4.10(a), (b) and (c) show the duty cycle control signals for phase A, B and C, respectively.

The control signals obtained from Figure 4.10 are compared with the triangular wave of switching frequency 1KHz with amplitude of one. When the control signals are greater than the triangular, the switches in the upper half of the inverter are switched ON. When the control signals are less than the triangular wave, the switches in the lower half of the inverter are switched ON while turning OFF the upper switches. Figure 4.11 shows the comparison of the control signals with the triangular wave to obtain transistor signals.

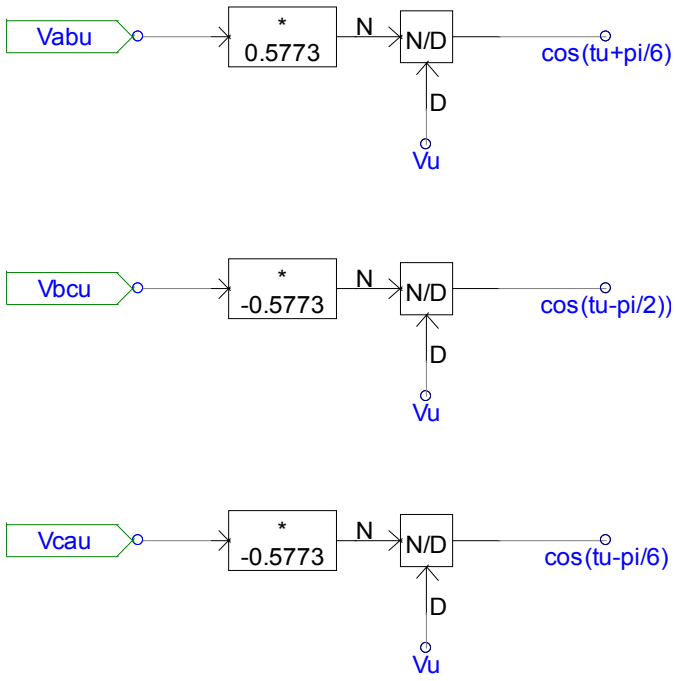

Figure 4.9 Intermediate step for obtaining duty cycle signals in PSCAD

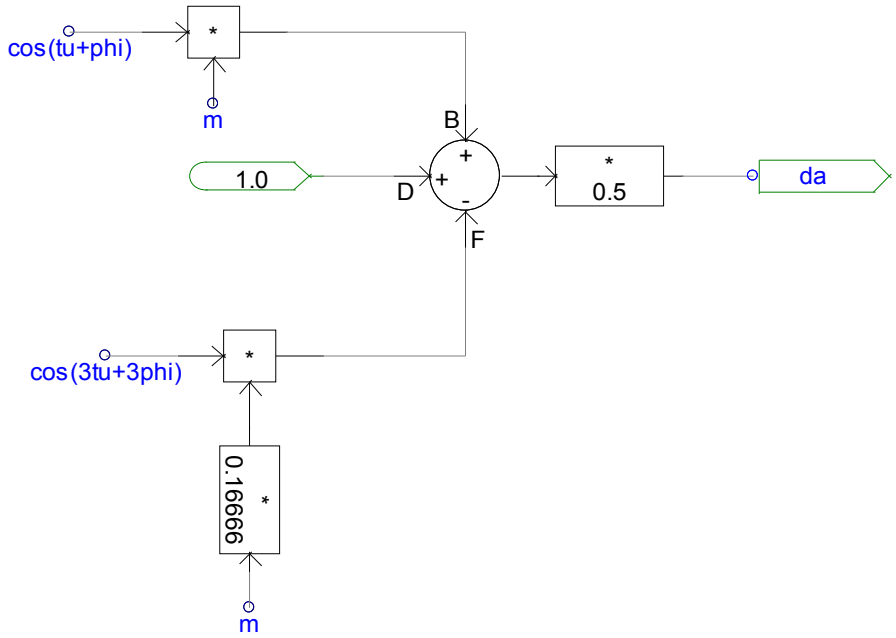

(a) Duty cycle control signal for Phase A

Figure 4.10 Duty cycle control signals in PSCAD

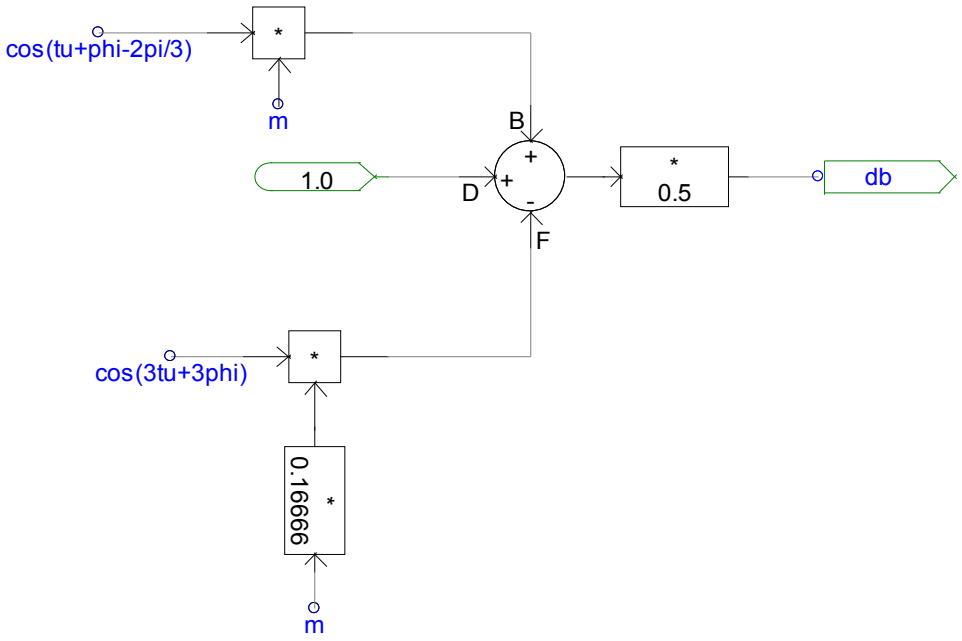

(b) Duty cycle control signal for Phase B

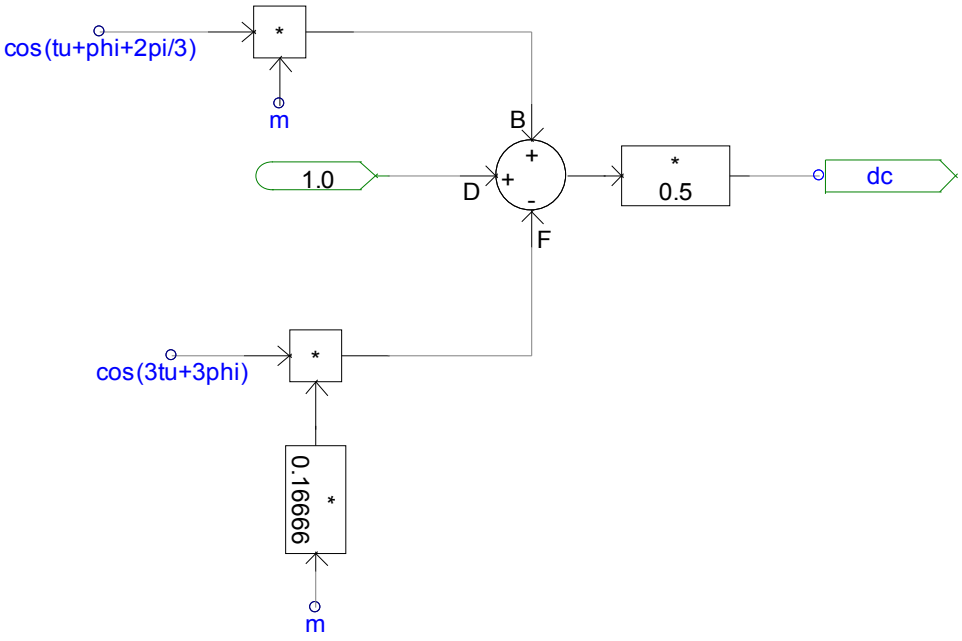

(c) Duty cycle control signal for Phase C

Figure 4.10 Duty cycle control signals in PSCAD (cont.)

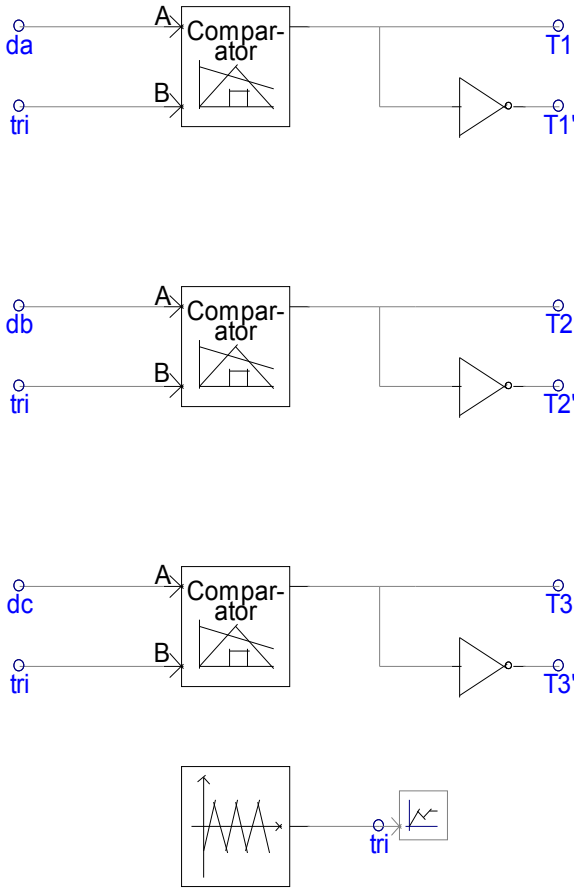

Figure 4.11 Determination of switching signals in PSCAD

4.2. SIMULATION RESULTS

This section consists of the results obtained in PSCAD 4.1.1 for the system shown in Figure 4.5. The simulation results consist of the fuel cell, the DC-DC converter and the DC-AC inverter characteristics. There are three subsections in this section. The first subsection consists of the simulation results obtained when a real power of 50 kW is commanded. The second subsection shows the simulation results corresponding to the limitation on the stack power (i.e. step change in P_{ref} from 400 to 500 kW). The third subsection deals with the results obtained for a step change in the real reference power from 50 to 100 kW for a zero reactive power injection.

4.2.1. Response for a Commanded Real Power of 50kW. This subsection consists of the fuel cell, the DC-DC converter and the DC-AC inverter characteristics for a reference power of 50kW.

4.2.1.1. SOFC characteristics. Figure 4.12 shows the response of the fuel cell for a commanded real power of 50kW. Figures 4.12(a) shows the stack voltage which reaches a steady state value of 438V in 5s. Figure 4.12(b) show stack current of the fuel cell which takes 5s to reach a steady state value of 120A. The slow response of the fuel cell is due to slow electrochemical reactions in the cell. This slow reaction is seen in the slow response of the fuel and the air flow. Figures 4.12(c) shows the fuel flow which depends on the response of the stack current. Figure 4.12(d) show the response of the air flow which depends on the fuel flow. The fuel and air flow take almost 20s to reach a steady state value. The stack current is limited based on the utilization range. The fuel utilization is initially high and gradually settles at an optimum value of 0.85 as shown in the Figure 4.12(e). Figure 4.12(f) shows the stack power which takes 5s to reach the commanded value of 50kW.

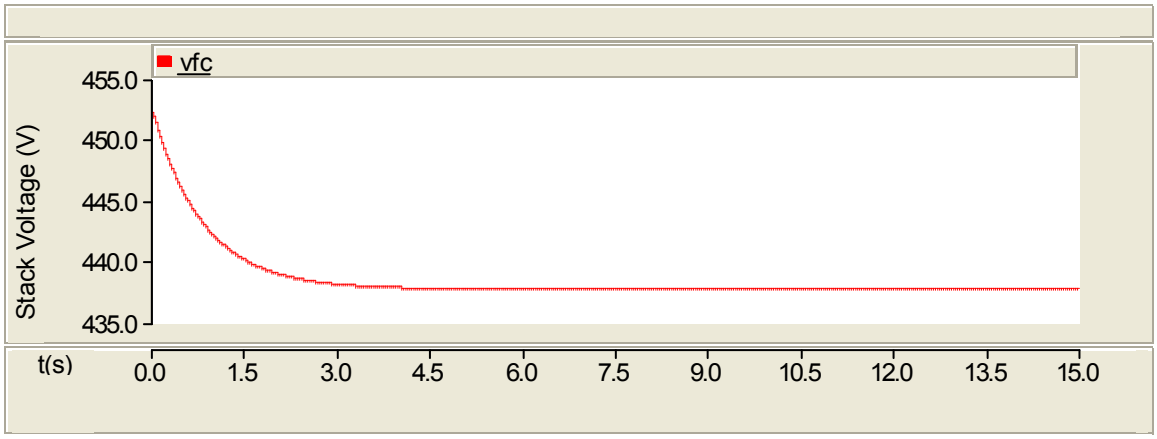

(a) Stack voltage

Figure 4.12 Response of the fuel cell for a commanded real power of 50kW

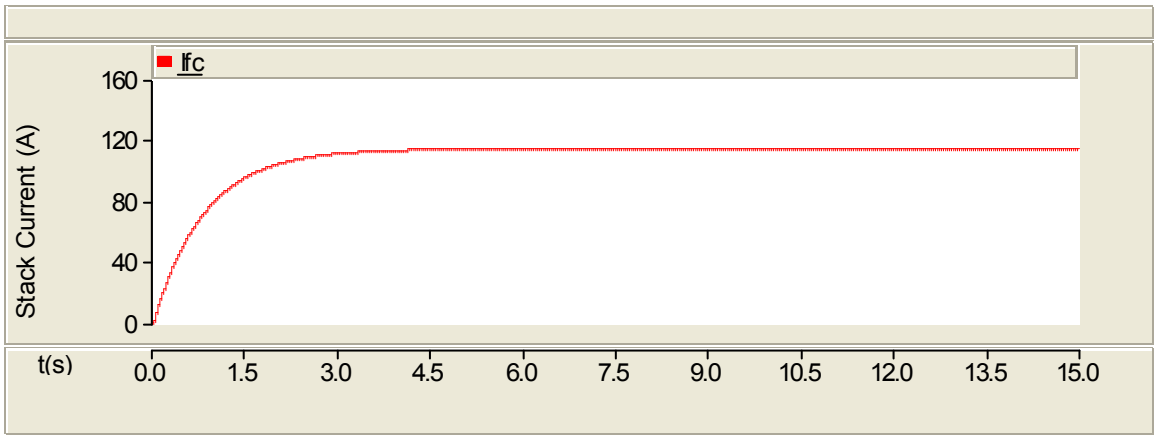

(b) Stack current

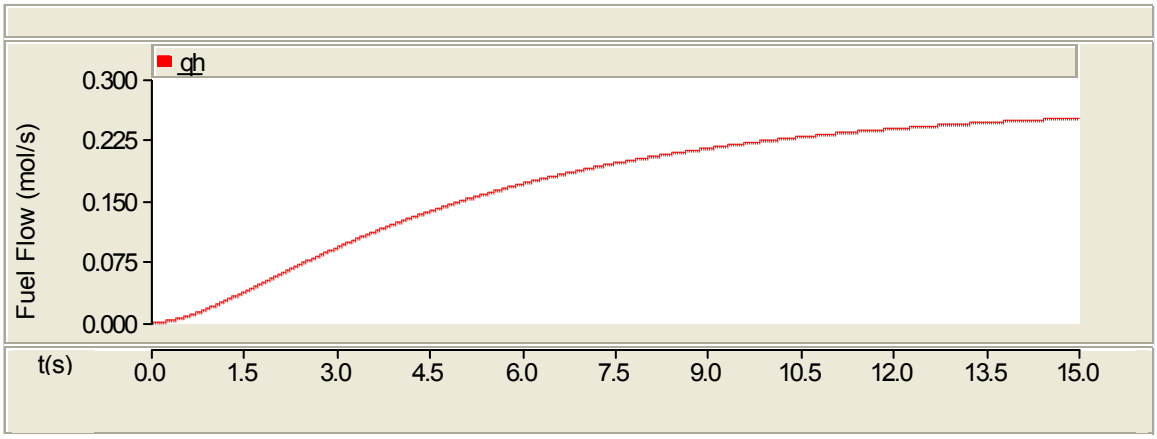

(c) Fuel flow

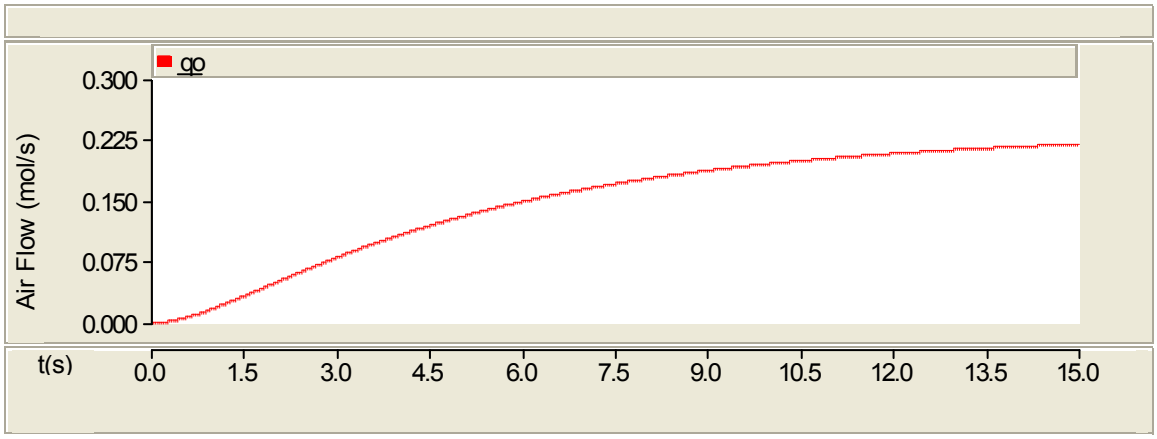

(d) Air flow

Figure 4.12 Response of the fuel cell for a commanded real power of 50kW (cont.)

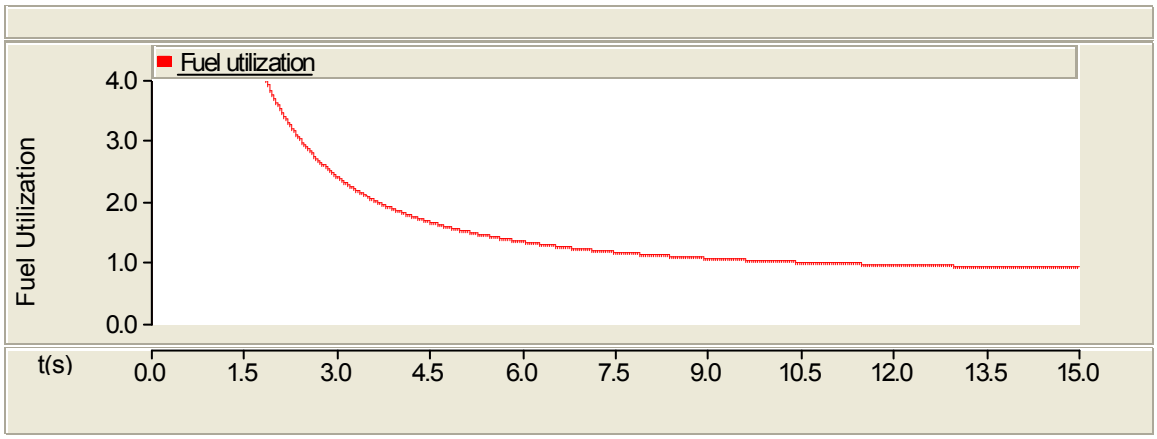

(e) Fuel utilization

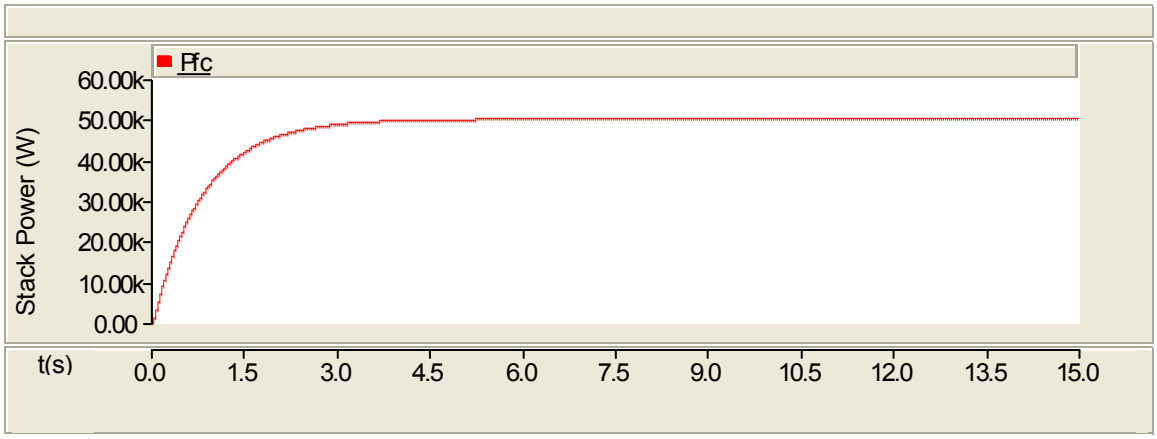

(f) Stack power

Figure 4.12 Response of the fuel cell for a commanded real power of 50kW (cont.)

4.2.1.2. DC-DC converter characteristics. Figure 4.13 shows the response of the converter for a commanded real power of 50kW. The converter duty cycle controller maintains the DC link voltage at 600V as shown in Figure 4.13(a). Figures 4.13(b) and (c) show the output current and power of the converter, respectively. Figure 4.13(d) shows the comparison between the stack power and the converter output power. Fuel cell power takes 5s whereas converter power takes 2.5s to reach the steady state value.

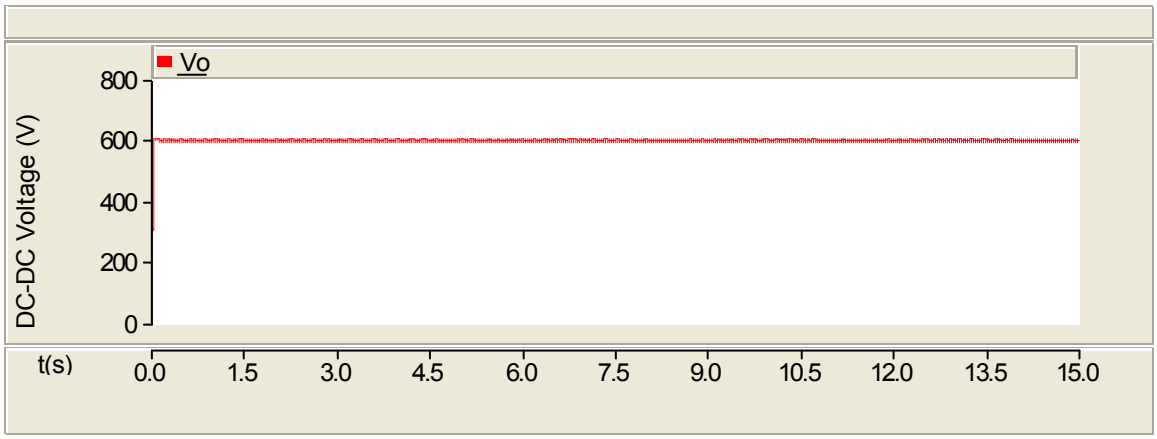

(a) Output voltage of the converter

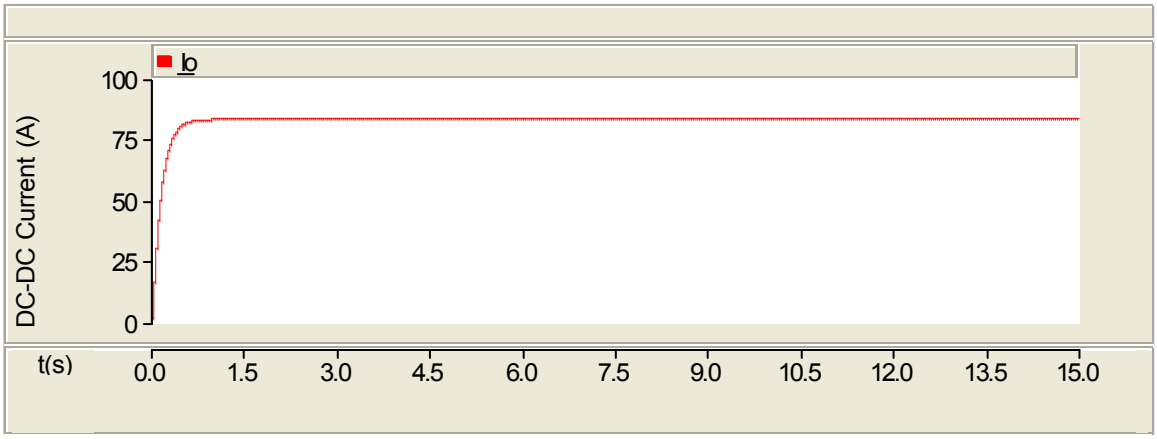

(b) Output current of the converter

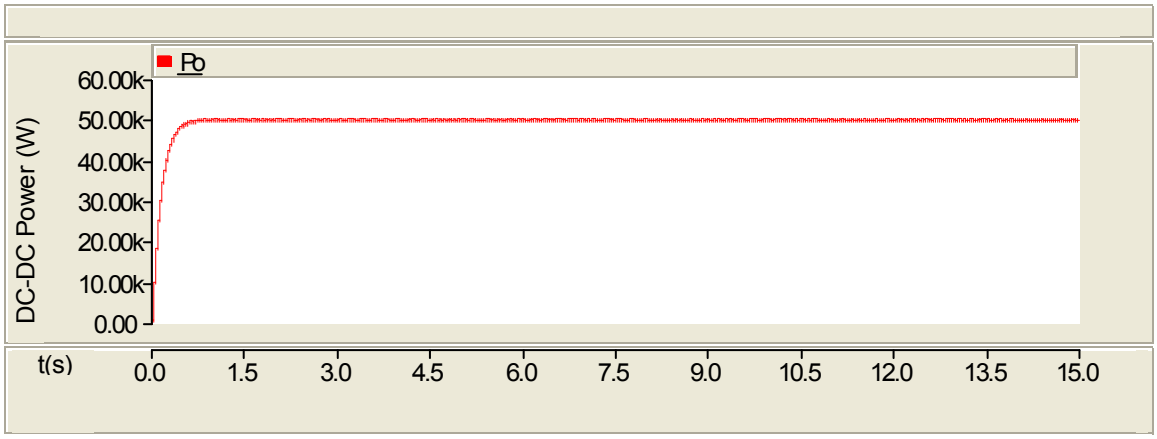

(c) Output power of the converter

Figure 4.13 Response of the converter for a commanded real power of 50kW

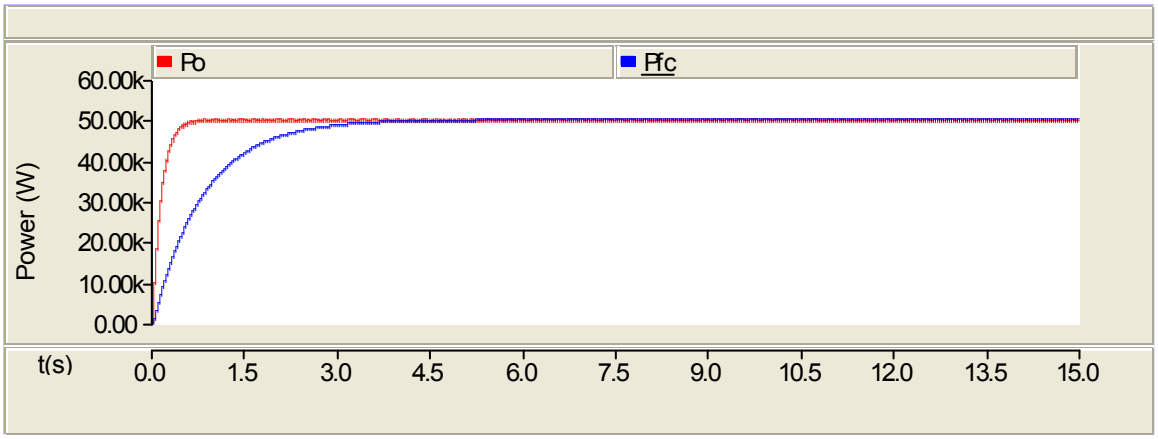

(d) Comparison between the fuel cell and the converter

Figure 4.13 Response of the converter for a commanded real power of 50kW (cont.)

4.2.1.3. DC-AC inverter characteristics. Figure 4.14 shows the response of the inverter for a commanded real power of 50kW. Figure 4.14(a) shows the utility side L-N voltage, the peak value of which is 10.2kV ($\sqrt{\frac{2}{3}}x12.5\,\text{kV}$). Figures 4.14(b) and (c) show the L-N voltage across the inverter and the transformer, respectively. These voltages consist of harmonics which are filtered out with an LC parallel filter (L = 0.011H and C = 200μF). Figure 4.14(d) shows the filtered L-N transformer voltage. Figure 4.14(e) shows the line current. There is no phase angle difference between the line current and the L-N utility voltage since the reactive power injection is assumed to be zero, as seen in Figure 4.14(f).

Figure 4.14(g) shows the real power injection with the filtered voltage. The real power takes 0.2s to reach the reference power of 50kW. Reactive power injection is assumed to be zero as shown in Figure 4.14(h). Figures 4.14(i) and (j) show the phase angle and the modulation index obtained from the PQ control. For a reference real power of 50kW and with the assumptions made, the phase angle of the inverter (ϕ_i) is 0.0128 radians and the modulation index is 1.115. The L-L rms value of the transformer voltage from the Q control is 12.498 kV as shown in Figure 4.14(k). Figure 4.14(l) shows the

comparison between the L-L rms value obtained from the Q control and the value measured from the system. Figure 4.14(m) shows the duty cycle control signals, each phase being displaced by 120^{o}. The duty cycle control signals should follow the L-N voltages on the utility side. Figure 4.14(n) shows the comparison between the duty cycle signal and the L-N utility voltage for phase A. Figure 4.14(o) shows the comparison of the phase A control signal with the triangular wave (switching frequency 1 KHz) to obtain the transistor T_1 as shown in Figure 4.14(p).

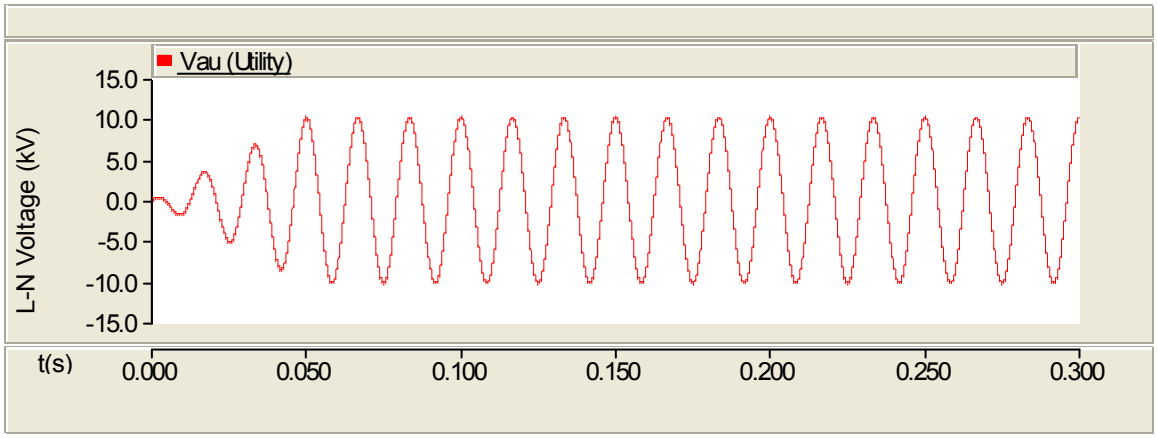

(a) Utility side line-neutral voltage

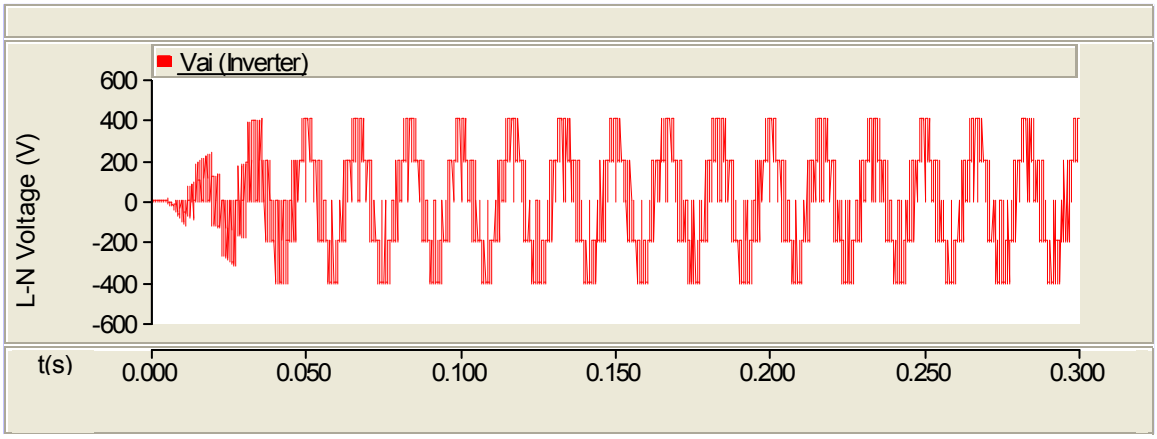

(b) Inverter line-neutral voltage (without filter)

Figure 4.14 Response of the inverter for a commanded real power of 50kW

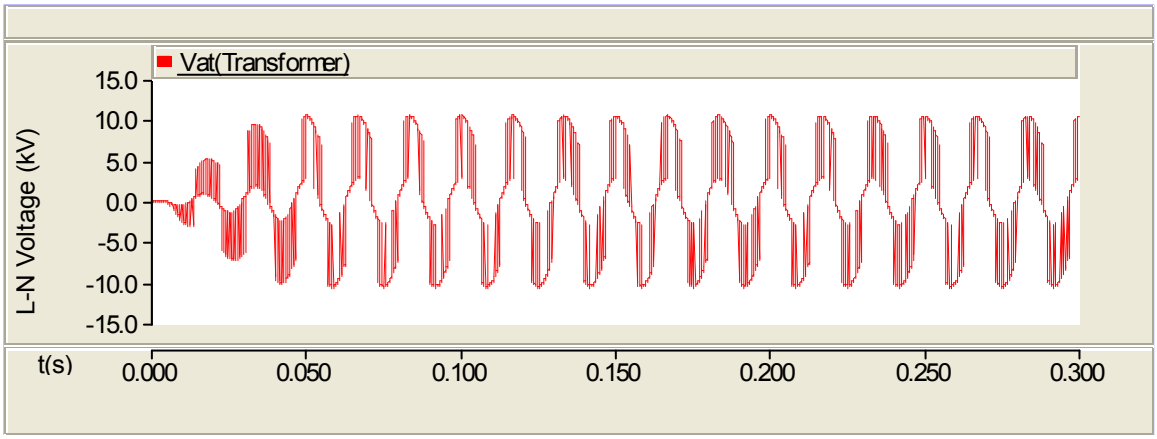

(c) Transformer line-neutral voltage (without filter)

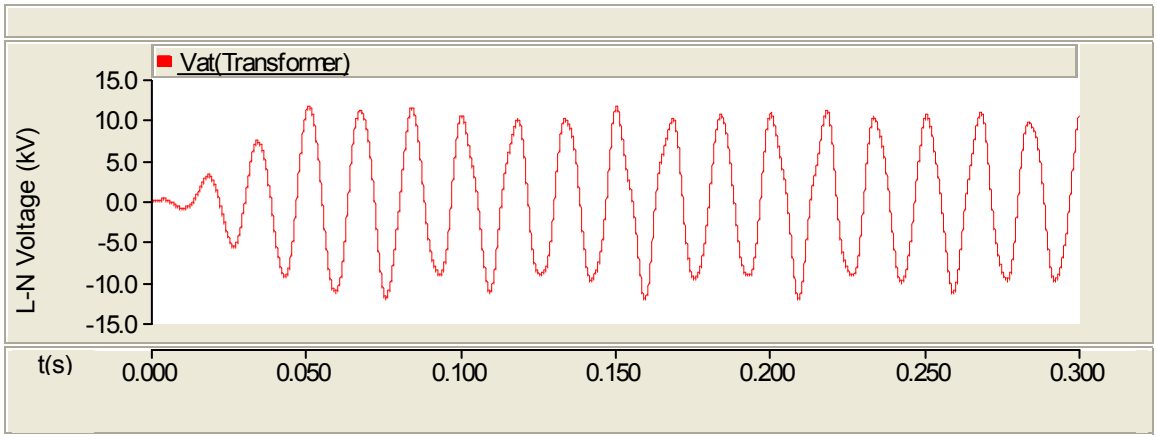

(d) Transformer line-neutral voltage (with filter)

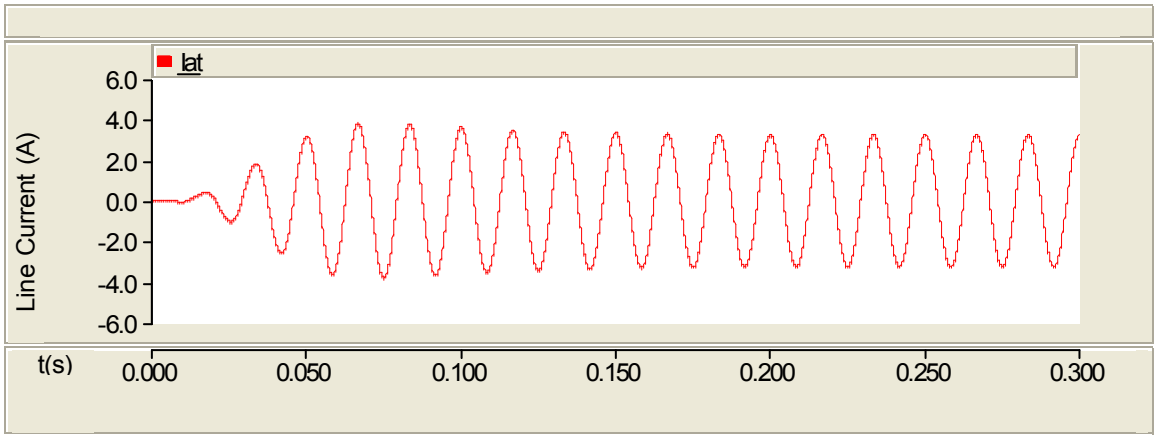

(e) Phase A line current after the transformer

Figure 4.14 Response of the inverter for a commanded real power of 50kW (cont.)

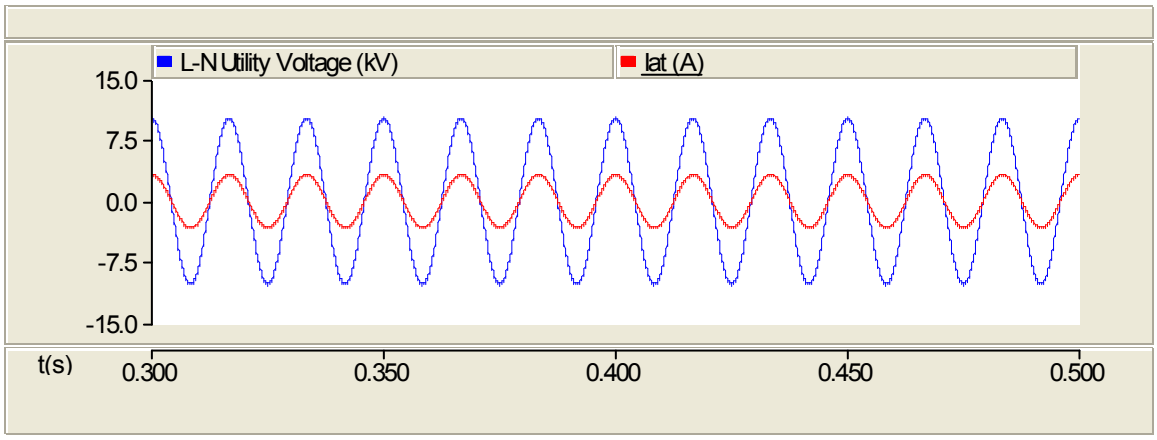

(f) Angle comparison between line current and L-L voltage (Transformer)

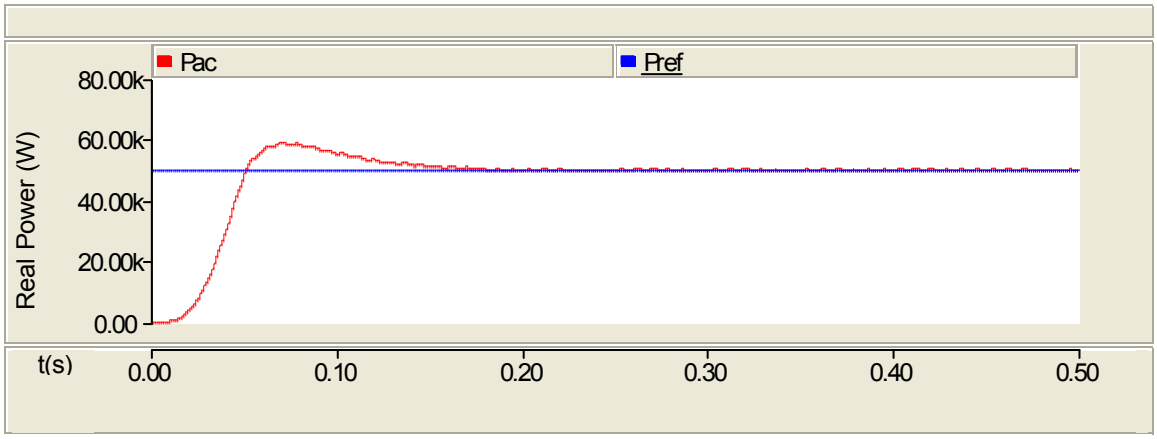

(g) Real power injection into the grid

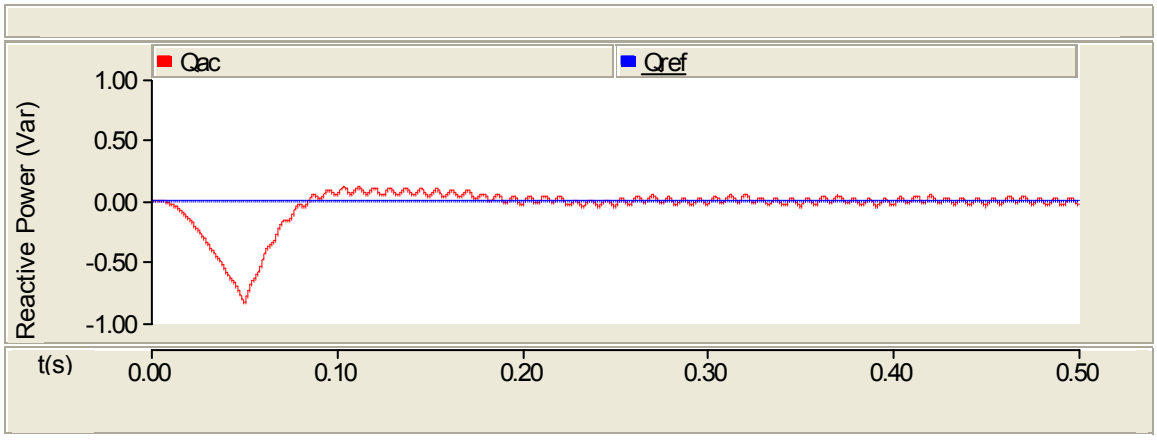

(h) Reactive power injection into the grid

Figure 4.14 Response of the inverter for a commanded real power of 50kW (cont.)

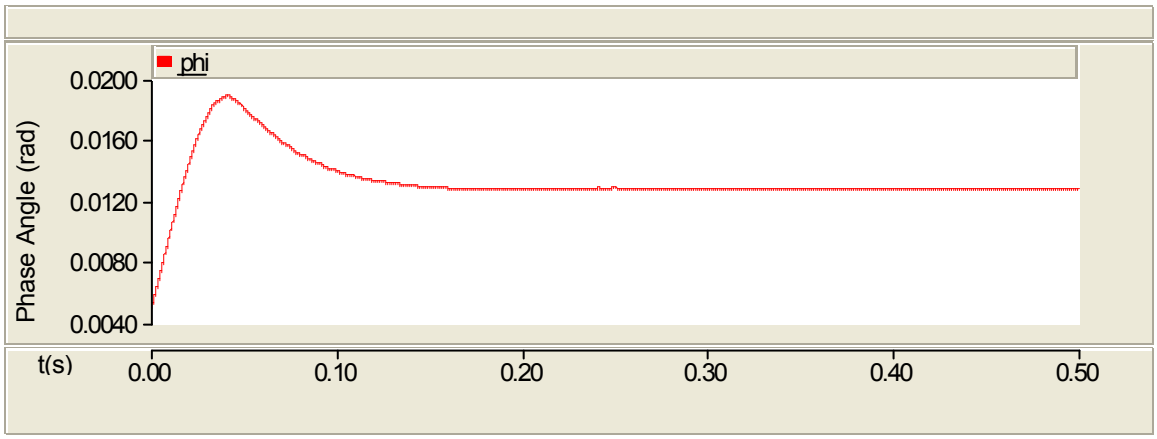

(i) Phase angle of the inverter from the P control

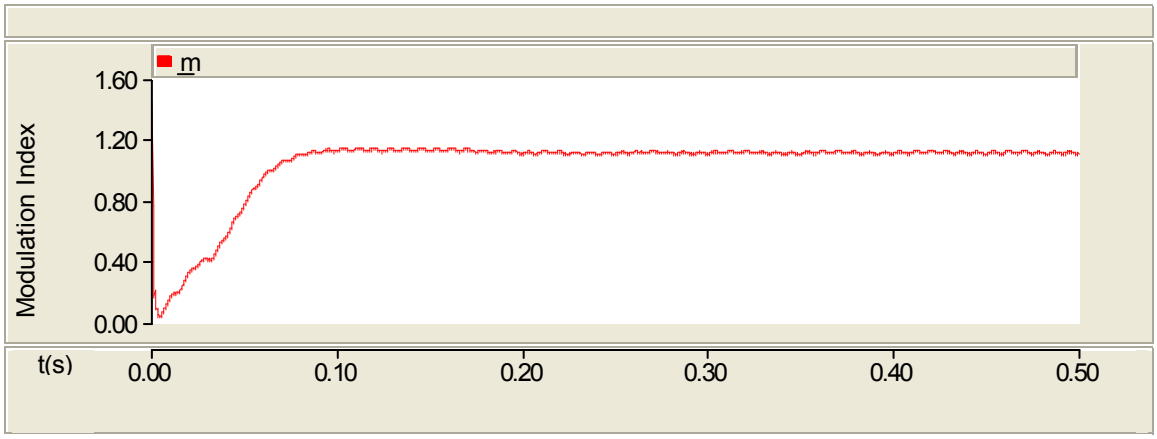

(j) Modulation index from the Q control

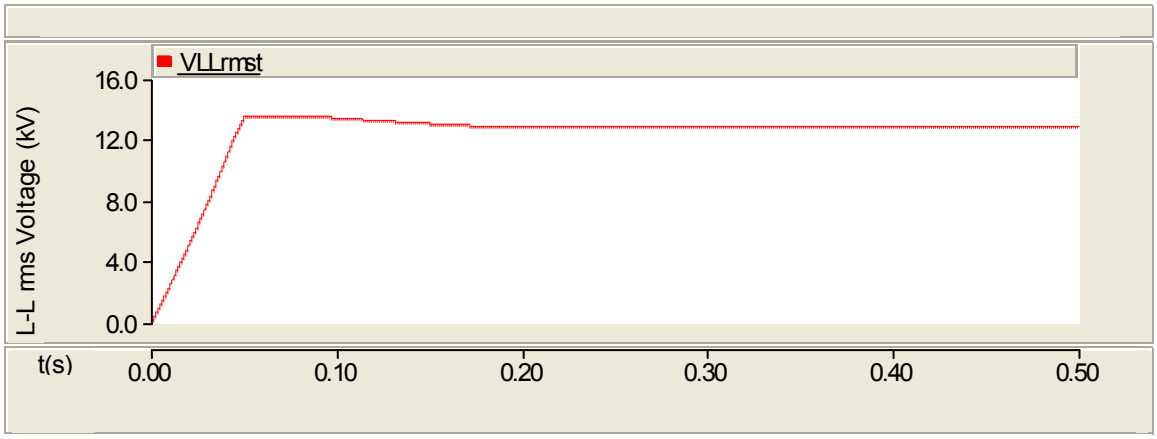

(k) L-L rms transformer voltage from the Q control

Figure 4.14 Response of the inverter for a commanded real power of 50kW (cont.)

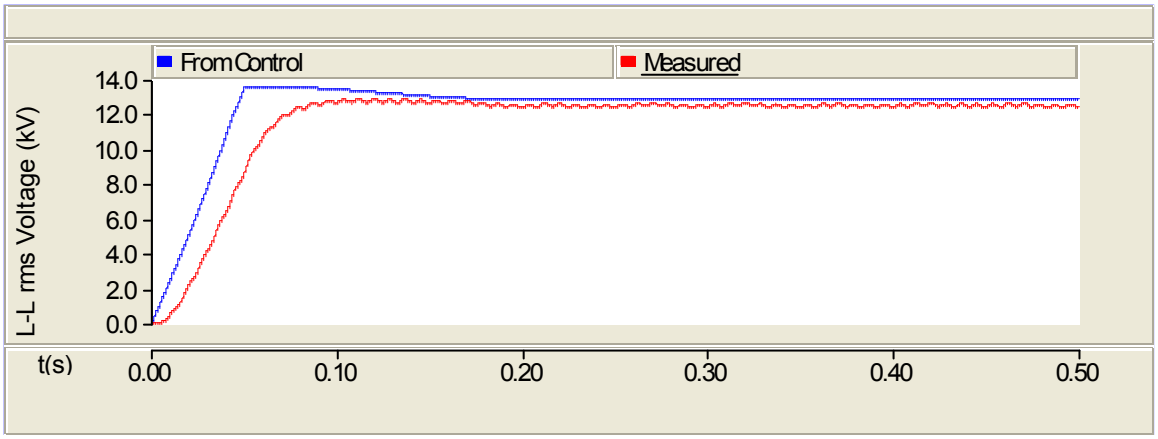

(l) Comparison of the controlled and measured value of L-L rms transformer voltage

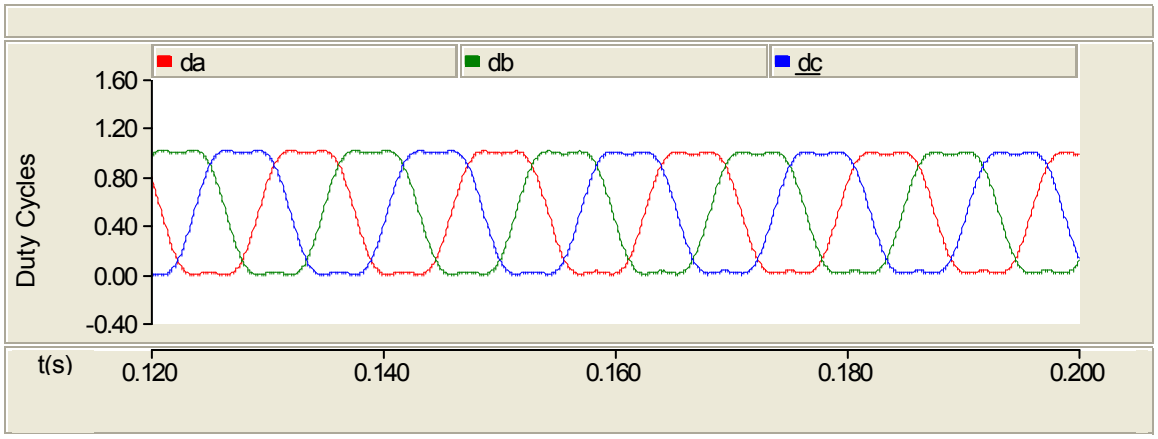

(m) Duty cycle control signals

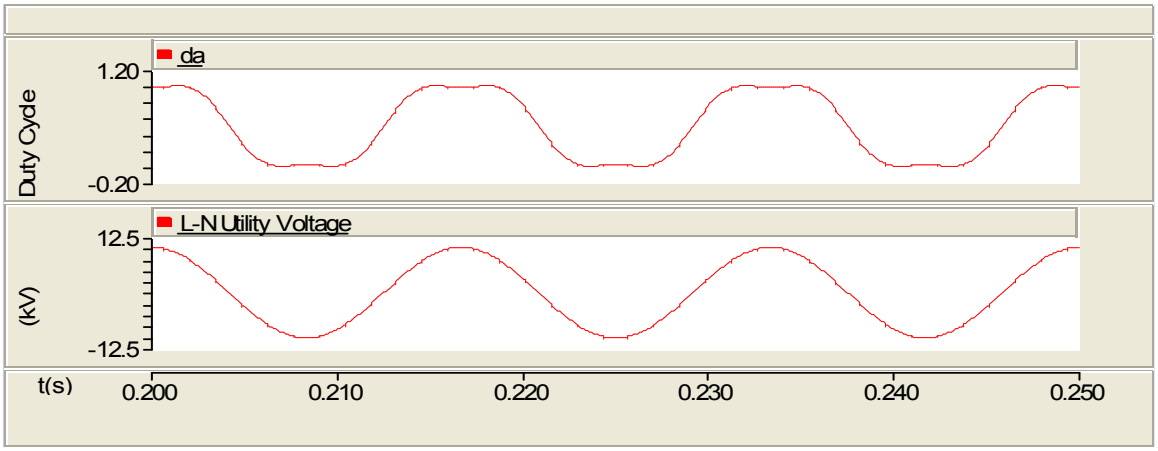

(n) Comparison of duty cycle and utility voltage for Phase A

Figure 4.14 Response of the inverter for a commanded real power of 50kW (cont.)

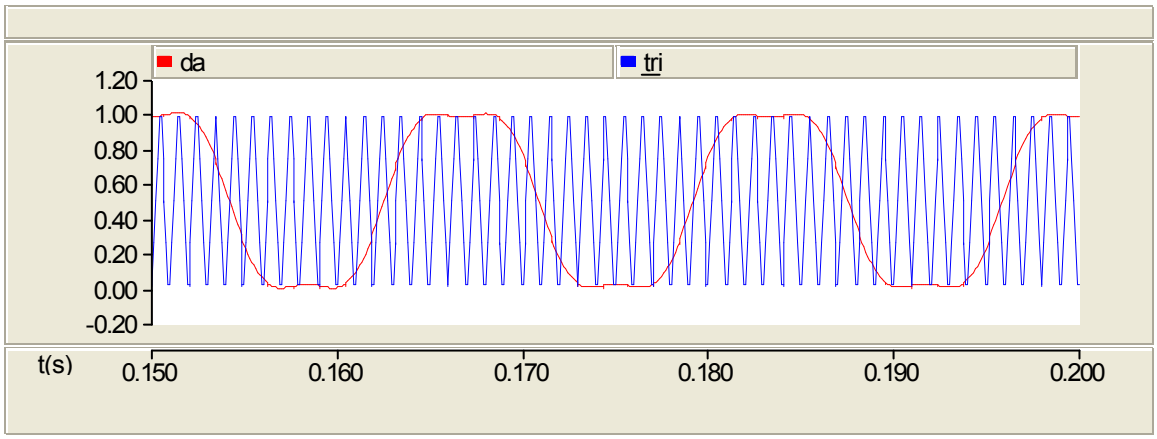

(o) Comparison of duty cycle signal with the triangular wave

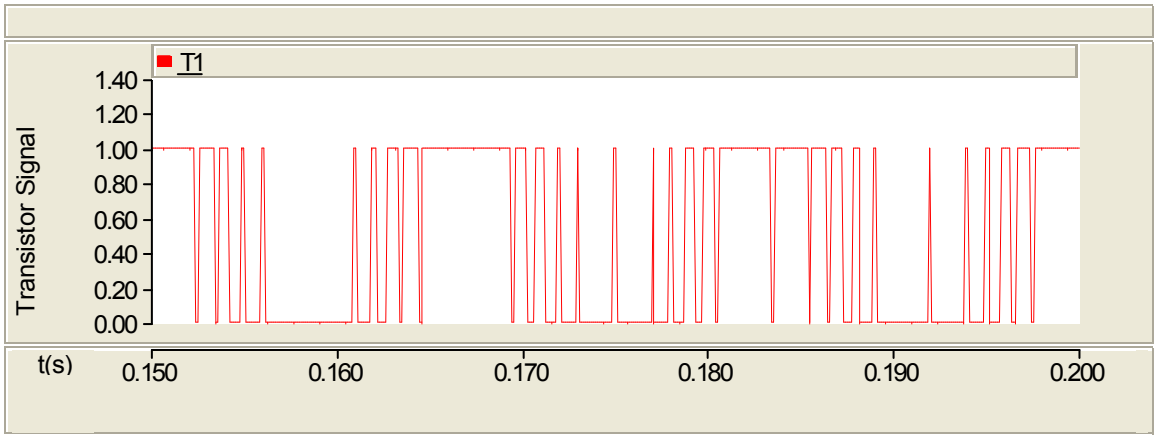

(p) Transistor signal for Phase A

Figure 4.14 Response of the inverter for a commanded real power of 50kW (cont.)

4.2.2. Response to Check the Limitation on the Fuel Cell. This subsection deals with the fuel cell, the DC-DC converter and the DC-AC inverter characteristics for a step change in the reference power from 400 to 500 kW.

4.2.2.1. SOFC characteristics. The maximum limit on the fuel cell stack power is 400kW. For any reference power beyond this level, the stack voltage drops to zero and oscillations can be observed. The reference power is stepped up from 400 to 500 kW at 15s. Figure 4.15 shows the response of the fuel cell for real power above the maximum

limit of 400kW. Figure 4.15(a) shows the response of the stack voltage which drops to zero after the step change in real power and loses stability. Figures 4.15(b), (c) and (d) show the response of the stack current, fuel flow and the air flow, respectively. Figure 4.15(e) shows the response of the fuel utilization. Figure 4.15(f) shows the response of the stack power which is no longer stable after the step change.

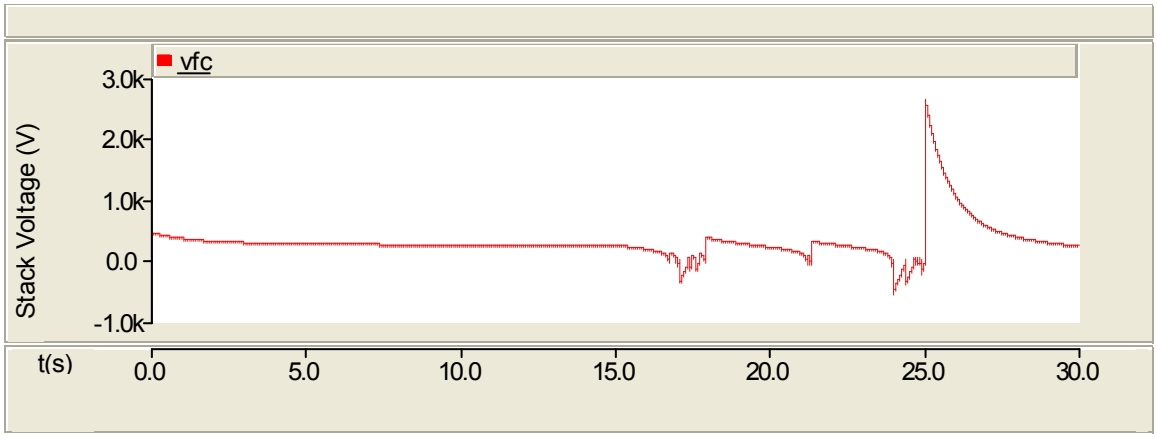

(a) Stack voltage

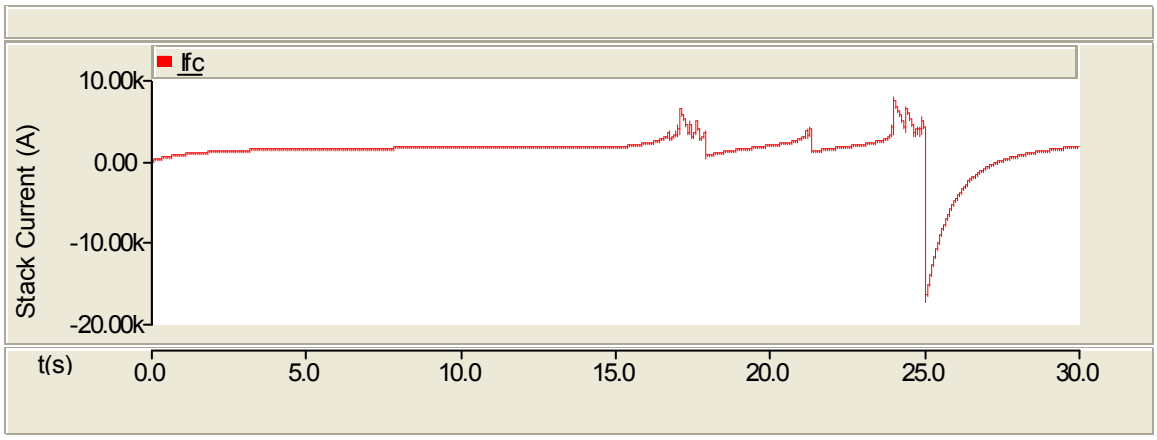

(b) Stack current

Figure 4.15 Response of the fuel cell for real power above the maximum limit of 400kW

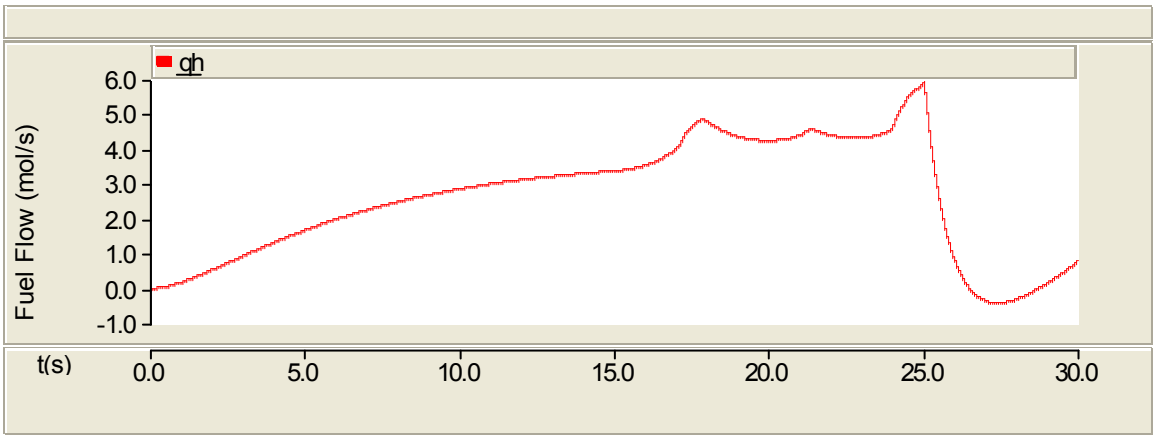

(c) Fuel flow

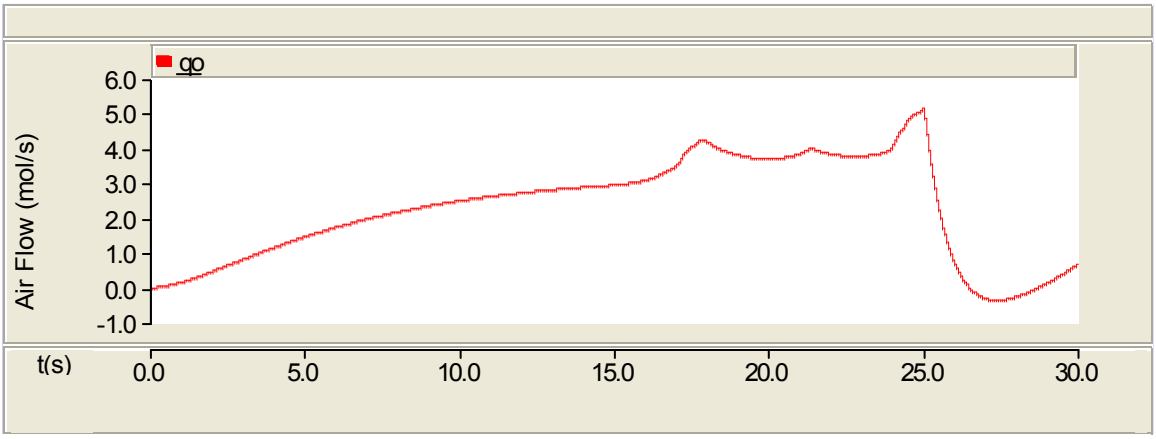

(d) Air flow

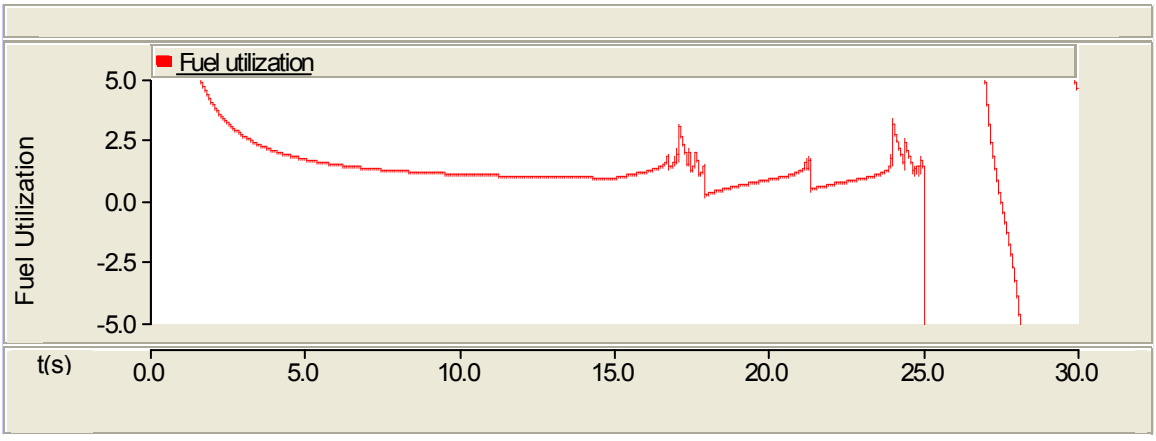

(e) Fuel utilization

Figure 4.15 Response of the fuel cell for real power above the maximum limit of 400kW (cont.)

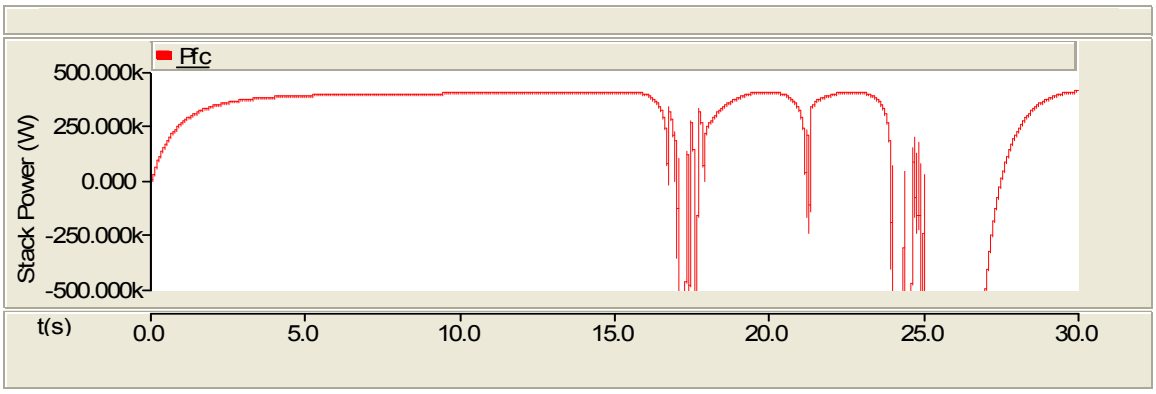

(f) Stack power

Figure 4.15 Response of the fuel cell for real power above the maximum limit of 400kW (cont.)

4.2.2.2. DC-DC converter characteristics. Figure 4.16 shows the response of the converter for real power above the maximum limit of 400kW. Figures 4.16(a), (b) and (c) show the converter voltage, current and power for step change in power to 500kW.

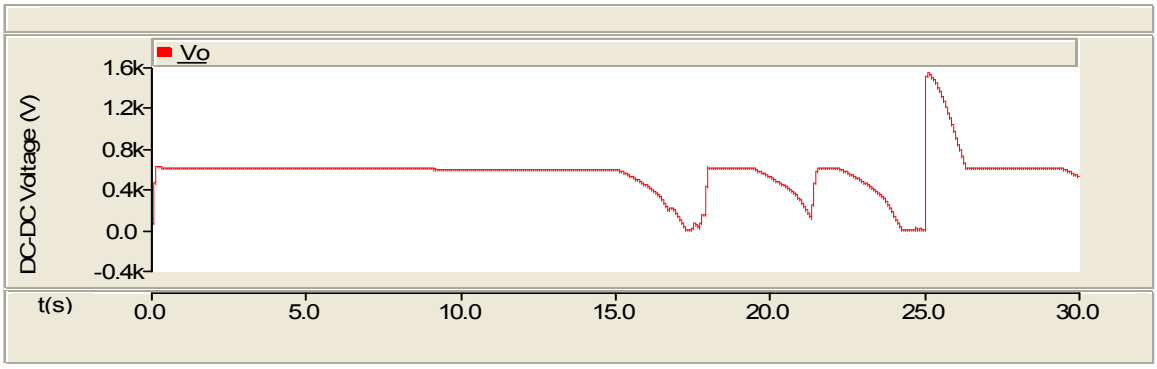

(a) Output voltage of the converter

Figure 4.16 Response of the converter for real power above the maximum limit of 400kW

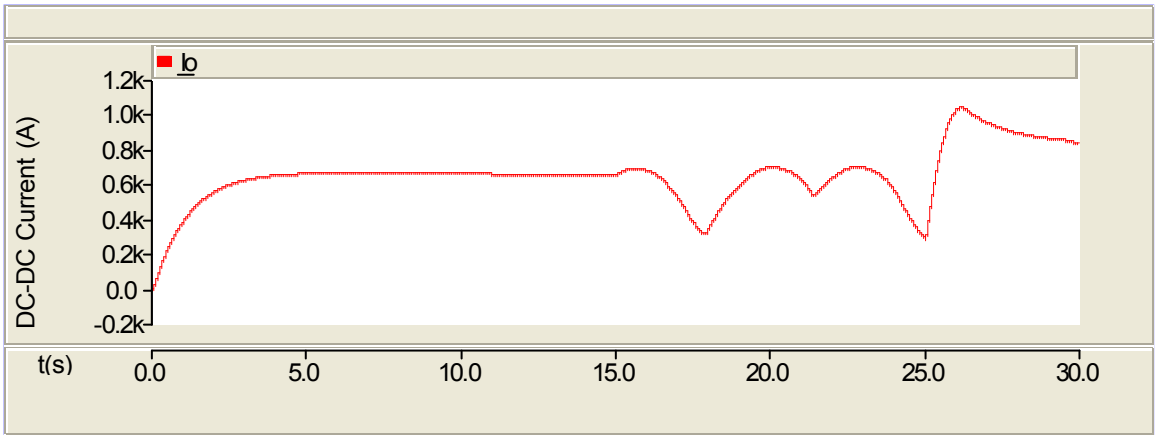

(b) Output current of the converter

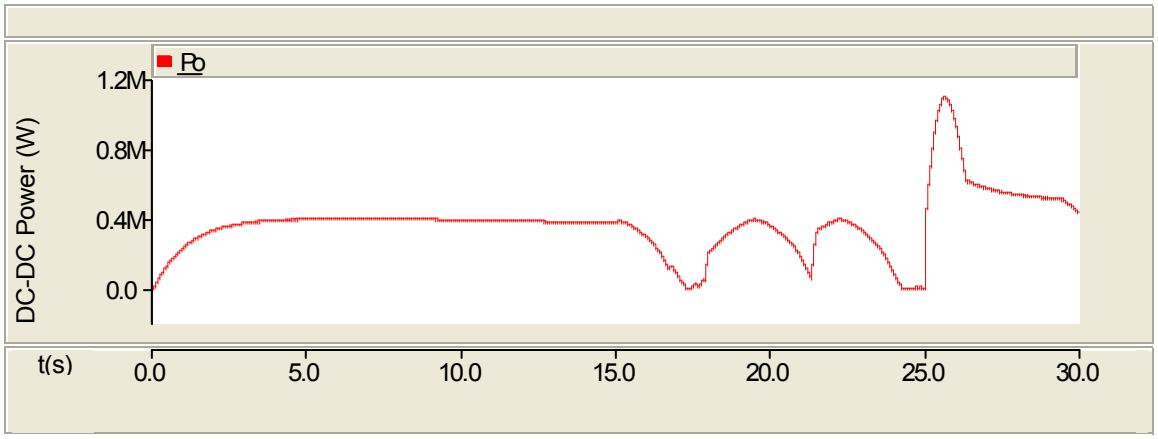

(c) Output power of the converter

Figure 4.16 Response of the converter for real power above the maximum limit of 400kW (cont.)

4.2.2.3. DC-AC inverter characteristics. This subsection deals with the inverter characteristics. Figure 4.17 shows the response of the inverter for real power above the maximum limit of 400kW. Figures 4.17(a) and (b) show the transformer line-neutral voltage and the line current, respectively. Figures 4.17(c) and (d) show the real power and reactive power injection into the grid, respectively, which are unstable after the step change in real power from 400 to 500kW. Figure 4.17(e) shows the phase angle and

Figures 4.17(f) and (g) show the modulation index and the line-line rms transformer voltage from the reactive power control, respectively.

Higher power can be commanded by either increasing the number of cells or by decreasing the fuel cell resistance. Increase in the number of cells, increases the capital as well as the running cost. Hence, it would be feasible to decrease the fuel cell resistance in order to command real power above the limit set by the fuel cell.

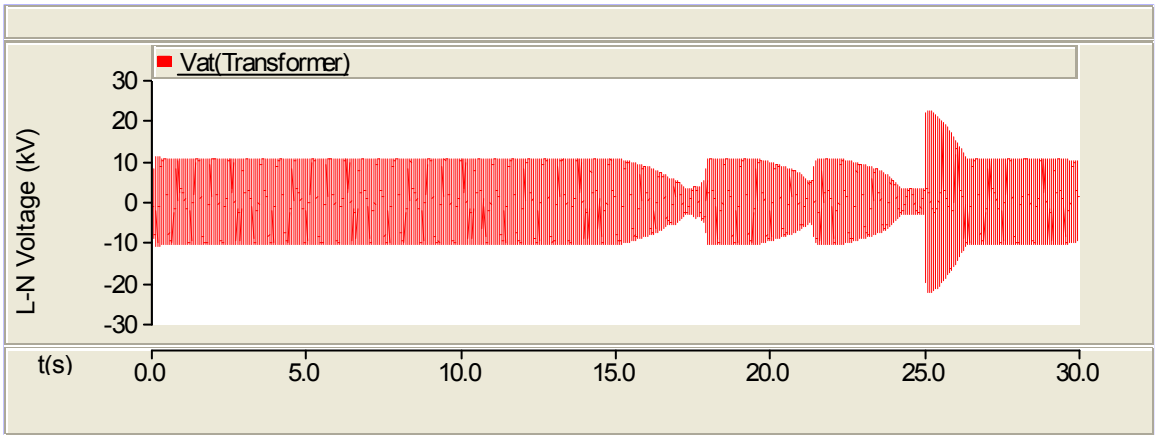

(a) Transformer line-neutral voltage

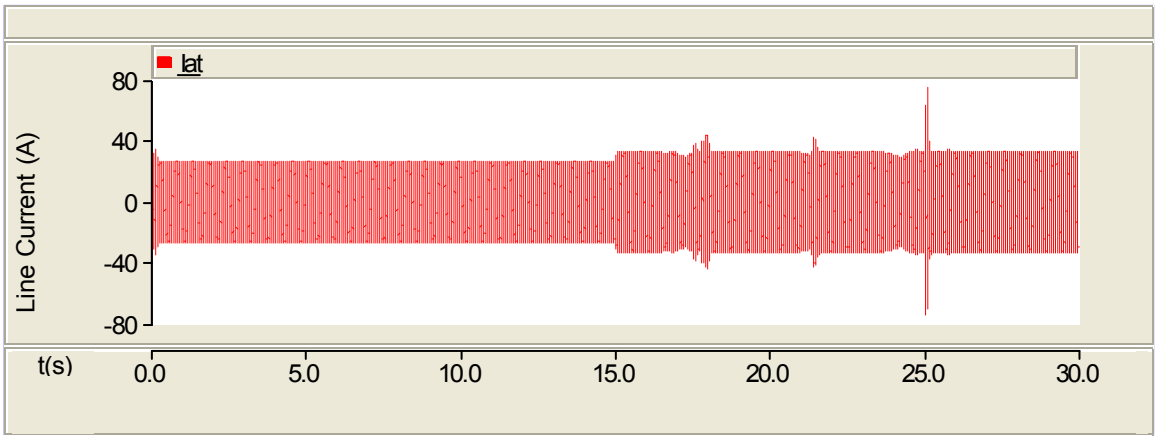

(b) Transformer line current in phase A

Figure 4.17 Response of the inverter for real power above the maximum limit of 400kW

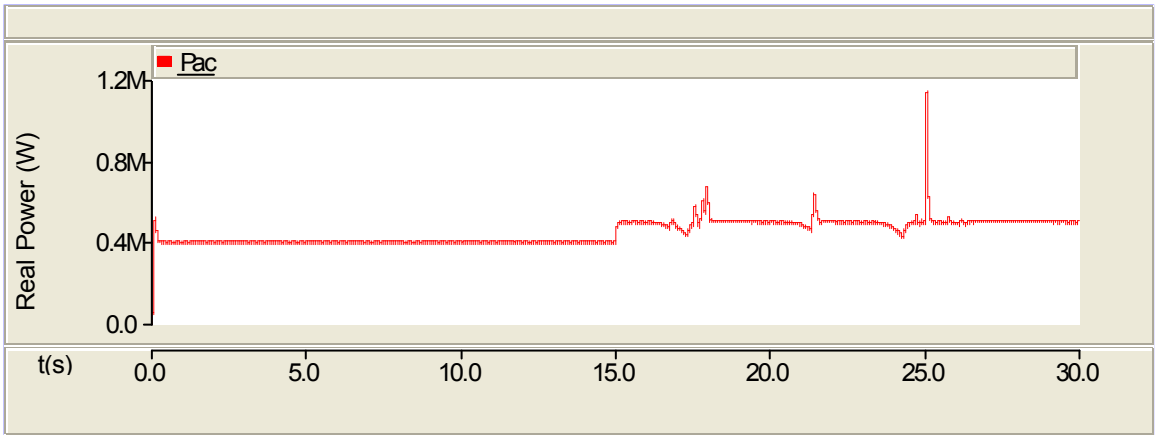

(c) Real power injection into the grid

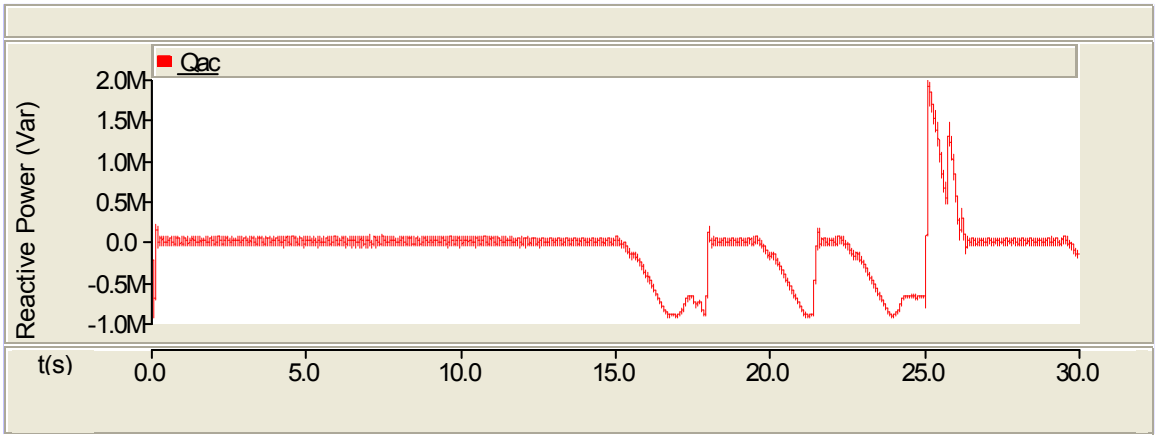

(d) Reactive power injection into the grid

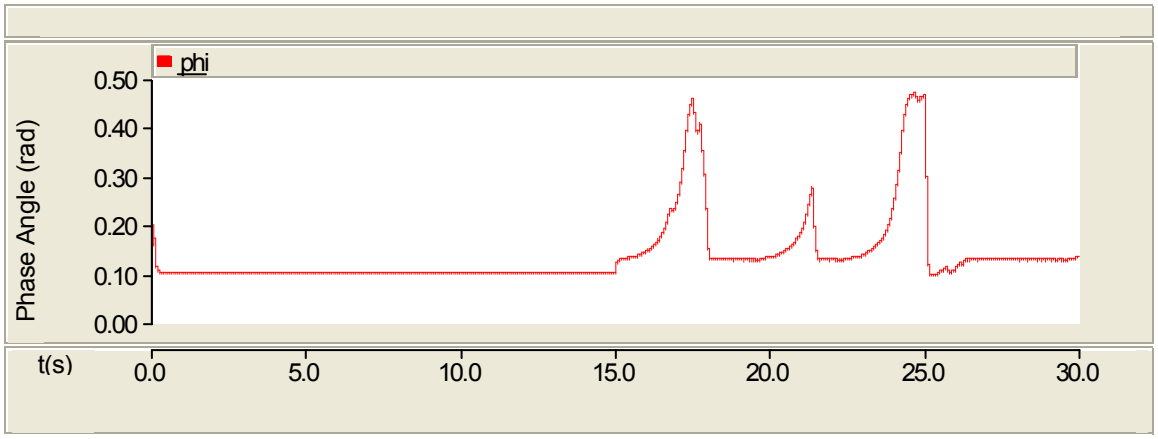

(e) Phase angle of the inverter from the P control

Figure 4.17 Response of the inverter for real power above the maximum limit of 400kW (cont.)

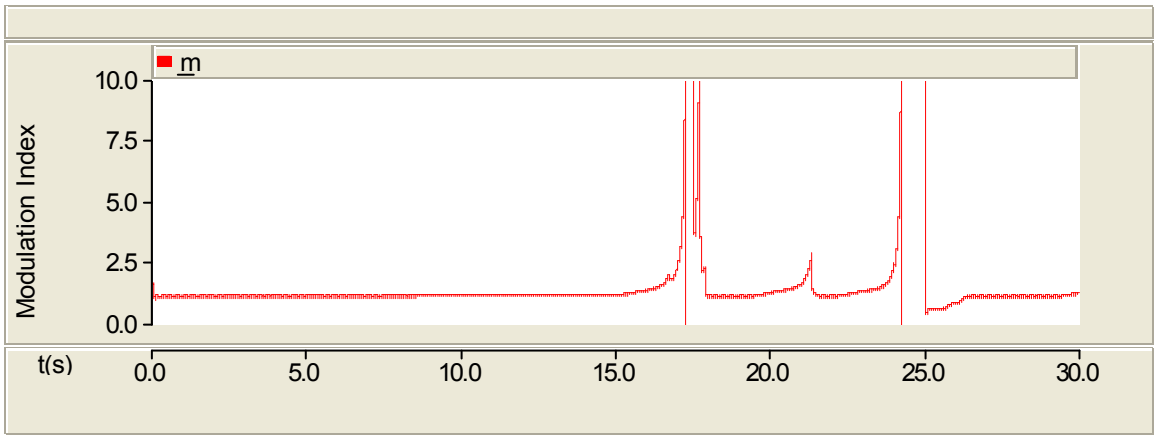

(f) Modulation index from the Q control

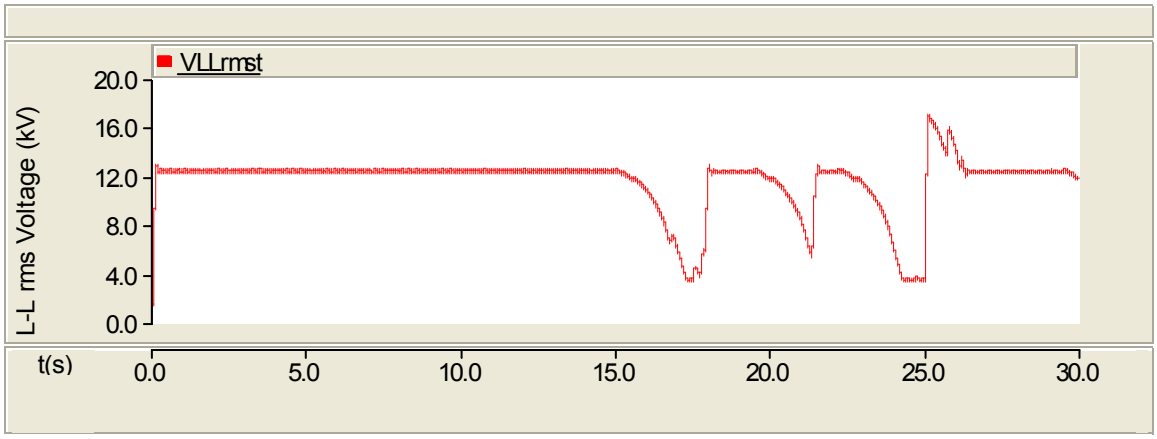

(g) L-L rms transformer voltage from the Q control

Figure 4.17 Response of the inverter for real power above the maximum limit of 400kW (cont.)

Higher power (i.e., above the set limit) can be commanded by decreasing the fuel cell resistance to 0.09 from 0.126Ω. Figure 4.18 shows the response of the fuel cell and the converter with reduced resistance. Internal stack resistance can be reduced by using electrodes with highest possible conductivity or by making the electrolyte as thin as possible. It may be difficult to reduce the thickness of the electrolyte because a fair amount of thickness is required to support onto which the electrodes are built and to

prevent any shorting between the electrodes. Further, the electrolyte needs to be wide enough to allow a circulating flow of it. Hence, resistance can be reduced by using higher conductivity electrode. Figures 4.18 (a), (b), (c) and (d) show the stack voltage, the stack power, the DC link voltage and the converter power for a step change in real power from 400 to 500kW.

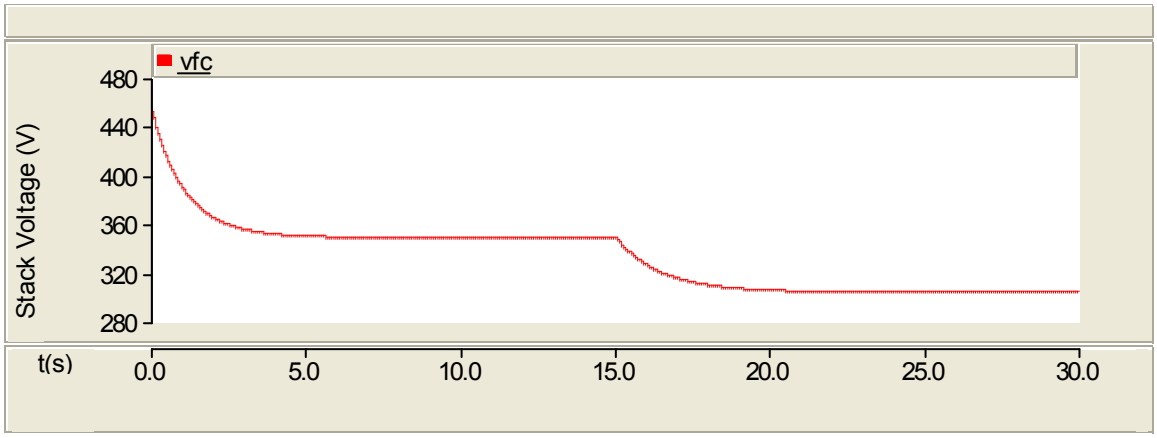

(a) Stack voltage (with reduced cell resistance)

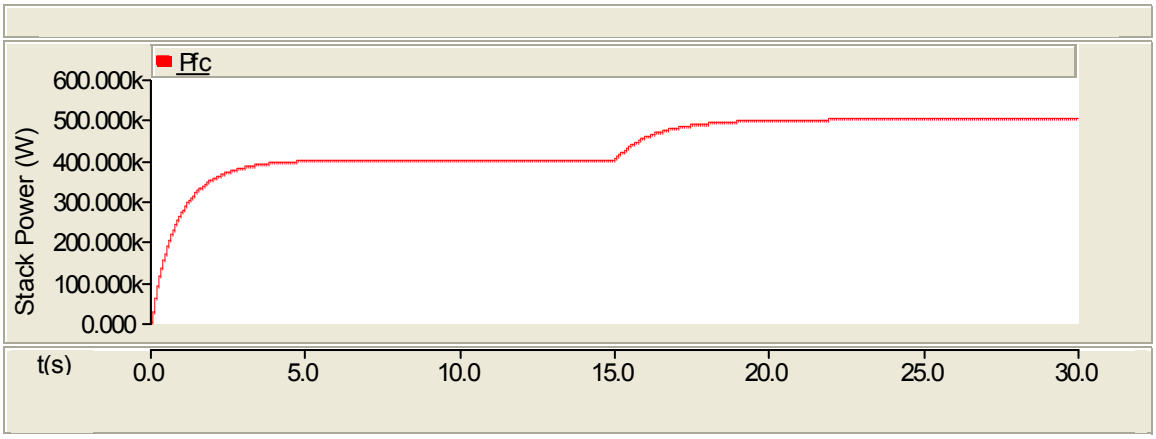

(b) Stack power (with reduced cell resistance)

Figure 4.18 Response of the fuel cell and the converter with reduced resistance

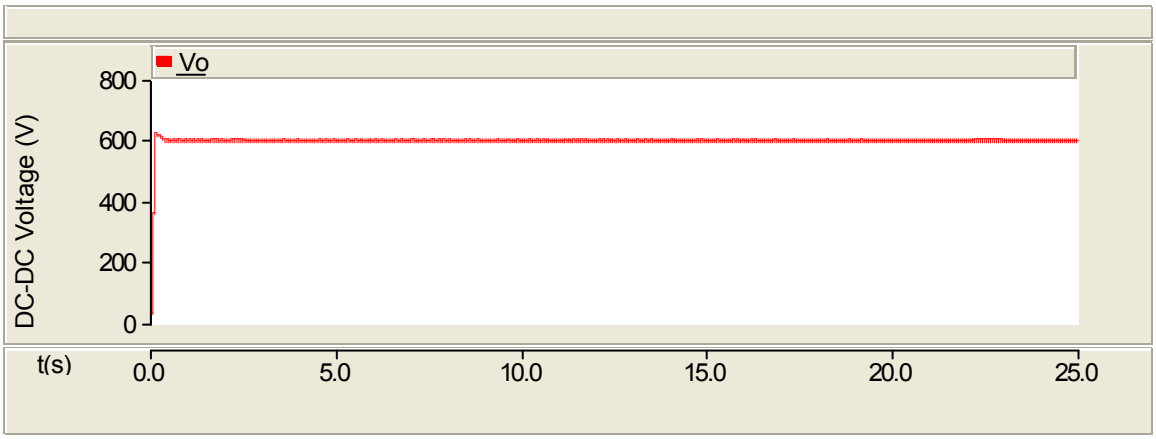

(c) Output voltage of the converter (with reduced cell resistance)

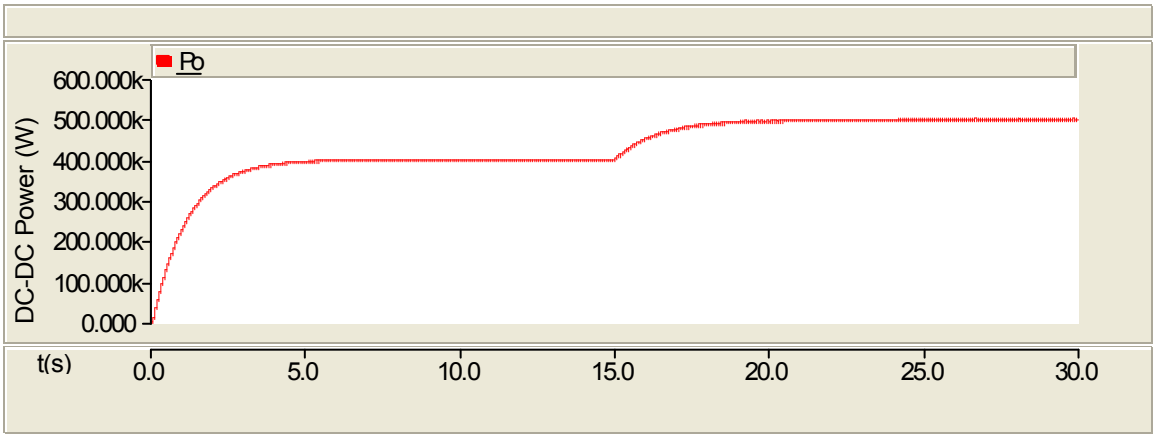

(d) Output power of the converter (with reduced cell resistance)

Figure 4.18 Response of the fuel cell and the converter with reduced resistance (cont).

4.2.3. Response for a Step Change in Real Power Reference. This subsection consists of the fuel cell, the DC-DC converter and the DC-AC inverter characteristics for a step change in the reference real power from 50 to 90kW. This subsection also the shows the comparison between the stack power, the DC-DC converter power and the DC-AC inverter power.

4.2.3.1. SOFC characteristics. Figure 4.19 shows the response of the fuel cell for step change in real power from 50 to 90kW. Figure 4.19(a) shows the gradual decrease in

the stack voltage from 438 to 425V. It takes around 5s to reach the new value. Figure 4.19(b) shows the change in the stack current from 120 to 225A. Figures 4.19(c) and (d) show the change in the fuel and air flow, respectively, which takes approximately 20s to reach the new value. Figure 4.19(e) shows the fuel utilization which gradually settles to an optimum value of 0.85 at around 10s. Figure 4.19(f) shows the change in the stack power from 50 to 90kW which takes around 5s to reach the new value.

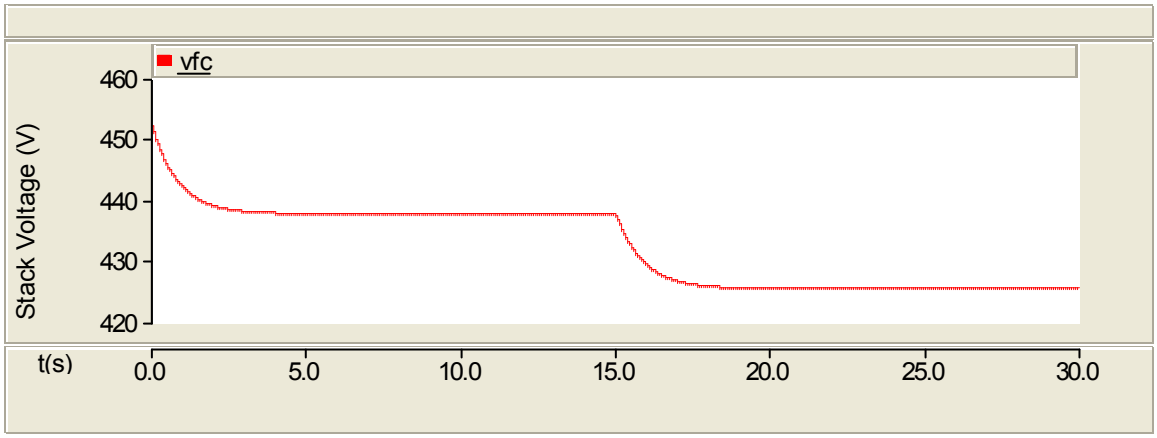

(a) Stack voltage

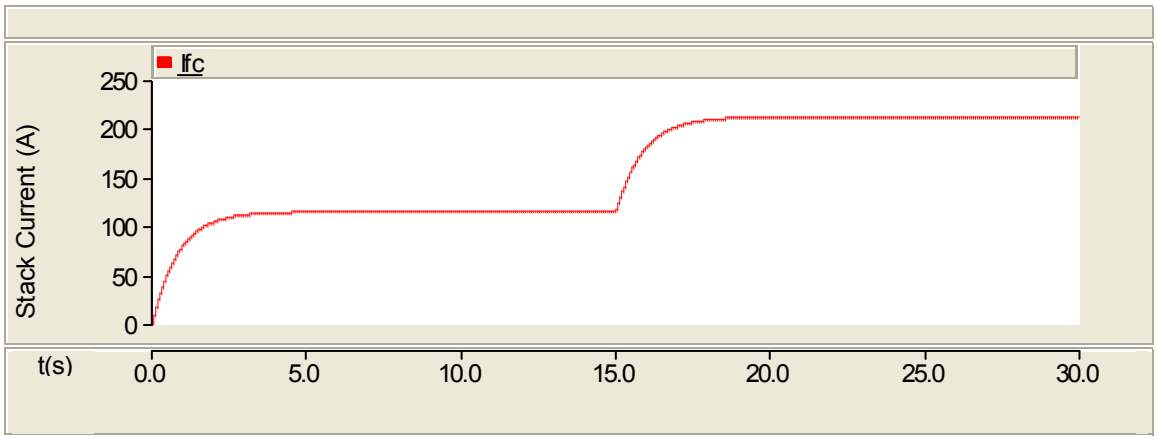

(b) Stack current

Figure 4.19 Response of the fuel cell for step change in real power from 50 to 90kW

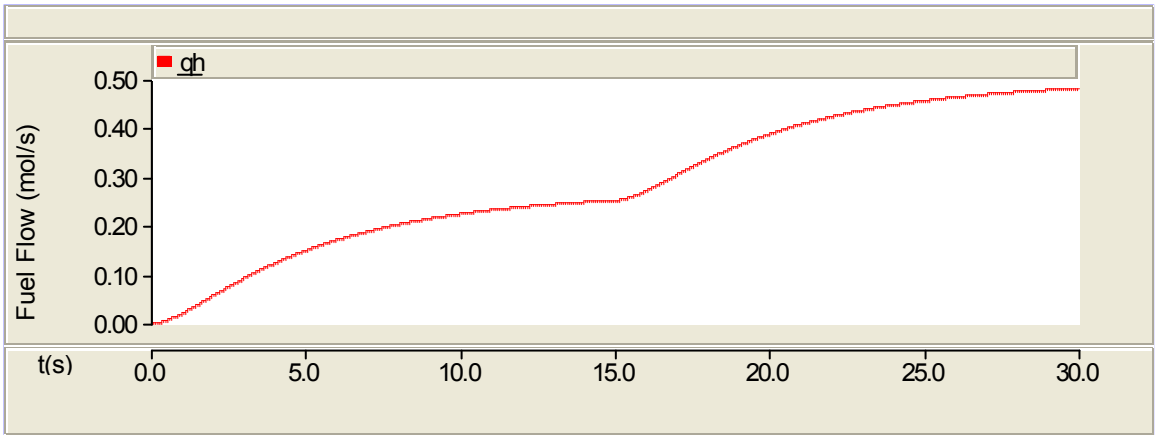

(c) Fuel flow

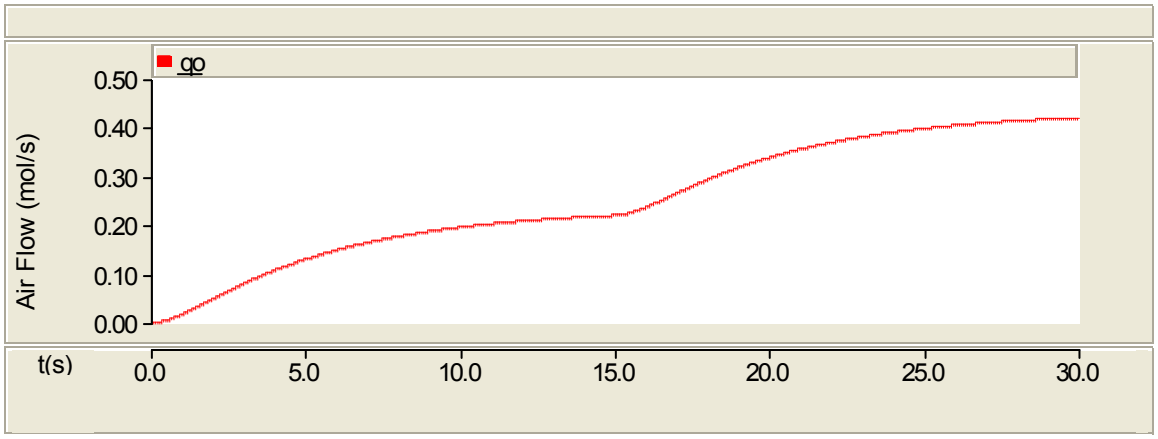

(d) Air flow

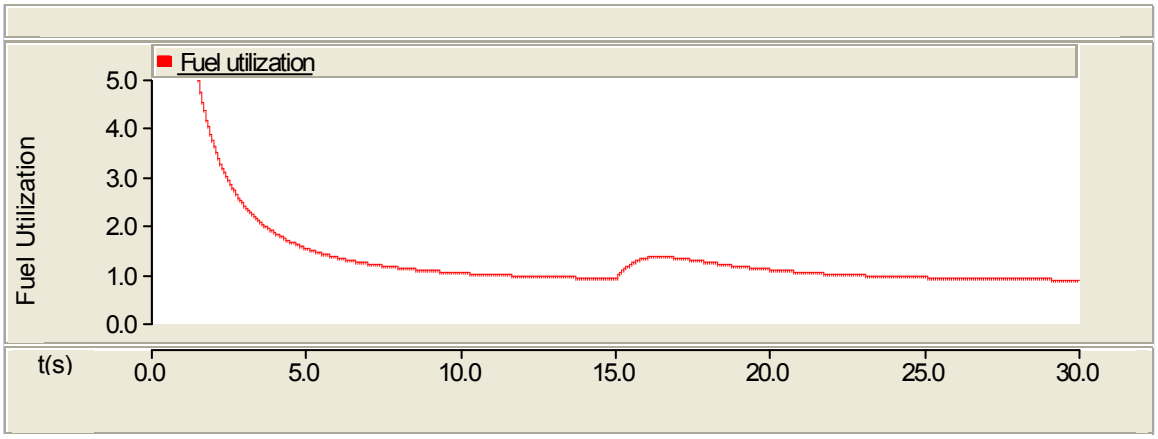

(e) Fuel utilization

Figure 4.19 Response of the fuel cell for step change in real power from 50 to 90kW (cont.)

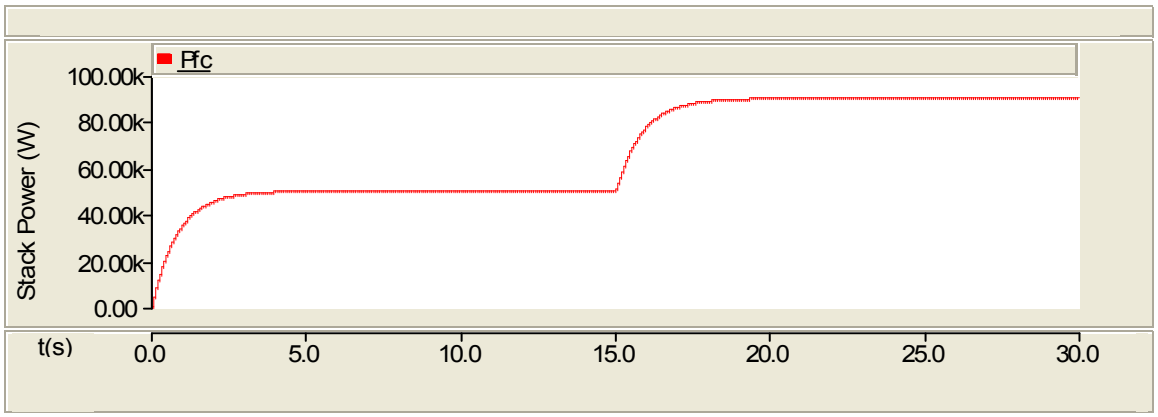

(f) Stack power

Figure 4.19 Response of the fuel cell for step change in real power from 50 to 90kW (cont.)

4.2.3.2. DC-DC converter characteristics. Figure 4.20 shows the response of the converter for step change in real power from 50 to 90kW. The feedback system maintains the output voltage at 600V as shown in Figure 4.20(a). Figures 4.20(b) and (c) show the current and the power of the converter respectively.

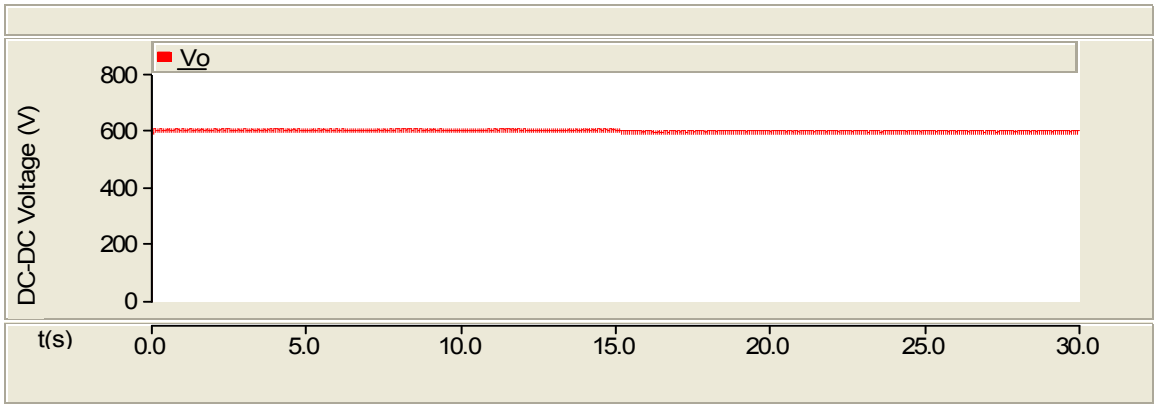

(a) Output voltage of the converter

Figure 4.20 Response of the converter for step change in real power from 50 to 90kW

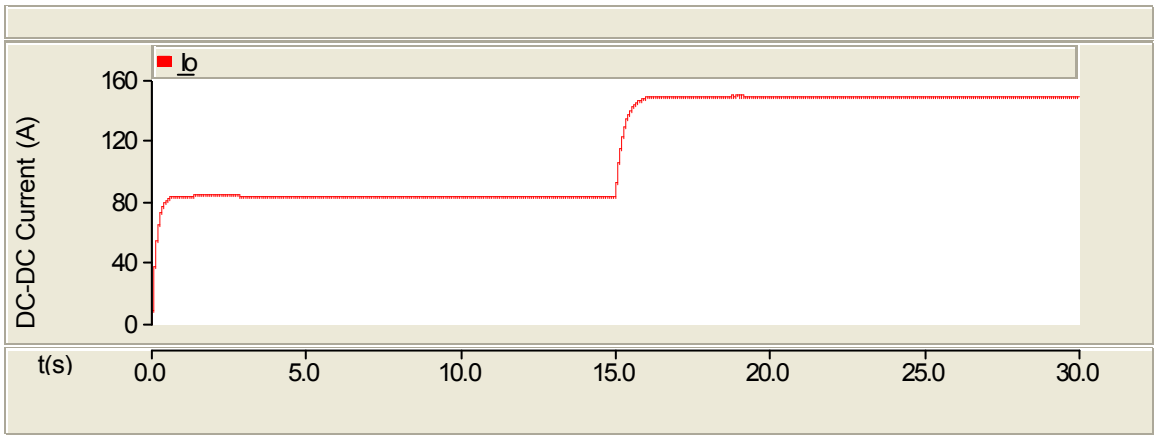

(b) Output current of the converter

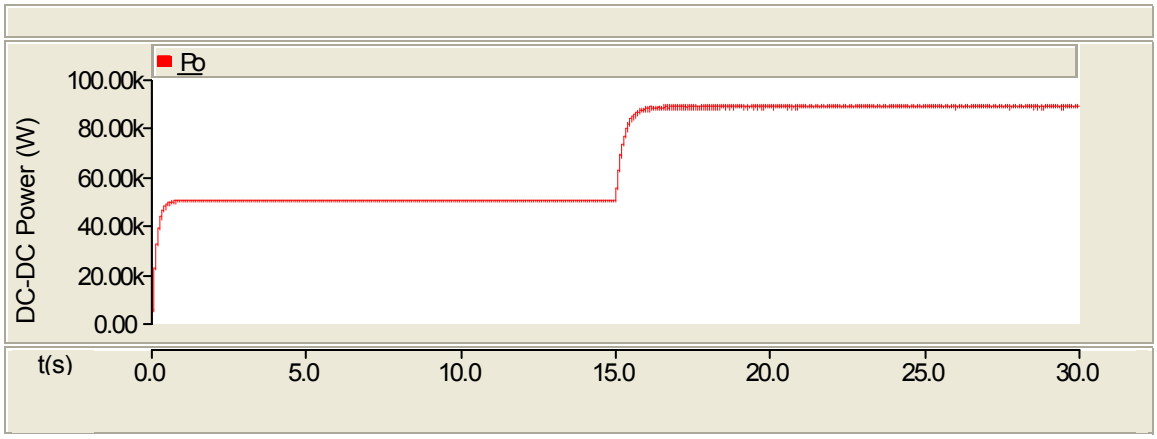

(c) Output power of the converter

Figure 4.20 Response of the converter for step change in real power from 50 to 90kW (cont.)

4.2.3.3. DC-AC inverter characteristics. The utility voltage need not be plotted since there will be no change on the utility side. Figure 4.21 shows the response of the inverter for step change in real power from 50 to 90kW.

Figure 4.21(a) shows the expanded view of transformer line-neutral voltage, similar to Figure 4.14(d). The small change in the voltage is not clearly seen in the figure. Figures 4.21(b) and (c) show the increase in the line current at the end of the transformer

and its expanded view, respectively. Figures 4.21(d) and (e) show the real and reactive power flow at the output of the transformer for a step change in reference real power. The real power takes 0.2s to reach the new steady value. The reactive power injection is assumed to be zero and this is evident from the Figure 4.21 (e).

Figures 4.21(f) and (g) show the phase angle of the inverter and the modulation index obtained from the PQ control. Real power controller controls the phase angle which increases from 0.0128 to 0.023 radians. The reactive power controller controls the modulation index which is maintained at 1.115 as shown in Figure 4.21(g). Figure 4.21(h) shows the L-L rms value of the transformer voltage obtained from the reactive power control; changes from 12.498 to 12.496 kV (negligible change) and cannot be seen in the figure. Figure 4.21(i) shows the measured value of the L-L rms transformer voltage.

Figure 4.21(j) shows the response of the fuel cell power (P_{fc}), DC-DC converter power (P_o) and the real power injection into the utility grid (P_{ac}) and Figure 4.21(k) shows its expanded view.

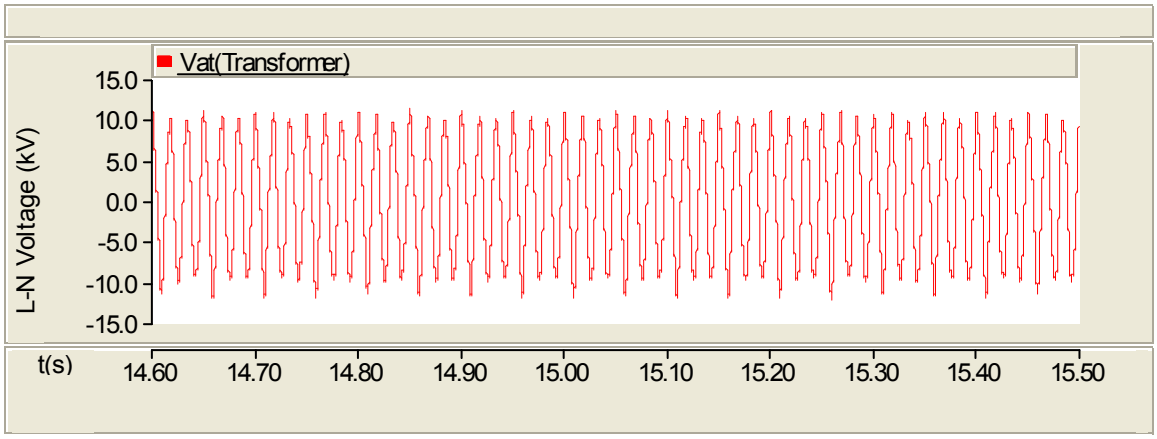

(a) Transformer line-neutral voltage (with filter)

Figure 4.21 Response of the inverter for step change in real power from 50 to 90kW

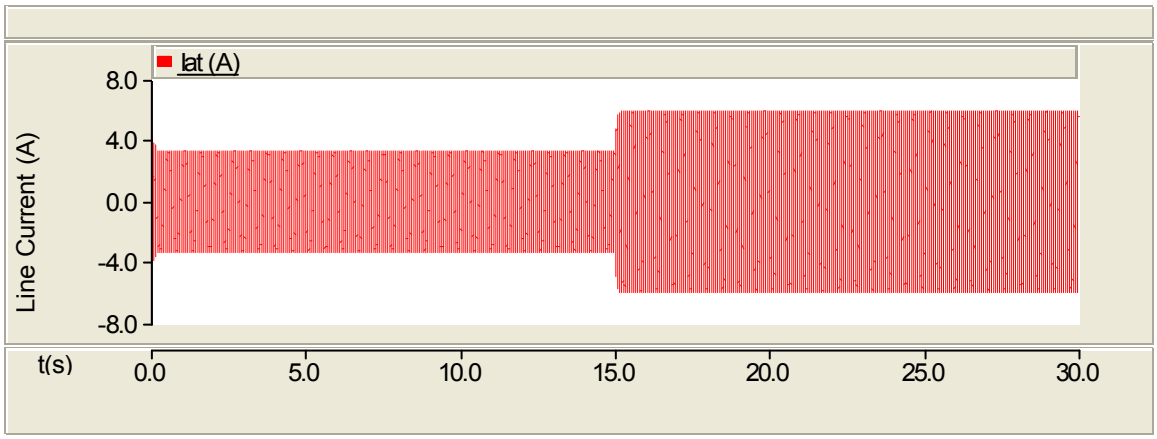

(b) Transformer line current in phase A

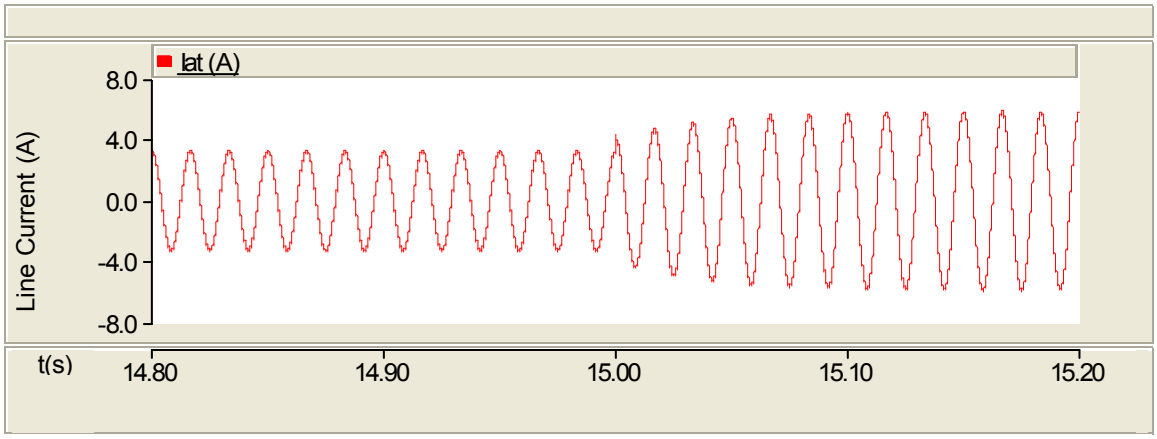

(c) Expanded view

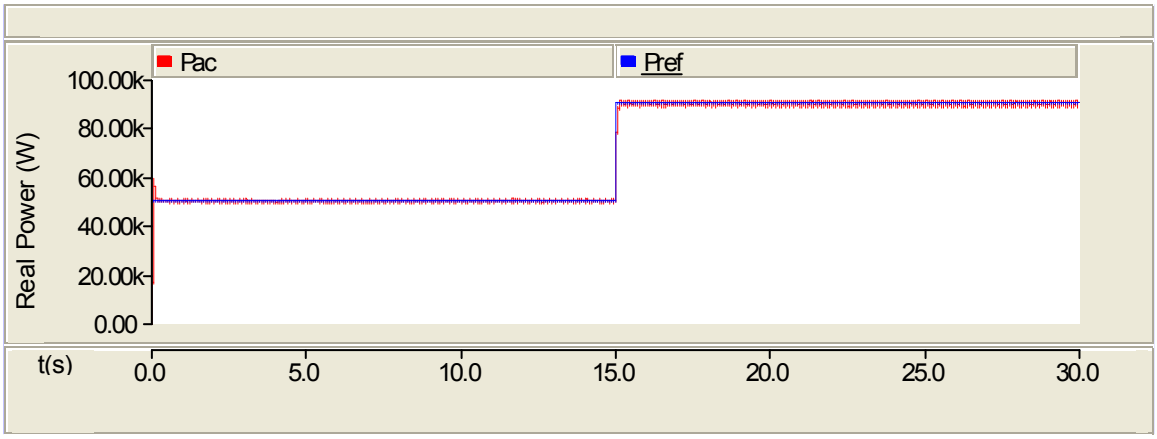

(d) Real power injection into the grid

Figure 4.21 Response of the inverter for step change in real power from 50 to 90kW (cont.)

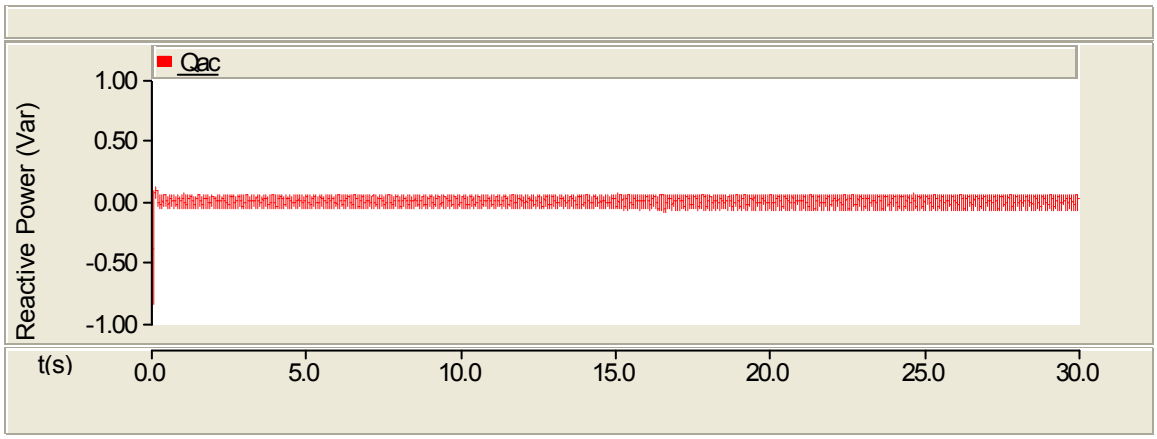

(e) Reactive power injection into the grid

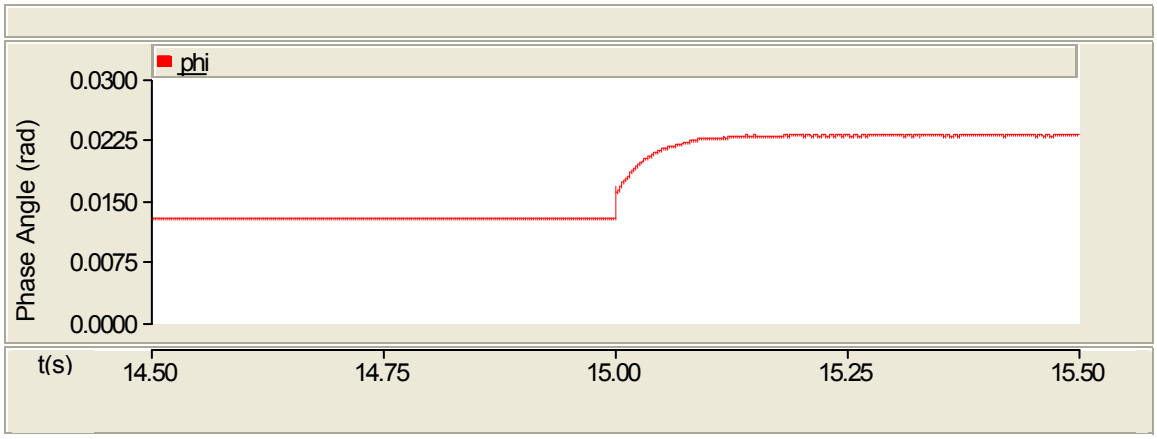

(f) Phase angle of the inverter from the P control

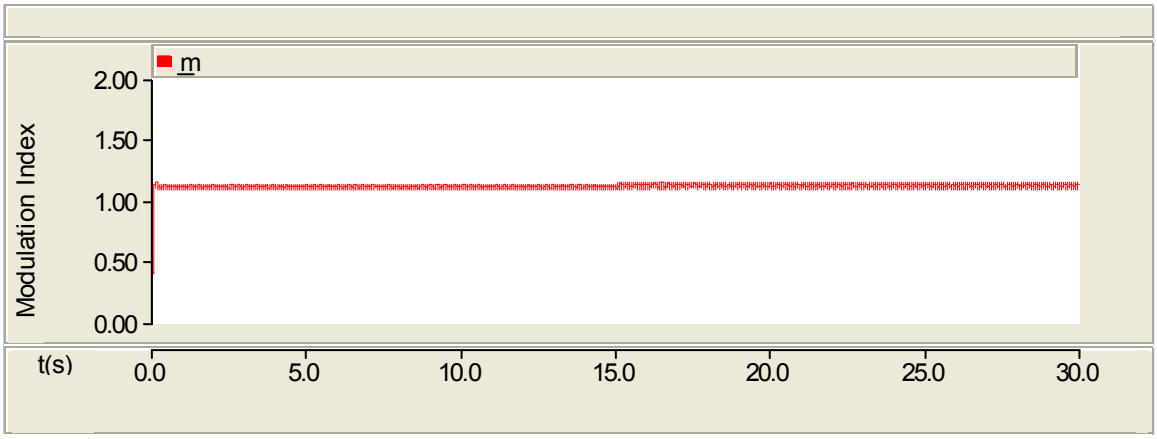

(g) Modulation index from the Q control

Figure 4.21 Response of the inverter for step change in real power from 50 to 90kW (cont.)

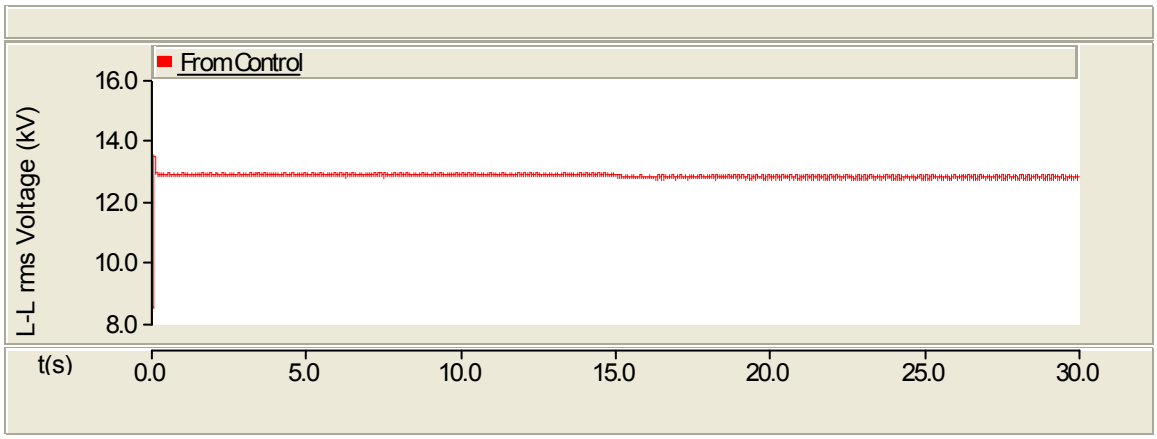

(h) L-L rms transformer voltage from the Q control

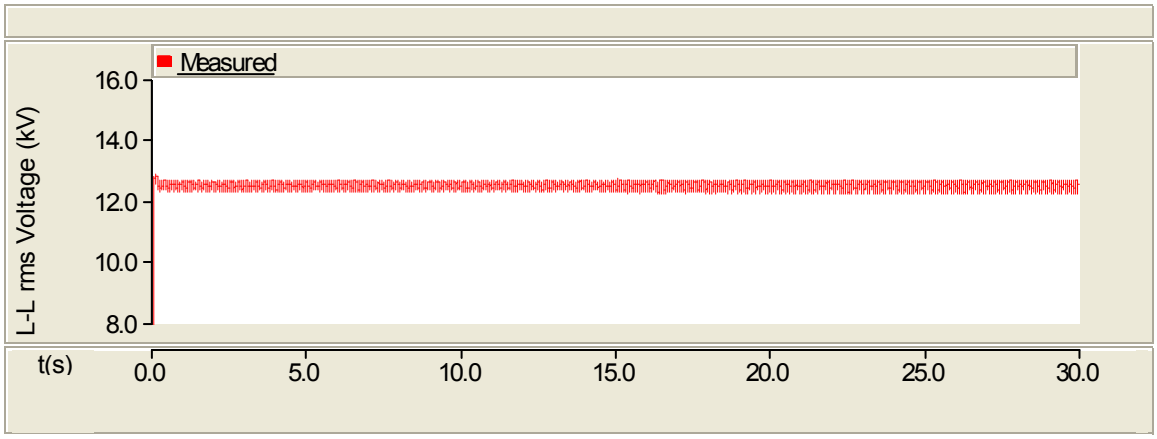

(i) L-L rms transformer voltage measured from the system

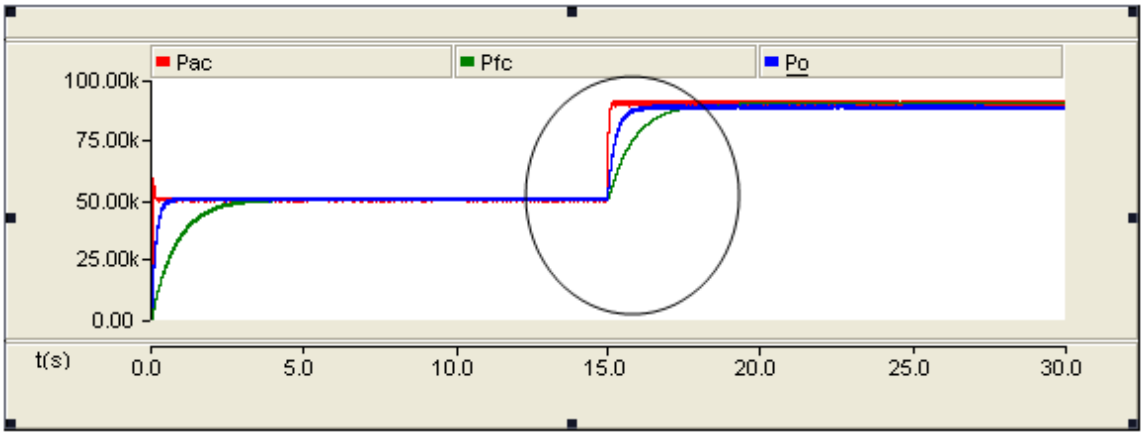

(j) Power characteristics

Figure 4.21 Response of the inverter for step change in real power from 50 to 90kW (cont.)

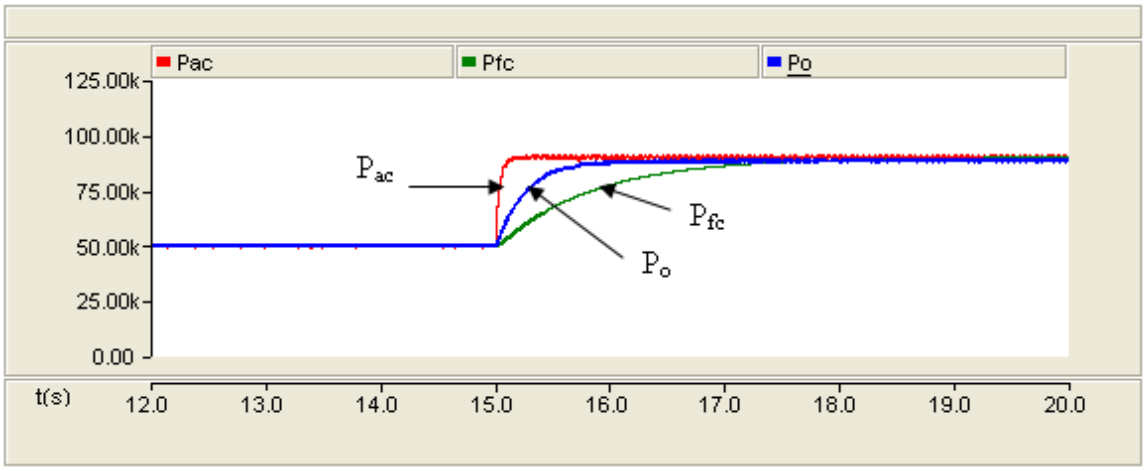

(k) Circular region expanded

Figure 4.21 Response of the inverter for step change in real power from 50 to 90kW (cont.)

The fuel cell power takes around 5s to reach the new steady value of 90kW. The response of the DC-DC converter is better than that of the fuel cell: it takes around 2.5s to reach the new steady state value. The real power flow into the utility grid takes less than 0.1s to reach the new steady state value.

The slow response of the SOFC, evident from Figure 4.21(k), is due to the slow change in the chemical reaction parameters after a change in the flow of reactants. The fast transient characteristic of the power electronic devices (DC-DC converter and the DC-AC inverter) has been utilized to improve the fuel cell performance when connected to the grid. Further, the DC link capacitor at the terminals of the DC-DC converter provides the extra power required to maintain the power balance between P_{fc} and P_o during the transient period. The difference between P_o and P_{ac} (i.e., the inverter output) during the transient period is made up by the same dc link capacitor; however, because a PI controller controls the inverter output, a faster response is obtained by optimizing the time constant of the integral portion of the controller. Thus, the slow response of the SOFC can be compensated with the help of the power conditioning unit.

The DC-DC converter improves the response by 50%. The response is further improved with the three phase DC-AC inverter. The real power flow into the grid takes less than 0.1s to reach the new steady value of 90kW from 50kW. The slow response of the fuel cell prevents it from grid-tie applications. The response time can be improved by 98% with the power conditioning units.

5. CONCLUSION AND FUTURE WORK

5.1. CONCLUSION

A dynamic model of the solid oxide fuel cell (SOFC) was developed in PSCAD. A DC-DC buck-boost converter topology and its closed loop control feedback system have been built. A three phase inverter has been modeled and connected between the SOFC-DC-DC system on the one side and the utility grid on the other side through an ideal transformer. A control strategy for the inverter switching signals has been discussed and modeled successfully.

The fuel cell, the converter and the inverter characteristics were obtained for a reference real power of 50kW. The response of the fuel cell stack power is compared with the response of the output power of the converter. The fuel cell power takes around 5s to reach the commanded value of 50kW whereas the converter output takes around 2.5s to reach the commanded value. The slow response of the fuel cell is due to the slow and gradual change in the fuel flow which is proportional to the stack current. The interconnection of the fuel cell with the converter boosts the stack voltages and also regulates it for continuous current. The fuel cell stack voltage drops to zero for discontinuous current and the system shuts down. The fuel cell unit shuts off for real power above the maximum limit. Additional power at the converter is provided by the inductor, connected in series with the equivalent load which acts as an energy storage. The inductor can be replaced by any energy storage device such as a capacitor or a battery for providing additional power during load transients.

The inverter control scheme uses a decoupled PQ control strategy to control the phase angle of the inverter and the voltage across the transformer. The characteristics for the system have been obtained. The transformer and inverter voltage waveforms have been plotted. The control variable (phase angle and modulation index) have been obtained from the proposed control scheme and plotted. The L-L rms voltage measured from the system is compared with the value obtained from the reactive control. The measured voltage oscillates with the average value being equal to that obtained from the control. The real power injection into the grid takes less than 0.1s to reach the

commanded value of 50kW. The reactive power injection has been assumed to be zero and was evident from the simulation results.

The maximum power limit on the fuel cell is 400kW. For any reference power beyond this limit, the fuel cell loses stability and drops to zero. This limit has been set by the parameters considered for the fuel cell data. Higher power can be commanded by either increasing the number of the cells, increasing the reversible standard potential or by decreasing the fuel cell resistance. A step change in the reference power from 400 to 500KW has been considered in order to observe the limitation of the fuel cell dynamics. The simulation results validate the maximum limit on the fuel cell. At the instant of step change, the stack voltage dropped to zero and oscillations were observed. This drop in voltage had its effect on the DC link voltage and consequently on the control variables and the real power injection into the grid. The reactive power was zero until the step change and after the step change, oscillations were observed in the reactive power as well.

The system was then subjected to a step change in the reference real power from 50 to 90kW. The fuel cell, the converter and the inverter characteristics were obtained. The characteristics of the fuel cell (voltage, current and power) have a slower gradual change at the instant of step change when compared with the converter characteristics. The DC link voltage was maintained at the reference value by the closed loop control system. The phase angle of the inverter depends on the real power injection. Hence for a step change in the real power, there is an increase in the phase angle of the inverter. Reactive power injections control the transformer voltage, which in turn controls the modulation index. At the instant of the step change, there is no increase in the rms value of line-line transformer voltage, owing to zero reactive power injection. The measured rms value slightly decreased whereas the value obtained from the control did not change.

The power characteristics of the system have been plotted. A comparison has been made between the response of the fuel cell power, DC-DC converter power and the real power injection into the utility grid. The power conditioning unit improved the slow response of the fuel cell. The response time improved by 50% with the DC-DC converter connected to SOFC. The response time has been further improved by an additional 40% (i.e. 90% overall) with the three phase inverter connection to the SOFC-DC-DC system.

The simulation results proved that the power conditioning unit made the fuel cell a potential distributed generation source for grid-tie applications.

5.2. FUTURE WORK

The fuel cell system developed in this thesis can be modified for improving the applicability of the system. In this thesis, the thermodynamic effect of the fuel cell has not been considered. Future work can involve inclusion of thermodynamic equations. The performance of the stack voltage with and without the temperature effect can be obtained and its overall effect on the load.

In this thesis, an infinite bus has been modeled for utility grid. The work can be further extended to a higher order bus system. Different placements of the fuel cell unit can be studied and analyzed. The performance of multiple units at multiple locations can also be studied. The performance of the fuel cell can also be tested by carrying out short circuit studies

APPENDIX-SYSTEM DATA

Table A.1 Parameters in SOFC model [10], [14] & [15]

	Representation	Value
T	Absolutely temperature	1273 K
F	Faraday's constant	96487 C/mol
R	Universal gas constant	8314 J/(kmol K)
E^o	Standard reversible cell potential	1.18 V
N	Number of cells in stack	384
K_r	Constant ,$K_r=N/4F$	0.996 x 10^{-6} kmol/(s A)
U_{max}	Maximum fuel utilization	0.9
U_{min}	Minimum fuel utilization	0.8
U_{opt}	Optimum fuel utilization	0.85
KH_2	Valve molar constant for hydrogen	8.43 x 10^{-4} kmol/(s atm)
KO_2	Valve molar constant for oxygen	2.81 x 10^{-4} kmol/(s atm)
KH_2O	Valve molar constant for water	2.52 x 10^{-3} kmol/(s atm)
τ_{H2}	Response time for hydrogen flow	26.1 s
τ_{H2O}	Response time for water flow	78.3 s
τ_{O2}	Response time for oxygen flow	2.91 s
R	Ohmic loss	0.126 Ω
T_e	Electrical response time	0.8 s
T_f	Fuel processor response time	5 s
r_{HO}	Ratio of hydrogen to oxygen	1.145

Table A.2 Parameters in buck-boost DC-DC converter

L	0.001H
C	5000μF
Filter inductance (L_f)	1.0H
R (Equivalent load)	7.2Ω
Switching frequency	6.5KHz

Table A.3 Electrical Data

DC-DC voltage (V_o)	600V
Line-line rms grid side voltage (V_{LLrmsu})	12.5kV
Turns ratio of the transformer (K_t)	30.5
Transformer leakage reactance (L_t)	0.106H

BIBLIOGRAPHY

[1] J. Padulles, G. W. Ault, and J. R. McDonald, "An Approach to the Dynamic Modeling of Fuel Cell Characteristics for Distributed Generation Operation," *IEEE- PES Winter Meeting*, vol. 1, Issue 1, pp. 134-138, January 2000.

[2] S. Pasricha, and S. R. Shaw, "A Dynamic PEM Fuel Cell Model," *IEEE Trans. Energy Conversion*, vol. 21, Issue 2, pp. 484-490, June 2006.

[3] P. R. Pathapati, X. Xue, and J. Tang, "A New Dynamic Model for Predicting Transient Phenomena in a PEM Fuel Cell System," *Renewable Energy*, vol. 30, Issue 1, pp. 1-22, January 2005.

[4] C. Wang, and M. H. Nehrir, "Dynamic Models and Model Validation for a PEM Fuel Cells Using Electrical Circuits," *IEEE Trans. Energy Conversion,* vol. 20, Issue 2, pp. 442-451, June 2005.

[5] D. J. Hall, and R. G. Colclaser, "Transient Modeling and Simulation of a Tubular Solid Oxide Fuel Cell," *IEEE Trans. Energy Conversion*, vol. 14, Issue 3, pp. 749-753, September 1999.

[6] E. Achenbach, "Three-dimensional and Time-dependent Simulation of a Planar SOFC Stack," *J. Power Sources*, vol. 49, Issue 1-3, pp. 333-348, April 1994.

[7] E. Achenbach, "Response of a Solid Oxide Fuel Cell to Load Change," *J. Power Sources*, vol. 57, Issue 1, pp. 105-109, September 1995.

[8] K. Sedghisigarchi, and A. Feliachi, "Dynamic and Transient Analysis of Power Distribution Systems with Fuel Cell-Part I: Fuel-Cell Dynamic Model," *IEEE Trans. Energy Conversion*, vol. 19, Issue 2, pp. 423-428, June 2004.

[9] C. Wang, and M. H. Nehrir, "A Physically-Based Dynamic Model for Solid Oxide Fuel Cells," accepted for *IEEE Trans. Energy Conversion* September 15, 2006.

[10] J. Padulles, G. W. Ault, and J. R. McDonald, "An Integrated SOFC Plant Dynamic Model for Power System Simulation," *J. Power Sources*, vol. 86, Issue 1-2, pp. 495-500, 2000.

[11] C. J. Hatziadoniu, A. A. Lobo, F. Pourboghrat, and M. Daneshdoost, "A Simplified Dynamic Model of Grid-Connected Fuel-Cell Generators," *IEEE Trans. Power Delivery*, vol. 17, Issue 2, pp. 467-473, April 2002.

[12] S. Stevandic, and J. Jiang, "A Standalone, Reduced-order Model and Control of a Grid-Connected Fuel Cell Power Plant," *IEEE-PES General Meeting*, vol. 2, pp. 679-686, July 2003.

[13] Z. Miao, M. A. Choudhry, R. L. Klein, and L. Fan, "Study of a Fuel cell Power Plant in Power Distribution System-Part I: Dynamic Model," *IEEE-PES General Meeting*, vol. 2, pp. 2220-2225, June 2004.

[14] Y. Zhu, and K. Tomsovic, "Development of Models for Analyzing the Load-Following Performance of Micro Turbines and Fuel Cells," *Electric Power Syst. Research*, vol. 62, Issue 1, pp. 1-11, May 2002.

[15] J. Wen, K. M. Smedley, and M. A. Pai, "Load-Following Improvement of Fuel Cells with Fast Transient OCC Inverter," *Proc. IEEE/ASME, Intl. Conf. on Advanced Intelligent Mechatronics*, pp. 140-145, July 2005.

[16] M. D. Lukas, K. Y. Lee, and H. G. Ayagh, "Development of a Stack Simulation Model for Control Study on Direct Reforming Molten Carbonate Fuel Cell Power Plant," *IEEE Trans. Energy Conversion*, vol. 14, pp. 1651-1657, December 1999.

[17] M. D. Lukas, K. Y. Lee, and H. G. Ayagh, " An Explicit Dynamic Model for Direct Reforming Carbonate Fuel Cell Stack," *IEEE Trans. Energy* Conversion, vol. 16, pp. 289-295, September 2001.

[18] F. Blaabjerg, Z. Chen, and S. B. Kjaer, "Power Electronics as Efficient Interface in Dispersed Power Generation Systems," *IEEE Trans. Power Electronics*, vol. 19, Issue 5, September 2004.

[19] G. K. Anderson, C. Klumpner, S. B. Kjaer, and F. Blaabjerg, "A New Power Inverter for Fuel Cells" *IEEE Conf. Power Electronics* Specialists, vol. 2, Issue 2, pp. 727-733, June 2002.

[20] C. Liu, T. Nergaard, L. Leslie, J. Ferrell, X. Huang, T. Shearer, J. Reichl, J. Lai, and J. Bates, "Power Balance Control and Voltage Conditioning for Fuel Cell Converter with Multiple Sources," *IEEE Conf. Power Electronics* Specialists, vol. 4, pp. 2001-2006, June 2002.

[21] J. J. Woo, "Modeling and Control of Fuel Cell Based Distributed Generation Systems," PhD Dissertation, Ohio State University, 2005.

[22] N. Mohan, T. M. Undeland, and W. P. Robbins, "Power Electronics, Converters, Applications and Design," 2nd Edition, John Wiley & Sons.

[23] C. Wang, and M. H. Nehrir, "Short-time Overloading Capability and Distributed Generation Applications of Solid Oxide Fuel Cells," accepted for *IEEE Trans. Energy Conversion* September 15, 2006.

[24] F. Jurado, J. R. Saenz, and L. Fernandez, "Neural Network Control of Grid-Connected Fuel Cell Plants for Enhancement of Power Quality," *IEEE Proc. Power Tech Conf.*, vol. 3, Issue 7, June 2003, Bologna, Italy.

[25] M. C. Chandorkar, M. D. Divan, and R. Adapa, "Control of Parallel Connected Inverters in Standalone AC Supply Systems," *IEEE Trans. Industry Applications*, vol. 29, Issue 1, pp. 136-143, January 1993.

[26] K. Ro, and S. Rahman, "Two-Loop Controller for Maximizing Performance of a Grid-Connected Photovoltaic-Fuel cell Hybrid Power Plant," *IEEE Trans. Energy Conversion*, vol. 13, Issue 3, pp. 276-281, September 1998.

[27] R. Lasseter, "Dynamic Models for Micro-turbines and Fuel Cells," *IEEE-PES Summer meeting*, vol.2, pp. 761-766, July 2001.

[28] C. Wang, and M. H. Nehrir, "Control of PEM Fuel Cell Distributed Generation Systems," *IEEE Trans. Energy Conversion*, vol. 21, Issue 2, pp. 586-595, June 2006.

[29] P. G. Barbosa, L. G. Rolim, E. H. Watanabe, and R. Hanitsch, "Control Strategy for Grid-Connected DC-AC Converters with Load Power Factor Correction," *IEEE Proc. Gener. Transm. Distrib.*, vol. 145, Issue 5, pp. 487-491, September 1998.

[30] D. Georgakis, and S. Papathanassiou, "Modeling of Grid-Connected Fuel Cell Plants," *Proc. CIGRE Power Systems with Dispersed Generation*, April 2005, Athens.

[31] B. Delfino, and F. Fornari, "Modeling and Control of an Integrated Fuel Cell-Wind Turbine System," *Proc. Power tech Conf.*, vol. 2, Issue 2, June 2003, Bologna, Italy

[32] A. Hajimiragha, "Generation Control in Small Isolated Power systems," Master Thesis, Royal Institute of Technology, Stockholm, 2005.

[33] http://www.ballard.com/be_a_customer/fuel_cells , date last visited: January 20, 2007, "Fuel Cells: Ballard Power Systems".

[34] http://www.powergeneration.siemens.com/en/fuelcells/commercialization , date last visited: March 10, 2007, "SOFC Product Commercialization".

[35] http://www.fuelcells.org/basics/apps.html , date last visited: January 20, 2007, "Fuel Cell Basics: Fuel Cells 2000".

[36] http://www.fuelcellmarkets.com/article_default_list.fcm , date last visited: March 10, 2007, "Fuel Cell Markets - Products & Services".

[37] "Small Stationary Applications - Fuel Cell Market Survey", Fuel Cell Today, 2003.

[38] "Small Stationary Applications - Fuel Cell Market Survey", Fuel Cell Today, 2006.

[39] "Large Stationary Applications - Fuel Cell Market Survey", Fuel Cell Today, 2006.

[40] K. Sedghisigarchi, and A. Feliachi, "Dynamic and Transient Analysis of Power Distribution Systems with Fuel Cell-Part II: Control and Stability Enhancement," *IEEE Trans. Energy Conversion*, vol. 19, Issue 2, pp. 429-434, June 2004.

[41] MATLAB/Simulink, version 7.1, Math works Inc, 1984-2005.

[42] Power Systems Computer Aided Design (PSCAD), version 4.1, Manitoba HVDC Research Center Inc, 2004.

[43] http://www.nfcrc.uci.edu/fcresources/FCexplained/challenges.htm , date last visited: January 20, 2007, "Fuel Cells Explained: National Fuel Cell Research Center".

[44] http://www.answers.com/topic/fuel-cell , date last visited: January 20, 2007.

[45] http://www.energy.ca.gov/distgen/equipment/fuel_cells/fuel_cells.html , date last visited: January 20, 2007, "California Distributed Energy Resource Guide", October 2005.

[46] http://www.engr.wisc.edu/me/faculty/klein_sanford/fuelcellreport193-1.pdf , date last visited: January 20, 2007, "Fuel Cells for Distributed Generation - A Technology and marketing Summary," March 2000.

[48] J. Larminie, and A. Dicks, "Fuel Cell Systems Explained", 2nd Edition, John Wiley & Sons, 2003.

[48] P. C. Krause, O. Wasynczuk and S. D. Suddhoff, "Analysis of Electric Machinery and Drives Systems," IEEE Press 2002.

VITA

Nagasmitha Akkinapragada was born on 9th August, 1980 in Hyderabad, a southern city of India. She received her primary and secondary in Hyderabad, India before joining Osmania University, Hyderabad, India to pursue her undergraduate degree in Electrical Engineering. She graduated with a Bachelor of Engineering degree in Electrical Engineering in May 2002. She worked in BPL Engineering Limited, India from August 2002 to June 2005 as an Assistant Manager. In August 2005, she joined the Masters' program in Electrical Engineering Department at University of Missouri-Rolla. Her research interests are power system analysis, distributed generation and electric machines and drives. She received her M.S. degree in Electrical Engineering in May 2007. She plans to pursue her career as a design engineer in the field of Electrical Engineering.